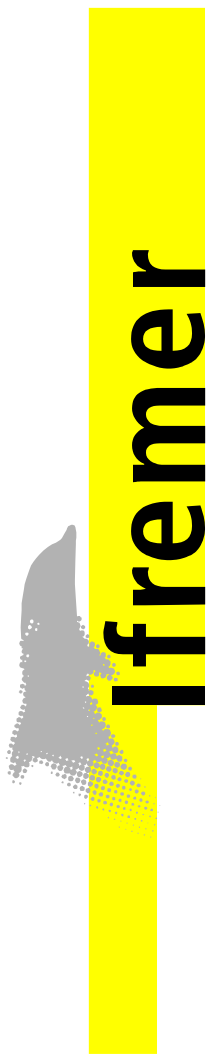


PDG-DOP-DCB-RDT-HO

Zakoua GUEDE
Michel OLAGNON
Hélène PINEAU (ACTIMAR – Brest)

Juin 2009 – R06 HO 09
(Rapport final)



ifremer

Validation of the Iterative Component Addition (ICA) formulas for the damage assessment of multimodal loading spectra

Validation of the Iterative Component Addition (ICA) formulas for the damage assessment of multimodal loading spectra

Distribution

Company	Addressees
TOTAL DGEP/TDO/TEC/GEO	Mrs V. Quiniou

Revision

Rev	Dates	authors	Checked by	Issue
0		Z. Guédé Zakoua.Guede@ifremer.fr M. Olagnon Michel.Olagnon@ifremer.fr H. Pineau pineau@actimar.fr	M. Olagnon	Final report



Validation of the Iterative Component Addition (ICA) formulas for the damage assessment of multimodal loading spectra

Z. Guédé & M. Olagnon

IFREMER - Centre de Brest, 29280 Plouzané, France

H. Pineau

ACTIMAR - 36 Quai de la Douane, 29200 Brest, France

ABSTRACT

The purpose of this study is to validate the use of the so-called Iterative Component Addition (ICA) formulas for the assessment of fatigue damage of marine structures subjected to complex (multimodal) wave loading conditions, as prevail in West Africa areas where the sea states are usually described as combinations of three wave systems (*e.g.* main swell, secondary swell and wind sea). In this context, operators specifications require to consider a very large set of fatigue loading cases, which lead to excessive computation times if the conventional procedure is used for fatigue assessment. The use of the ICA formulas is expected to simplify the evaluation of the damage and to allow a drastic reduction of computation time, keeping a slight level of conservatism. The present work intends to validate those formulas on an industrial application. One is especially interested in the accuracy of the ICA-based approach for fatigue damage assessment, the ease of use of this approach and the computation times it involves.

The scope of the study is limited for simplicity purposes to cases where the structural dynamic response is linear. Its actual industrial application deals with the assessment of the fatigue damage induced by the vertical bending moment of an FPSO hull girder subjected to wave loading in a West Africa area. In this report, we define the occurrence probabilities of all the fatigue loading cases to be applied as required by the operator specifications. Then, to validate the use of the ICA formula, the fatigue damage is estimated according to two main approaches. The first one, which serves as a reference solution, uses a conventional method and computes the damages of the sea states from the metocean database only. The other one uses ICA formulas and compute the damages of all possible sea states defined by the operator specifications. For this last approach, a full application of ICA formulas based on a partition of wave systems response spectra is also carried out and some analytical formulas for the damage of unimodal spectra are set up. Between both approaches, some intermediate computations are made to estimate the individual effects of the approximations introduced.

The occurrence probabilities of the fatigue loading cases derived from the metocean specifications exhibit some significant discrepancies from the statistics of the metocean database. Namely, they provide a lower significant height for the sea states with only a main swell and a larger one for sea states with the three wave systems. As to the application of ICA formulas, it is shown to provide accurate results. We can note that the ICA results are close to the reference solution and that most of the conservatism comes from the discretization defined for the statistical analysis. Moreover, the implementation of the ICA-based approach is simple on the actual industrial application. With appropriate change of programming language and optimization of the procedure, dramatic improvements have been obtained in the computation time, with nearly 2 million combinations of sea states processed in less than one minute.

Two main difficulties were encountered in this study. The first one concerns the two-slopes S-N curve, as a combined spectrum may have cycles amplitudes that are larger than the stress threshold of the S-N curve while its individual components do not. That was solved by providing a method to estimate two-slope damage from the two single-slope ones. The second difficulty stems from the discrepancies observed between the statistics on the metocean database and the sea states probabilistic model derived from the metocean specifications, which raises some questions on the construction of fully relevant metocean specifications. Though some progress was made, that second difficulty is not yet satisfactorily solved.

However, this study appears as a mighty step in the development of a global framework for fatigue damage assessment under multimodal loading conditions with the ICA formulas.

NOMENCLATURE

Variables

t	<i>time</i> in seconds
ω	<i>frequency</i> in rad/s
H_S	<i>significant waveheight</i>
T_p	<i>peak period</i> of the wave spectrum
ω_p	<i>peak frequency</i> of the wave spectrum
θ_p	<i>peak direction</i> of the wave spectrum
$S_w(\omega)$	<i>wave power spectral density</i>
$S_{BM}(\omega)$	<i>structural response power spectral density</i>
λ_k	<i>spectral moment</i> of order k
m or k	<i>slope parameter of the S-N curve</i> ¹
$\log \bar{a}$	<i>S-N curve parameter</i> ¹
S_c	<i>Threshold of the S-N curve</i>
N	<i>number of peaks</i> or <i>number of rainflow cycles</i> ²
d or D	<i>fatigue damage</i> ²
σ	standard deviation
χ	skewness
κ	kurtosis

Abbreviation

MS:	Main Swell ;
SS:	Secondary Swell ;
WS:	Wind Sea
RAO	Response Amplitude Operator
VWBM	Vertical Wave Bending Moment
PDF	Probability Density Function
CDF	Cumulative Density Functin
jPDF	Joint Probability Density Function
ICA	Iterative Component Addition

¹For 2 slopes subscript 1 for low-cycles fatigue regime and subscript 2 for high-cycles fatigue regime.

²It can have a second subscript that refers to the signal under consideration.

1 Introduction

Fine descriptions of sea state climate, introducing partitions of the sea states into several wave systems components, that have become the rule for climate in some areas lead to quite complex fatigue damage assessment. In particular, this is the case for the West Africa areas where sea states are usually described as combinations of up to three wave systems (*e.g.* main swell, secondary swell and wind sea). In this context, the set of fatigue loading cases to be dealt with for fatigue analysis must cover all possible combinations of the wave system components, which constitute a very large set (*e.g.* with 10^6 to 10^9 elements). Thus, a full damage computation by selecting all the combinations that may have a significant effect, simulating them and the corresponding stress time histories and counting their cycles is quite unpractical. However, it would be computationally acceptable and even efficient if one were able to compute easily the damage induced by a sea state made of several wave systems components in terms of the damages due to its components taken separately. That way, full damage computation would be needed only for each of the wave systems components, the amount of which is much lower than the number of the sea states to be considered (10^2 to 10^3).

To estimate the damage due to a sea state with several wave systems, one can make use of analytical formulas, which were set up for the evaluation of fatigue under loads with multimodal spectral densities (*i.e.* spectra with several peaks). Those such formulas consider a multimodal spectrum as the sum of unimodal spectra (*i.e.* spectra with one peak), corresponding respectively to each peak of the multimodal spectrum under consideration, and express the damage of the multimodal spectrum in terms of the damage of those individual unimodal spectra and of their respective spectral parameters. However, most of those formulas ([5], [7]) are dedicated to bi-modal spectra only and for which each mode is narrow-band, whereas, in practice loads spectra exhibit more than two modes and not necessarily narrow-band. In addition, they may be overly conservative when the spectral peaks are not widely separate in frequency.

In 2007, the authors have conducted some studies to set up formulas for the estimation, in a conservative manner, of the fatigue damage induced by a multimodal spectrum in terms of the damages of each of its components taken independently. The proposed formulas called Iterative Component Addition (ICA) were shown to meet the main expectations of engineering design, *e.g.* simple fatigue damage calculation with low computation time and reasonable conservatism [14]. Moreover, those formulas can be iteratively applied when more than two components need to be combined, as is the case in practice.

In addition, two-slopes S-N curves are often required. The ICA formulas may accept a two slope S-N curve with some increase in computational complexity. Still, we have been able to develop additional formulas, see Appendix A, that allow to approximate quite satisfactorily the damage corresponding to a two slope S-N curve from the damages corresponding to each of the slopes.

The issue here is to validate the use of ICA formulas on a realistic fatigue design application.

Since the formulas work by combining structural response spectra corresponding to the wave systems spectra present in the sea state, one has to assume a linear relation between the wave components and their respective load effects to ensure that any combination of wave systems in a given sea state induces an equivalent combination on the response spectra. It may be noted at this point that some sorts of non-linearities could still be taken into account, namely those that affect in a simple way (for instance, by an amplification factor depending only on the significant wave heights of the combined wave systems) the response spectral components, but that this was not attempted in the present study.

Thus, the scope of the study is limited to structural responses represented by a linear dynamic system (*i.e.* with RAOs). The retained industrial application is based on an actual FPSO design at a West Africa location. Wave loads are computed from the set of metocean data provided by the operator. The structural response considered is the Vertical Wave Bending Moment (**VWBM**) at the midship of an FPSO hull girder and is assumed to be linear, and thus fully defined by the Response Operator Amplitudes (RAO) that were provided by Bureau Veritas. The fatigue design requirements are based on the Bureau Veritas guidelines [2] and a fatigue design life of 100 years is considered.

To validate the use of ICA formulas, the fatigue damage on the actual structure is evaluated according to two lines of approach. The first one is based on the metocean database and serves as a reference solution, while the second one uses the ICA formulas in connection with a global climate description such as the metocean specifications provided by the operator. Between the two approaches, some intermediate computations are carried out especially to estimate the effects of various approximations such as the discretization made for the statistical analysis, and the conservatism level of ICA formulas on the actual sea states. Additionally, one has to estimate the occurrence probabilities of all the operational sea states to compute the fatigue damage from the metocean specifications. A probabilistic model is also defined

and discussed for this purpose, and further developments are suggested.

The present report is organised as follows: the second section describes the scope of the study, the different approaches are introduced and their respective issues discussed; the third section presents the industrial application dealt with; the fourth section shows a complete statistical analysis of the metocean data so as to provide occurrence probabilities of the fatigue wave loading cases from the metocean specifications; the fifth section is dedicated to the fatigue damage assessment according to various approaches; the sixth section summarizes the procedure that is eventually proposed to deal with the computational performance issues; a last section discusses the obtained results and concludes the study.

2 Scope of the study

The purpose of the global study is to validate a methodology for robust and cost-effective evaluation of fatigue damage for the design of marine structures, in the case of multiple loading systems (for instance, wind sea, several swells and even responses at natural frequencies). It is as such a development of some questions raised in the “Joint Probabilities & Response Based Design” project [10].

In the previous stages of the study, we compared the performance of combination methods making use of the standard deviation, zero-crossing frequency, spectral bandwidth and induced rainflow damage of each component taken in isolation. The present phase deals with a practical application case, in order to identify and solve the operational problems that a designer is faced with to apply specifications describing the wave climate on the location of interest in terms of wave systems rather than sea states.

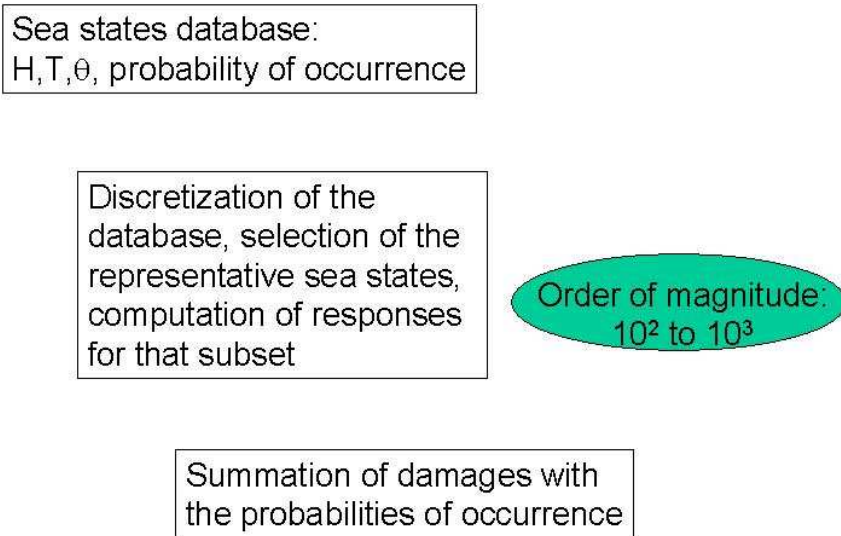


Figure 1: The standard method for design fatigue computation.

When environment is described by sea states and their occurrence probabilities, fatigue damage estimation for the foreseen life of the structure can be performed as described in Figure 1, where the complex computations of response and stresses in the structural details need only to be carried out for a reduced number of sea states, usually less than a thousand.

Unfortunately, those sea states descriptions are not sufficiently refined for regions where they are made of several well-distinct wave systems where sea states with the same global H_S , T_p and θ_m may have dramatically diverse effects on the structural response and thus fatigue.

An effort has been undertaken in the recent years to describe such sea states, frequent in the West Africa areas for instance, as combinations of several wave systems. Software packages such as SPOP [8] have been developed to extract the wave systems information from the hindcast or measured wave spectra, and thus allow modeling and reconstruction of multimodal spectral shapes. It allows accurate description of the structural responses as the combinations (often simply the sums under linear assumption) of the responses, taken and computed individually, to the identified systems of the sea state.

However, the diversity of the sea states and of the responses increases in proportion to the accuracy of their representations. Fatigue computations need to take into account each of the possible loading and response cases that the structure is likely to experience over its planned lifespan, and those computations are resource-demanding because of the complexity of the structures and of the rainflow cycle-counting method that is consensually accepted as the reference one. Thus, when the wave climate is described as statistics of wave systems, one could apply the conventional method to the sea state database consisting of all possible combinations of wave systems, but one would then be faced with untractable computational resources demand. For instance, assuming at most three types of simultaneous wave systems are to be considered (main swell, secondary swell, wind sea), the number of possible combinations is then typically the cube of the number of discretization classes for a given wave system. This discretization is comparable to that of the sea states in the conventional procedure, and thus the order of magnitude of the number of complex computations is raised to between millions and a billion, which is somewhat unpractical (Fig.2).

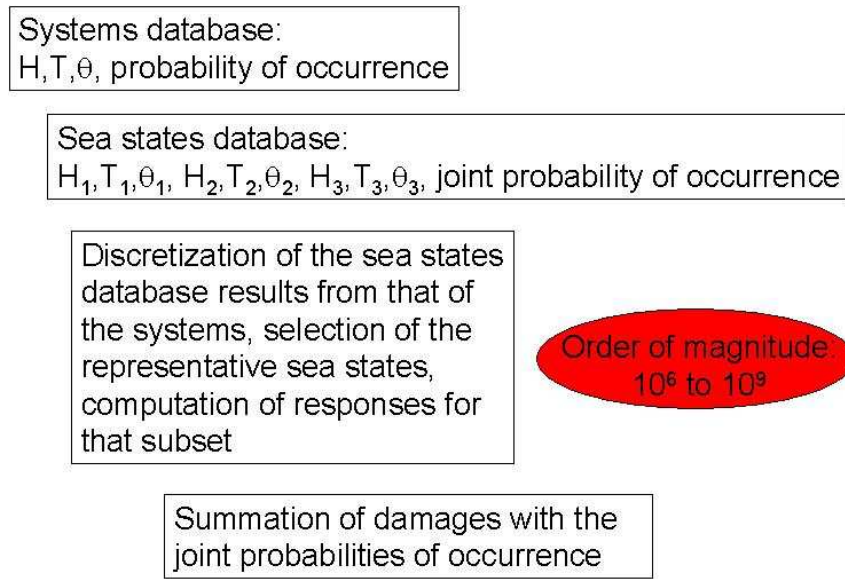


Figure 2: The reference method for wave systems climate description.

In the earlier stages of this study, we introduced the ICA method that we believe has a larger domain of validity than the previously existing ones, with the aim to postpone the combination stage to the “individual wave system’s” damages, keeping thus the number of complex computations to figures comparable with those in the original method, as shown by figure 3. It should however be noted that joint probabilities still need to be accurately estimated for all possible combinations.

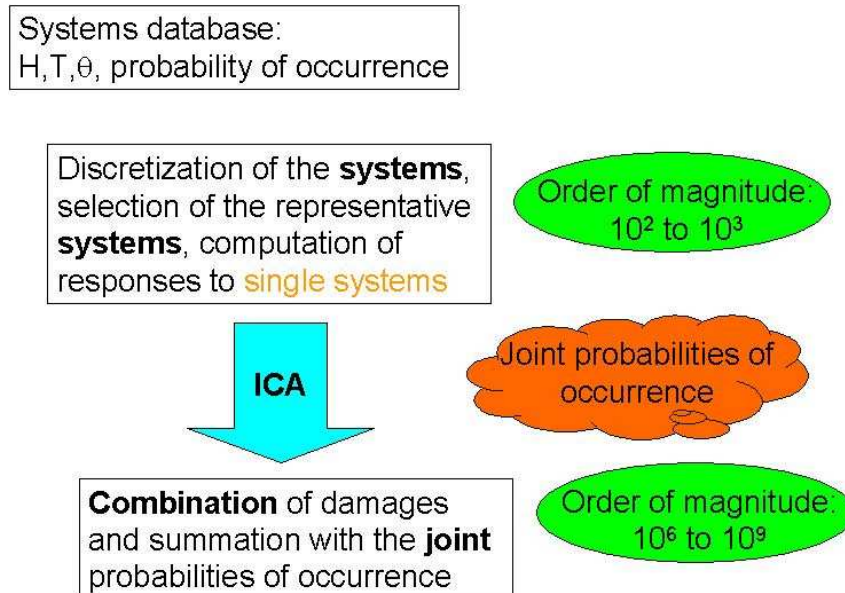


Figure 3: Reduction of computation time by use of the ICA method.

The ICA method was tested in academic cases in those previous stages of the study. In the present stage, we apply it an actual case (though with a simplified response model defined by RAOs rather than fully non-linear) to further validate that procedure. The first validation uses a reference fatigue computation carried out on the actual measured sea states, and a calculation by combination of the individual systems damages (see Fig. 4).

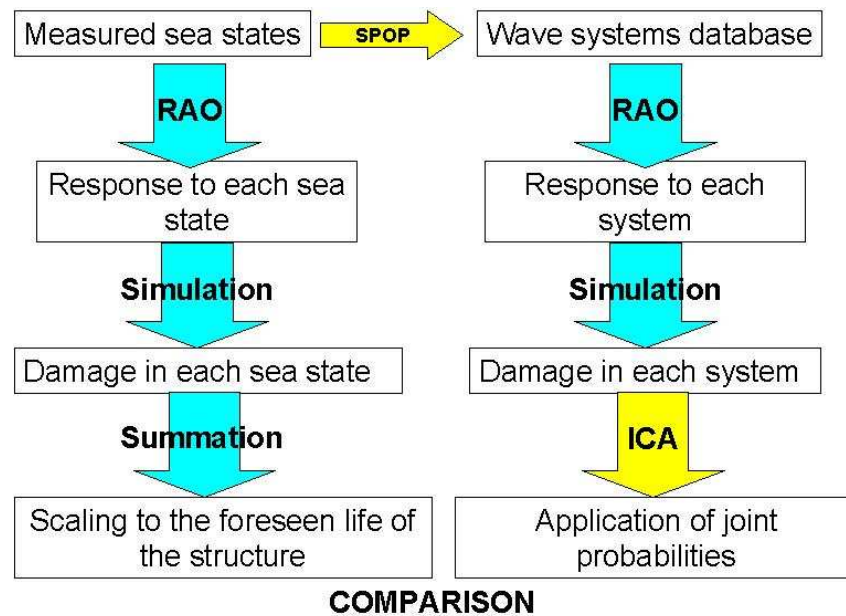


Figure 4: Practical validation of the ICA method.

The main difficulties encountered at this stage came from the construction of the joint probabilities to be used to weight the systems combinations. Most of the observed differences in the comparison could be tracked to the discretization used for the parameters of the systems, to the application of the exclusion criteria between systems defined in the metocean specifications, and to the assumptions of independence between those systems. Apart from those database description specific problems, satisfactory validation was obtained for the ICA method itself as detailed in the following.

Other difficulties came from the double slope S-N curve formulas, differing for ranges beyond and within a threshold, that are recommended by classification societies, and that are not well suited to combination. The main problem is that there may well be no actual cycle range beyond the threshold in each of the components to be combined, but some may appear in the combination, and thus the information on the damage created by those cycles cannot be obtained directly from the damages of the components. The development of a workaround had to be carried out.

In addition, the use of simulations to derive the rainflow damage of the original components was still a time-consuming step.

The next step is described in Figure 5. It consists in identifying modes on the response spectra rather than systems in the loading waves ones. Simulations are thus avoided, and the ICA method is used with "purer" peaks than for the responses to individual wave systems.

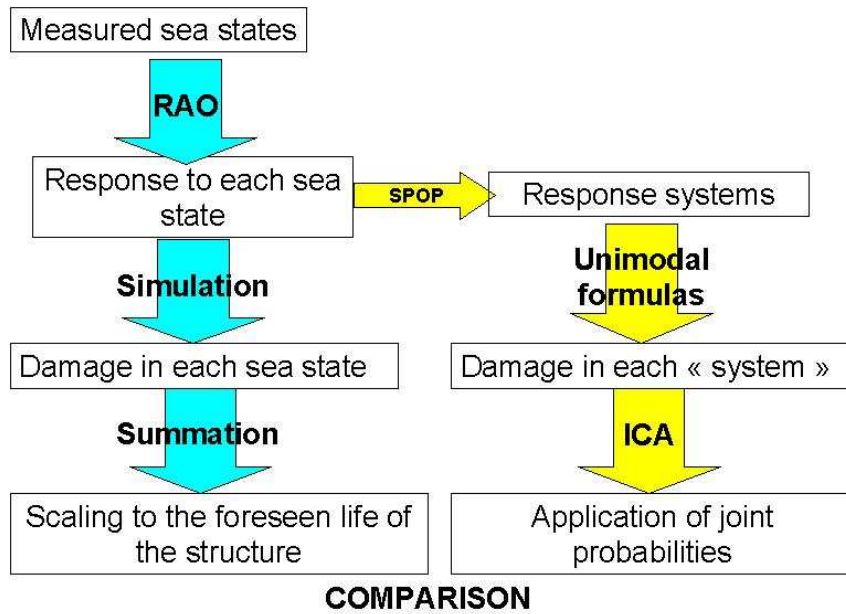


Figure 5: Faster use of the ICA method.

A final goal is to be able to construct a "response systems database", as shown on Figure 6, directly from the observed wave systems and the structure's RAOs.

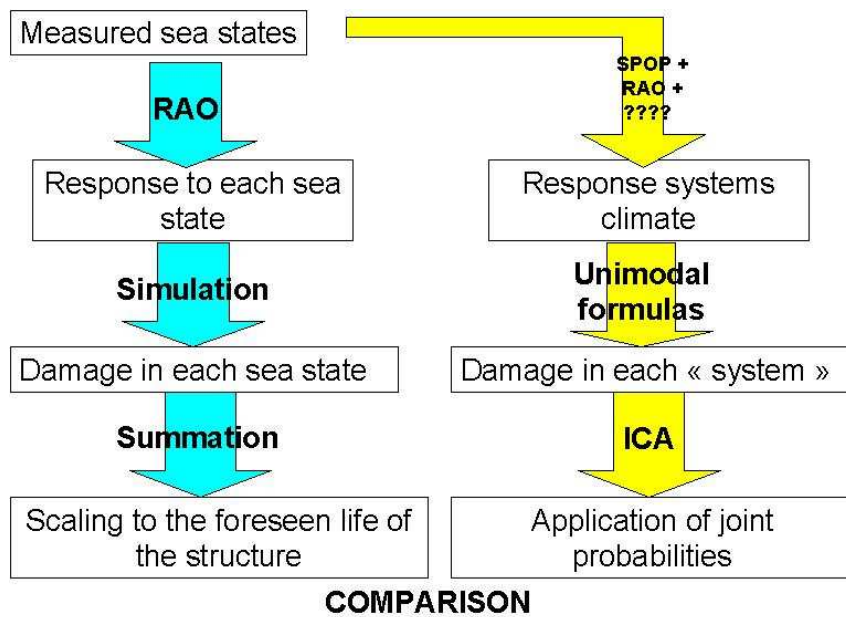


Figure 6: Further improvement in the use of the ICA method.

The various approaches used to compute the fatigue damage in the actual study are listed in table 1 with their respective issues.

Finally, note that, in connection but separate from this study, some work has been carried out on the application of the ICA formulas to assess the damage due to load spectra the main bodies of which are considered isolately from their tail yielding such a spectrum with two components or pseudo-modes. That specific study is described in appendix F.

Fatigue damage assessment from actual metocean database

	Description	Issue
1	<i>Time-domain simulation based damage assessment</i> - from the metocean database - from the partition of the response spectra database	Reference solution Effect of the partition
2	<i>ICA-based damage assessment</i> - from the sea states in the metocean database - from statistical analysis on the metocean data	Conservatism level of ICA Effect of discretization and ICA

Fatigue damage assessment from metocean climate prediction

	Description	Issue
3	ICA with the damages of the <i>wave systems components</i> applied on climate prediction under assumptions (H1) ^a and (H2) ^b	Validation of ICA
4	ICA with the damages of the <i>response systems components</i> applied on climate prediction under assumptions (H1) ^a and (H2) ^b	Validation of fully analytical damage assessment based on ICA

^a **(H1)** : overall independence of wave systems components

^b **(H2)** : independence of wave systems components within a given combination type

Table 1: Approaches for fatigue damage assessment and their respective issues.

3 Description of the industrial application

The retained industrial application is based on an actual FPSO hull girder design at a West Africa location. The wave loads are computed from the set of metocean data provided by the operator. The structural response considered is the Vertical Wave Bending Moment (**VWBM**) at the midship of the FPSO hull girder and is assumed to be linear, and thus fully defined by the Response Operator Amplitudes (RAO) that were provided by Bureau Veritas. The fatigue design requirements are based on the Bureau Veritas guidelines [2]. For the sake of simplicity, a fatigue design life of 100 years is considered in this application.

3.1 Wave loading

For West Africa location, new methods have been set up to describe the metocean climate with more accuracy [8]. In this actual study, the metocean climate data consists of 17672 records of the individual wave systems directional spectral parameters. Those data are sorted by recording dates. Systems having the same date belong to one single sea state. There are at most three wave system components in any sea state, identified as either main swell, secondary swell or wind sea.

It is assumed that any wave system is completely described by the directional wave spectrum:

$$S_w(\omega, \theta) = S(\omega) \cdot D(\theta)$$

where $S(\omega)$ is the wave energy spectrum and $D(\theta)$ is the direction distribution. The suggested model for $S(\omega)$ is a Wallops spectrum:

$$S(\omega) = \frac{\left(\frac{4l+1}{4}\omega_p^4\right)}{\Gamma(l)} \frac{H_S}{\omega^{4l+1}} \exp\left[-\frac{4l+1}{4}\left(\frac{\omega}{\omega_p}\right)^{-4}\right]$$

where H_S and ω_p are respectively the significant height and the peak frequency. The parameter l of the Wallops spectrum model is given in term of ω_p by a polynomial approximation [15]:

$$l(\omega_p) = 0.00205 \cdot \left(\frac{2\pi}{\omega_p}\right)^3 - 0.00290 \cdot \left(\frac{2\pi}{\omega_p}\right)^2 + 0.12665 \cdot \left(\frac{2\pi}{\omega_p}\right) + 0.22932$$

Note that in that approximation, $l(\omega_p)$ can be sometimes lower than one, which makes no sense in practice as the fourth spectral moment is then infinite. In that case, we decided to set the value of $l(\omega_p)$ to one (Pierson-Moskovitz spectrum). A typical shape of the Wallops spectrum is shown in Figure 7.

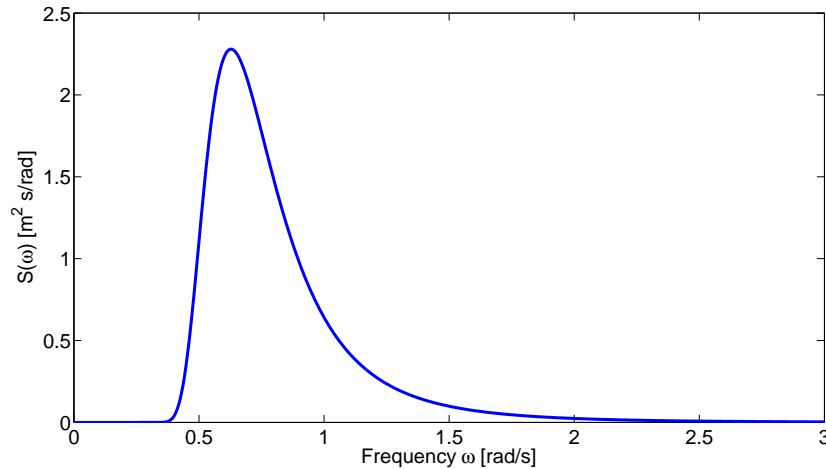


Figure 7: Wallops spectrum model

The suggested model for the direction distribution is a Wrapped-Normal function, the equation of which is:

$$D(\omega) = \frac{1}{\sqrt{2\pi}\sigma_{sw}} \sum_{k=-5}^{k=5} \exp \left[-\frac{1}{2} \left(\frac{\theta - \bar{\theta} - 2k\pi}{\sigma_{sw}} \right)^2 \right]$$

$\bar{\theta}$, the mean wave direction is set to θ_p the peak direction. σ_{sw} is the standard deviation and gives a measure of the spreading. However, in the actual study, the directional spreading is neglected, and the wave spectrum is supposed to be unidirectional in its peak direction (*i.e.* $S_w(\omega) = S(\omega) \cdot \delta_{\theta_p}$). This approximation does not affect the relevance of the analysis results for the issues considered here.

3.2 Mechanical modelling

The present study focuses on the fatigue at a detail in a FPSO deck around midship due to the *Vertical Wave Bending Moment*. The nominal stress σ_n at deck is obtained by: $\sigma_n = M_B/S_M$, where M_B is the vertical wave bending moment and S_M is the section modulus at deck and is set to the value 110m^3 according to Bureau Veritas requirements [2].

The corresponding Response Amplitude Operator (RAO), provided by Bureau Veritas, is a function of both incidence direction and frequency. It is given for 25 incidence angles from 0 to 360 and 53 frequencies from 0 to 2 rad/s. Then, that RAO is linearly interpolated to agree with the actual wave loading direction and frequency sampling (Figure 8). From the linearity assumption, the power spectral density of the VWBM is given by:

$$S_{BM}(\omega) = \int_{\theta} |RAO(\omega, \theta)|^2 \cdot S_w(\omega, \theta) d\theta, \text{ in fact, } S_{BM}(\omega) = |RAO(\omega, \theta_p)|^2 \cdot S_w(\omega) \quad (1)$$

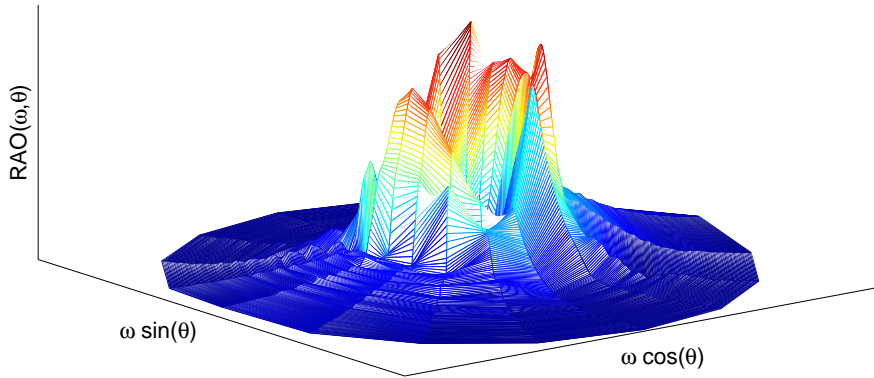


Figure 8: Directional RAO

Note that, in the actual study, the direction convention for the RAO does not meet that of the wave. The RAO is defined with incidence direction "from", counterclockwise by reference to the back centerline of the ship, while the wave direction convention is stated as: "from", clockwise by reference to the geographic north. To convert the wave incidence angle according to the RAO incidence convention, the following relation is used:

$$\theta_r = 360^\circ - \theta_w + 22.5^\circ \quad (2)$$

denoting θ_r , the RAO incidence, and θ_w the wave incidence direction. The wave incidence angles convention and the FPSO position is shown on Figure 9.

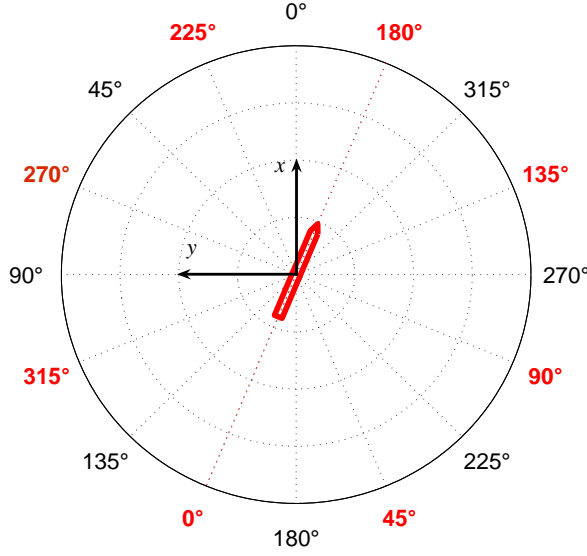


Figure 9: Vessel coordinate system and RAO incidence angles convention

3.3 Fatigue design requirements

A two slopes S-N curve is used for fatigue assessment. It has the following general expression:

$$N = \begin{cases} K_1 \Delta\sigma^{-m_1} & \text{if } N \leq 10^7 \text{ (i.e. } \Delta\sigma \geq S_c) \\ K_2 \Delta\sigma^{-m_2} & \text{if } N > 10^7 \text{ (i.e. } \Delta\sigma < S_c) \end{cases}$$

where $\Delta\sigma$ is the rainflow cycle range and N the number of cycles. K_1 , K_2 , m_1 , m_2 and S_c are characteristics parameters. The values used for the S-N curve parameters are shown in table 2. They correspond to basic DEn B S-N curves from Bureau Veritas guideline [2].

K_1	m_1	K_2	m_2	S_c	SCF
5.80210^{12}	3	4.03610^{16}	5	83.40 MPa	4.0

Table 2: DEn B S-N curve [2]

Note that the stress concentration factor SCF is not realistic, it is intentionally exaggerated to make the life of the structure close to the design lifetime.

4 Metocean climate prediction

The long-term fatigue damage assessment requires the knowledge of all the possible fatigue loading cases that are likely to occur over the design lifetime. However, the available metocean data cover a much shorter period of only almost three years. Therefore, a metocean climate on the design lifetime needs to be predicted. In the actual study, that prediction uses the statistical properties of the wave systems derived from the metocean data in connection with some convenient hypotheses on the way those wave systems combine with each other.

4.1 Preliminary processing of the metocean data: Partition & Assemblage

Those metocean data correspond to 8040 sea states, which represents, assuming that a stationary sea state lasts for 3 hours, a period of *2 years 9 months and 15 days*. Before making any statistical analysis on the data, two operations are carried out:

- a *partition* (classification) of the sea states,
- and an *assemblage* (merging), in any sea state, of those components which are sufficiently close.

4.1.1 Partition

The sea states are partitioned into, at most, three wave systems, identified either as main swell, secondary swell or wind sea. That partition is based on the following rules:

- To distinguish wind sea from swells, a threshold of 7.5s is normally set for the peak periods. However, when the components are either all above or all below the threshold, the wind sea component is always the one with the lowest peak period.
- When there are two simultaneous swells, the secondary swell is the one with the highest geographic angle. If the two geographic angles are equal, the secondary swell is the one with the lowest significant wave height.

The partition of the sea states is achieved with a program provided by the operator.

4.1.2 Assemblage

It is specified that 2 components i and j of a given sea state such that:

$$\frac{1}{1.2} < \frac{T_{p,i}}{T_{p,j}} < 1.2 \text{ and } |\theta_{p,i} - \theta_{p,j}| < 45^\circ \quad (3)$$

must be assembled. The new component has new parameters H_S , T_p and θ , which have to be computed.

From the relations: $\lambda_0 = \lambda_{0,i} + \lambda_{0,j}$ and $H_S = 4\sqrt{\lambda_0}$, we get:

$$H_S = \sqrt{H_{S,i}^2 + H_{S,j}^2} \quad (4)$$

To compute T_p , it is assumed that it is in a constant ratio to T_z :

$$T_p \approx T_z = \sqrt{\frac{\lambda_0}{\lambda_2}} = \sqrt{\frac{\lambda_{0,i} + \lambda_{0,j}}{\lambda_{2,i} + \lambda_{2,j}}} \quad (5)$$

Reporting in the previous equation (E.q.(5)) the expression of $T_{p,i}$ and $T_{p,j}$ in terms of their respective spectral moments, we get:

$$T_p = \frac{H_S \cdot T_{p,i} \cdot T_{p,j}}{\sqrt{H_{S,i}^2 \cdot T_{p,j}^2 + H_{S,j}^2 \cdot T_{p,i}^2}} \quad (6)$$

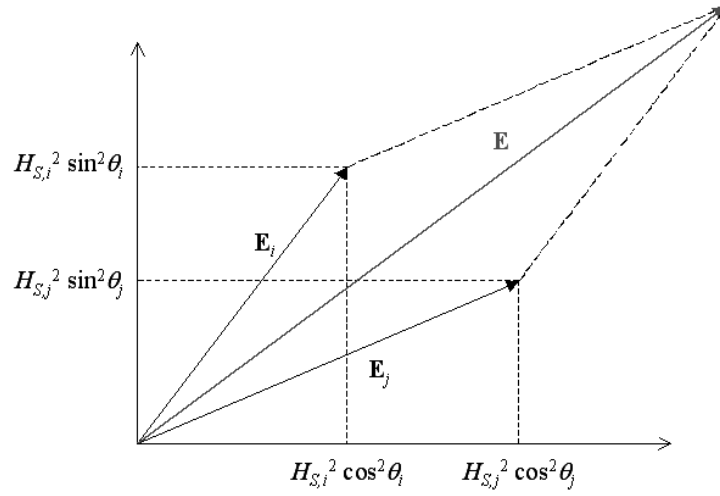


Figure 10: Direction of the assembled system.

To estimate the direction of the assembled systems, components are represented by energy vectors, $\mathbf{E}_i = H_{S,i}^2 [\cos^2 \theta_i \sin^2 \theta_i]^t$ and $\mathbf{E}_j = H_{S,j}^2 [\cos^2 \theta_j \sin^2 \theta_j]^t$ (Figure 10). Then, the direction of the assembled systems is such that of the sum vector $\mathbf{E} = \mathbf{E}_i + \mathbf{E}_j$. Referring the coordinates with respect to vector \mathbf{E}_i , we can write:

$$\tan^2 \theta = \frac{H_{S,j}^2 \sin^2 (\theta_j - \theta_i)}{H_{S,i}^2 + H_{S,j}^2 \cos^2 (\theta_j - \theta_i)} \quad (7)$$

$$\theta = \arctan \left[\frac{H_{S,j} \sin (\theta_j - \theta_i)}{\sqrt{H_{S,i}^2 + H_{S,j}^2 \cos^2 (\theta_j - \theta_i)}} \right] + \theta_i \quad (8)$$

4.1.3 Results of the metocean data partition & assemblage

The proportions of the main swell, secondary swell and wind sea in all the sea states are shown in table 3, and the proportions of their combinations that occur in the set of actual sea states are given in table 4.

	after partition		after assemblage	
	Number	Frequency [%]	Number	Frequency [%]
main swell	8038	99.97	8037	99.96
secondary swell	5464	67.96	5289	65.78
wind sea	4169	51.85	4088	50.85

Table 3: Proportions of the components.

	after partition		after assemblage	
	Number	Frequency [%]	Number	Frequency [%]
MS only	1158	14.40	1212	15.07
MS + SS	2713	33.74	2740	34.08
MS + WS	1416	17.61	1536	19.10
MS + SS+ WS	2751	34.22	2549	31.70
no MS (i.e. WS only)	2	0.03	3	0.05
Total	8040	100	8040	100

Table 4: Proportions of the combinations.

The results show that a main swell component is almost always present in the sea states, as well after partition as after assemblage. There is no major change in the distribution of the combination types after the assemblage except the fact that the number of sea states with three components has been reduced while it has increased in the other categories. Finally, one can consider that only four significant types of combinations occur in the metocean data:

- only main swell (15%);
- main and secondary swell without wind sea (34%);
- main swell and wind sea without secondary swell (19%);
- all three components are present (32%).

4.2 Statistical analysis of the metocean data

To perform a statistical analysis of the metocean data, the environmental parameters (*e.g.* H_S , T_p , θ) must be discretized. As one will see in the sequel, that discretization will have a significant effect on the damage assessment. From that discretization, the statistical analysis provides :

- some statistical properties of the environmental parameters of the sea states in the metocean database ;
- the joint distribution of the environmental parameters for any given wave system.

The joint distribution of the wave system parameters is necessary to compute the occurrence probabilities of the combinations of wave systems components that are predicted by the metocean climate.

4.2.1 Discretization

Since unrealistic combinations are excluded, one has to pay attention, in the choice of the bins locations, that the exclusion of a given combination based on the values of the bins is equivalent to the exclusion of a combination of any elements of the corresponding discretization intervals. This equivalence is particularly difficult to achieve with the peak period parameter T_p for which the exclusion criteria is expressed in terms of a ratio (see Eq. (3)). For example, let us consider a discretization of T_p with an interval length of 1s. A combination containing at least two components, which peak periods are 11s and 10s, meet the assemblage criterion ($11/10 = 1.1 < 1.2$). However, a combination of two components, which peak periods are 11.4s and 9.4s, do not meet the assemblage criterion ($11.4/9.4 = 1.21 > 1.2$), although those peak periods belong to the previous discretization intervals. To avoid a discrepancy between the exclusion of class intervals combinations and that of their respective elements, we chose to discretise $\log T_p$ instead of T_p . The histogram bins are given in table 5.

Parameter	Bins interval	Disc. path length	Number
H_S	[0.25m ; 3.25m]	0.5m	7
$\log(T_p)$	[$\log 3$; $\log 22.5$]	$\log(1.2)/2$	23
θ	[0° ; 348.75°]	22.5°	16

Table 5: Histogram bins of the environmental parameters

4.2.2 Statistical properties of sea states from the metocean database

For the various combination categories, some statistical properties of the global environmental parameters are computed from the metocean database (Table 6). Those global parameters are obtained from the assemblage equations (4), (6) and (8) for a sea state, which is a combination of wave systems. For a parameter X (*e.g.* H_S , T_p , θ), the following statistical characteristics are computed :

- \bar{X} the mean value, σ_X the standard deviation, χ_X the skewness and κ_X the kurtosis ;
- $X_{1/3}$ (resp. $X_{1/10}$) the mean of the values of the parameter X for the third (resp. the tenth) of the sea states with the larger H_S .

	MS only	MS+SS	MS+WS	MS+SS+WS
$\overline{H_S}$ [m]	1.59	1.40	1.25	1.22
σ_{H_S} [m]	0.48	0.40	0.32	0.32
χ_{H_S} [m ³]	0.95	1.01	1.16	1.19
κ_{H_S} [m ⁴]	3.65	4.35	5.81	5.15
$H_{S,1/3}$ [m]	2.14	1.85	1.60	1.58
$H_{S,1/10}$ [m]	2.63	2.23	1.90	1.91
$\overline{T_p}$ [s]	12.23	11.21	9.06	9.36
σ_{T_p} [s]	2.00	1.51	1.63	1.82
χ_{T_p} [s ³]	0.15	0.45	0.23	0.14
κ_{T_p} [s ⁴]	2.39	3.03	2.71	2.61
$T_{p,1/3}$ [s]	14.48	12.90	10.90	11.38
$T_{p,1/10}$ [s]	15.73	14.15	12.06	12.62
θ	208.26	202.08	210.50	206.09
σ_θ	8.84	7.05	10.47	8.91
χ_θ	0.38	0.24	1.16	0.55
κ_θ	2.79	4.05	8.89	3.32
$\theta_{1/3}$	218.10	209.66	222.00	216.20
$\theta_{1/10}$	225.23	215.39	229.71	223.30

Table 6: Statistical properties of environmental parameters from the metocean database.

The Table 6 shows that the average of the significant wave height is largest for sea states with only a main swell, followed by those with both swells, which means H_S is larger than that of a main swell + a wind sea. The combination of the three wave systems has the lowest mean H_S . Note also that both combinations "MS+WS" and "MS+SS+WS" have close statistical properties for the parameters H_S and T_p . The results show also that $\overline{\theta}$, $\theta_{1/3}$ and $\theta_{1/10}$ are in the southwest sector, which means that the sea states with the larger H_S come from this sector.

In addition, the occurrence frequencies of the sea states can be derived by a basic empirical statistical analysis on the metocean data. First all the values of the environmental parameters that appear in the database are discretized by replacement with the value of the closest bin. Then one has to count the number of times a sea state is repeated in the database. Finally, the occurrence frequency of any sea state is the number of times it is repeated divided by the size of the database.

312 triplets of environmental parameters (H_S, T_p, θ) defining each observed wave system component, appear in the sea state data (*i.e.* any sea state is the combination of at most three elements of this set of 312 triplets). Counting the number of repeated sea states, it is found that $N_c = 3877$ different combinations do actually occur. Their respective frequencies of occurrence are computed (Figure 11).

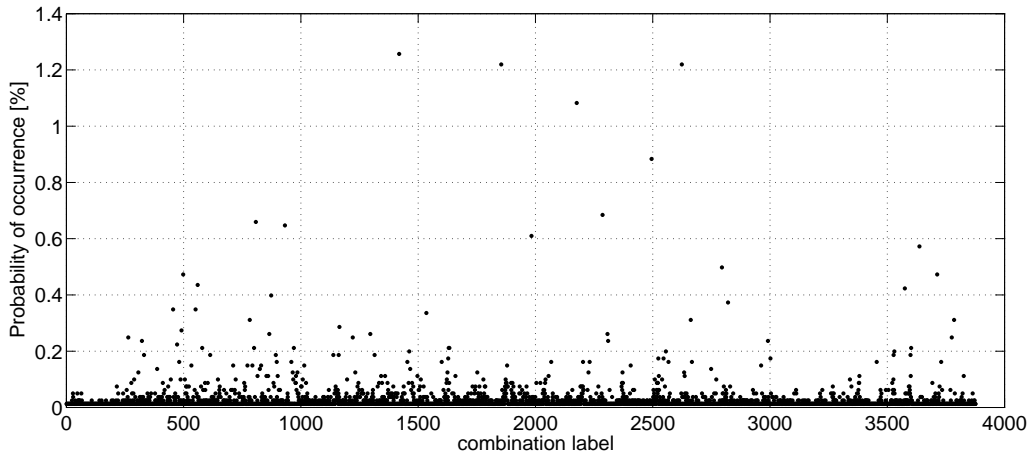


Figure 11: Probability of occurrence of any observed combination.

4.2.3 Joint distribution of (H_S, T_p, θ) for a given wave system

The joint distribution of the environmental parameters is estimated according to the following formula:

$$f(H_S, T_p, \theta) = f_{H_S, T_p}(H_S, T_p | \theta) \cdot f_\theta(\theta) \quad (9)$$

where $f_{H_S, T_p}(H_S, T_p | \theta)$ is the conditional joint probability density function of H_S and T_p given the direction θ , and $f_\theta(\theta)$ is the probability density function of the direction. Those distributions are estimated empirically with the discretization of the intervals of the observed values of the environmental parameters (see table 5). Hence, $f_\theta(\theta)$ is approximated by an histogram of θ , while $f_{H_S, T_p}(H_S, T_p | \theta)$ is estimated as the directional scatter-diagrams of $H_S - T_p$. The probability density function involved in the expression of the joint distribution are given by:

$$f_\theta(\theta_c) = \frac{k_\theta}{n_\theta \cdot \Delta\theta}$$

$$f_{H_S, T_p}(H_{S,c}, T_{p,c} | \theta_c) = \frac{k_{H_S - T_p}}{n_{H_S - T_p}(\theta_c) \cdot \Delta H_S \cdot \Delta T_p}$$

where $k_{H_S - T_p}$ is the directional scatter-diagram given the direction θ and k_θ is the direction histogram; n_θ is the size of the set of the actual wave system in the database and $n_{H_S - T_p}(\theta_c)$ is the number of elements in that set with the direction θ_c . The joint distribution of spectral parameter for the three types of wave systems (*e.g.* main swell, secondary swell and wind sea) are depicted in appendix E.

4.3 Metocean climate prediction

The prediction of the metocean climate uses the available metocean data in connection with some assumptions on the way the wave systems components combine with each other.

4.3.1 Hypotheses

Two distinct assumptions are considered:

- (H1) \equiv *independence assumption of the wave systems components whatever the type of combination is:*
It is assumed that all the wave system components can combine with any other wave system components.
- (H2) \equiv *independence assumption of the wave systems components observed in a given combination kind:*
In this case the independence assumption applies only for the observed wave systems components belonging to the type of combination under consideration, with different probabilities for each type of combination.

One imposes that sea states and their respective occurrence probabilities, that are a result of each assumption must meet some characteristics of the metocean database. Thus,

- both metocean climate predictions must show the combination categories in the same proportions as those observed in the metocean database (Table 4).
- the wave systems combinations that do not meet the partition and assemblage criteria must be excluded, since the preliminary processing performed on the metocean data has ruled out those kind of combinations.
- the metocean climate predications must not yield unrealistic wave systems components combinations. An unrealistic combination is one :
 - with a wind sea of higher peak period than that of one of the swells;
 - with two swells such that the secondary swell has the lowest geographic angle ;
 - with two swells having the same geographic angle but such that the secondary swell has the highest significant height ;

4.3.2 Method for the assessment of the combinations occurrence probabilities

The construction of the new probabilistic model is based on the following principle: the occurrence probabilities of all the possible combinations of wave system components are given by the ones derived from an independence assumption (*i.e.* estimated as the product of the respective frequencies of their wave systems components) truncated to the set of realistic combinations (*i.e.* removing combinations that meet the exclusion criteria).

The probability of occurrence of any kind of combination is set equal to its frequency of occurrence in the metocean data (see table 4). Now let us explain how to construct the probability of occurrence of any combination of wave systems components.

Main swell only: When a sea state is composed of only one main swell, any MS component may occur. The occurrence probabilities of any sea state of this kind read:

$$\Pr(MS = i | \text{MS only}) = f_{H,T,\theta}^{(MS)}(H_{S,i}, T_{p,i}, \theta_{w,i}) \cdot \Delta H_S \cdot \Delta T_p \cdot \Delta \theta$$

The conditional probability $\Pr(MS = i | \text{MS only})$ must be multiplied by the probability of occurrence of a sea state with main swell only.

Combination of two systems (*e.g.* MS+SS or MS+WS): Let us consider that we have to recombine sea states that contain one main swell and one secondary swell. The case of MS+WS is similar, simply replacing SS by WS.

Assuming that a sea state contains two swells, any combination of main swell and secondary swell components may occur, unless it is unrealistic. The occurrence probability of a combination that involves MS = i and SS = j is:

$$\Pr(MS = i, SS = j) = \Pr(SS = j | MS = i) \cdot \Pr(MS = i) \quad (10)$$

In fact, some MS component can not be combined with some SS component because of the exclusion criteria. The conditional probability $\Pr(SS = j | MS = i)$ is regarded as a truncature of the probability under independence assumption to the set of possible combinations. Thus, given a MS component i , the probability that any SS component j is combined with MS= i when it is possible, is given by:

$$\Pr(SS = j | MS = i) = \frac{\Pr(SS = j)}{\sum_{\substack{SS \text{ possible} \\ \text{with MS}=i}} \Pr(SS)}$$

Reporting the expressions of those probabilities in terms of the PDF, we have:

$$\Pr(SS = j, MS = i) = \frac{\Pr(MS = i) \cdot \Pr(SS = j)}{\sum_{SS \text{ possible}} \Pr(SS)} \quad (11)$$

where

$$\begin{aligned} \Pr(MS = i) &= f_{H,T,\theta}^{(MS)}(H_{S,i}, T_{p,i}, \theta_i) \cdot \Delta H_S \cdot \Delta T_p \cdot \Delta \theta \\ \Pr(SS = j) &= f_{H,T,\theta}^{(MS)}(H_{S,j}, T_{p,j}, \theta_j) \cdot \Delta H_S \cdot \Delta T_p \cdot \Delta \theta \end{aligned}$$

Note that the obtained probability must be multiplied by the occurrence probability of a sea state with two swells.

Main swell + Secondary swell + Wind sea: For this case, the same reasoning as for the combination of two wave systems is applied, considering that the combination MS+SS+WS is a combination of the wave systems (MS+SS) and WS. The probability of occurrence is obtained replacing in Eq.(11) "MS= i ", by "(MS= i ,SS= j)" and "SS= j " by "WS= k ".

4.3.3 Results & Discussion

The numbers of possible sea states predicted by both assumptions (H1) and (H2) are given in Table 7. That number is much larger under (H1).

cpnt. type	MS only	MS + SS	MS + WS	MS + SS + WS	Total
nb. cpnts. under (H1)	169	13899	24852	1862087	1901007
nb. cpnts. under (H2)	70	7590	8204	773821	789616

Table 7: Numbers of combinations from the metocean climate description.

The statistical properties which were computed from the metocean data (Table 6) are also evaluated from the metocean climate prediction under both assumptions (H1) and (H2) (see Table 8).

Under (H1), the sea states which are combination of the three wave systems take the largest values for $\overline{H_S}$, $H_{S,1/3}$ and $H_{S,1/10}$. The sea states with only a main swell take the smallest values of those characteristics. Between both extreme, the combination "MS+SS" take larger values for the same characteristics than the combination "MS+WS". It means the sea states with the larger H_S frequently occur in combination category "MS+SS+WS". Note also that the statistical characteristics for parameter H_S and T_p in combination categories "MS+WS" and "MS+SS+WS", which were those of the metocean data, are quite different under assumption (H1), especially for $H_{S,1/3}$, $H_{S,1/10}$, $T_{p,1/3}$ and $T_{p,1/10}$. Concerning the global directions, their averages are in the southwest sector as well as the directions of the sea states with larger H_S .

However, under (H2), one observes that the order of importance of the average significant heights is reversed compared to the previous assumption, which means that the sea states with only a main swell take more frequently the largest H_S values. Still, the discrepancy between $H_{S,1/3}$, $H_{S,1/10}$, $T_{p,1/3}$ and $T_{p,1/10}$ in combination categories "MS+WS" and "MS+SS+WS" is much smaller than under (H1), and the global directions averages and the directions of the sea states with larger H_S are also found in the southwest sector.

The observed discrepancies between the statistics from the metocean database and from the metocean description with (H1) is due to the fact that the assumption (H1) allows all the main swell components observed in the database to occur alone or combined with the other wave systems.

Under the assumption (H2), the mean values of H_S in the various combination types follow the same order as those from the metocean data. However, $\overline{H_S}$ is larger for "MS only" and "MS+WS", and lower for "MS+SS" and "MS+SS+WS".

Note that, for all the combination types and whatever the metocean description is, the sea states with the larger H_S have very close peak periods and directions.

From these results, the independance assumption is not satisfactory in version (H1) nor in version (H2), even if the version (H2) appears close to the observed metocean data. A more satisfactory metocean climate prediction could be based on statistics of events (systems coming from a single storm, and arriving to the site over a period of several hours to several days with a specific time-evolution pattern) rather than on the metocean data.

under assumption (H1)					under assumption (H2)				
	MS only	MS+SS	MS+WS	MS+SS+WS		MS only	MS+SS	MS+WS	MS+SS+WS
$\overline{H_S}$ [m]	0.99	1.27	1.20	1.43	$\overline{H_S}$ [m]	1.64	1.32	1.27	1.15
σ_{H_S} [m]	0.49	0.50	0.46	0.47	σ_{H_S} [m]	0.50	0.44	0.36	0.35
χ_{H_S} [m ³]	0.97	0.71	0.96	0.74	χ_{H_S} [m ³]	0.85	0.51	0.64	0.44
κ_{H_S} [m ⁴]	4.65	3.96	4.88	4.13	κ_{H_S} [m ⁴]	3.52	3.51	4.57	4.14
$H_{S,1/3}$ [m]	1.25	1.77	1.46	1.92	$H_{S,1/3}$ [m]	2.25	1.77	1.46	1.48
$H_{S,1/10}$ [m]	1.75	2.15	1.90	2.28	$H_{S,1/10}$ [m]	2.75	2.15	1.90	1.79
$\overline{T_p}$ [s]	11.08	11.72	8.69	9.45	$\overline{T_p}$ [s]	12.24	11.19	9.12	8.98
σ_{T_p} [s]	2.49	1.94	2.21	2.06	σ_{T_p} [s]	2.02	1.81	1.87	2.13
χ_{T_p} [s ³]	0.68	0.33	0.52	0.26	χ_{T_p} [s ³]	0.24	0.67	0.26	0.31
κ_{T_p} [s ⁴]	3.40	3.03	3.06	2.80	κ_{T_p} [s ⁴]	2.63	3.32	2.81	2.85
$T_{p,1/3}$ [s]	11.26	11.78	10.01	9.08	$T_{p,1/3}$ [s]	12.34	11.56	9.68	10.09
$T_{p,1/10}$ [s]	13.52	11.85	11.78	13.55	$T_{p,1/10}$ [s]	12.34	12.37	10.26	9.90
$\overline{\theta}$	205.80	205.96	205.76	205.92	$\overline{\theta}$	207.35	203.01	209.81	205.95
σ_θ	9.14	9.10	9.07	9.03	σ_θ	9.47	5.95	11.54	8.82
χ_θ	1.62	1.64	1.62	1.63	χ_θ	1.42	0.51	1.39	1.44
κ_θ	7.93	7.97	7.90	7.95	κ_θ	3.53	14.83	6.29	5.57
$\theta_{1/3}$	225	202.63	224.80	202.5	$\theta_{1/3}$	202.5	202.77	224.80	202.57
$\theta_{1/10}$	225	225	224.84	202.5	$\theta_{1/10}$	202.5	202.82	202.35	202.77

Table 8: Statistical properties of environmental parameters from the metocean climate prediction.

5 Fatigue damage assessment

The fatigue damage is now estimated according to the various approaches shown in table 1.

5.1 Damage assessment from metocean database

In this section,

- the fatigue damage from the metocean data is computed by a time-domain simulation method ;
- the conservatism level of ICA formulas and the effects of the discretization of environmental parameters are estimated over the metocean data.

At this stage, it is important to note that the ICA formulas (appendix A) assume that the components damages, from which combined damage is computed, are obtained with a single slope S-N curve. Therefore, ICA formulas can not be directly applied to a damage obtained from a two slopes S-N curve, as it is the case in the actual application. Thus, some work have been done to derive analytical formulas which allow to compute the double slope rainflow damage, in a slightly conservative manner, by combining the single slope damages. Those formulas, identified by (a), (b), (c) and (d), in the order of their respective conservatism level, are presented in appendix C.

5.1.1 Fatigue damage from metocean data

Method

The fatigue damage is computed from the 8040 sea states that are observed in the metocean database. Hence, it is implicitly assumed that all the sea states which can occur during the entire life of the structure belong to the metocean database and that their respective frequencies of occurrence are the same as those that they have in the database. Then, the fatigue damage over the design lifetime is estimated according to the following method based on time-domain simulations. First, the power spectral density of the response of each sea state from the database is computed with the actual RAO under the linear assumption using equations (1) & (2). Then, a number n_g of time series is generated for each of those response spectra. That number n_g is chosen such that the total number of time series generated covers exactly the design lifetime. Hence, for a design lifetime of 100 years, one chose $n_g = 36$, which gives a total number of time series equal to $N_t = 36 \cdot 8040 = 289440$. The damages due to those time series are computed by counting the cycles by the Rainflow method and by cumulating the elementary damages produced by each cycle according to Miner's rule [11]. Finally, the time series damages d_k are simply summed to get the total damage D_t .

$$D_t = \sum_{k=1}^{N_t} d_k$$

The result obtained is considered as the *reference solution*, since it is based on the metocean database and is provided by an acknowledged method for fatigue damage assessment.

Results & Discussion

The results of the analysis are given in tables 9 & 10. Table 9 provides, for the different categories of combinations which have been identified in the metocean database, the following fatigue damages and their ratios to the reference solution:

- D_t , the total fatigue damage ;
- $D_{H_{3,1/3}}$ (resp. $D_{H_{3,1/10}}$) the damage produced by the sea states with significant wave heights in the highest third (resp. the highest tenth) of the wave heights and their respective proportion in the total damage.

That table shows that the sea states with the third highest significant wave height produce around 90% of the damage in each category of combination. On the other hand, the sea states with the tenth

Sea sates	Freq. Occ.	D_t	$D_{H_s,1/3}$		$D_{H_s,1/10}$	
			Value	Ratio \cdot / D_t	Value	Ratio \cdot / D_t
MS ONLY	15.07%	0.2863	0.2557	89.31%	0.1492	52.11%
MS+SS	34.08%	0.2542	0.2314	91.04%	0.1618	63.66%
MS+WS	19.01%	0.0604	0.0567	93.89%	0.0438	72.55%
MS+SS+WS	31.70%	0.0748	0.0692	92.57%	0.0547	73.17%
ALL	100%	0.6757	0.6358	94.09%	0.4772	70.62%

Table 9: Fatigue damages from the metocean database - *Reference solution*.

highest significant wave height give 52% to 73% of the damage in each combination category and 70% of the total damage. Hence, a relatively small number of sea states causes a large amount of the total damage. One can also notice, that the damage due to the sea states with only a main swell (15% of the sea states) corresponds to 40% of the total damage, and the damage from the swells (*e.g.* MS only & MS+SS), which have 40% of occurrence frequency, produces 80% of the total damage. However, note that, that result depends on the particular response under consideration. In fact, that response is driven by swell. One could come to a different conclusion with another structural response, if it were driven by wind sea for instance.

5.1.2 Conservatism level of ICA formulas and Discretization effects

Method

At this stage, it is also interesting to estimate from that reference solution the conservatism level of the ICA formulas and the effect of the discretization of the environmental parameters. Concerning the conservatism level of the ICA formulas, one has to compute with the ICA formulas the expected damage due to sea states that are partitionned into several wave systems in terms of the damages of their respective wave systems components. Note that damage of a given wave system component is computed here by a time-domain simulation method averaging 100 runs. That number was chosen sufficiently large for an accurate estimation. After calculating the individual damages of all the wave systems identified in the metocean database, the damages of all the sea states with several wave systems are computed by ICA formulas. Then, the total damage on the design lifetime is obtained by scaling the fatigue damage over the database duration by the factor n_g .

To assess the effect of the discretization of environmental parameters, the total damage is computed using ICA formulas in connection with the sea states statistics derived from the metocean database (see section 4.2.2). Let us recall that the statistical analysis performed on the metocean database allowed to identify 312 wave systems components and $N_c = 3877$ combinations of those components. Thus, only the damages due to the 312 wave systems components are computed by the time-domain simulation method. From those damages, the damages of the 3877 combinations identified are estimated using the ICA formulas. To get the expected damage over the database duration, the damages of the combinations are weighted by their respective occurrence probabilities (Figure 11) and summed. As previously, the total damage on the design lifetime is obtained by scaling the fatigue damage over the database duration by the factor n_g .

Results & Discussion

The conservatism level of ICA formulas over the sea states of the database that contain more than one wave system is depicted on figure 12.

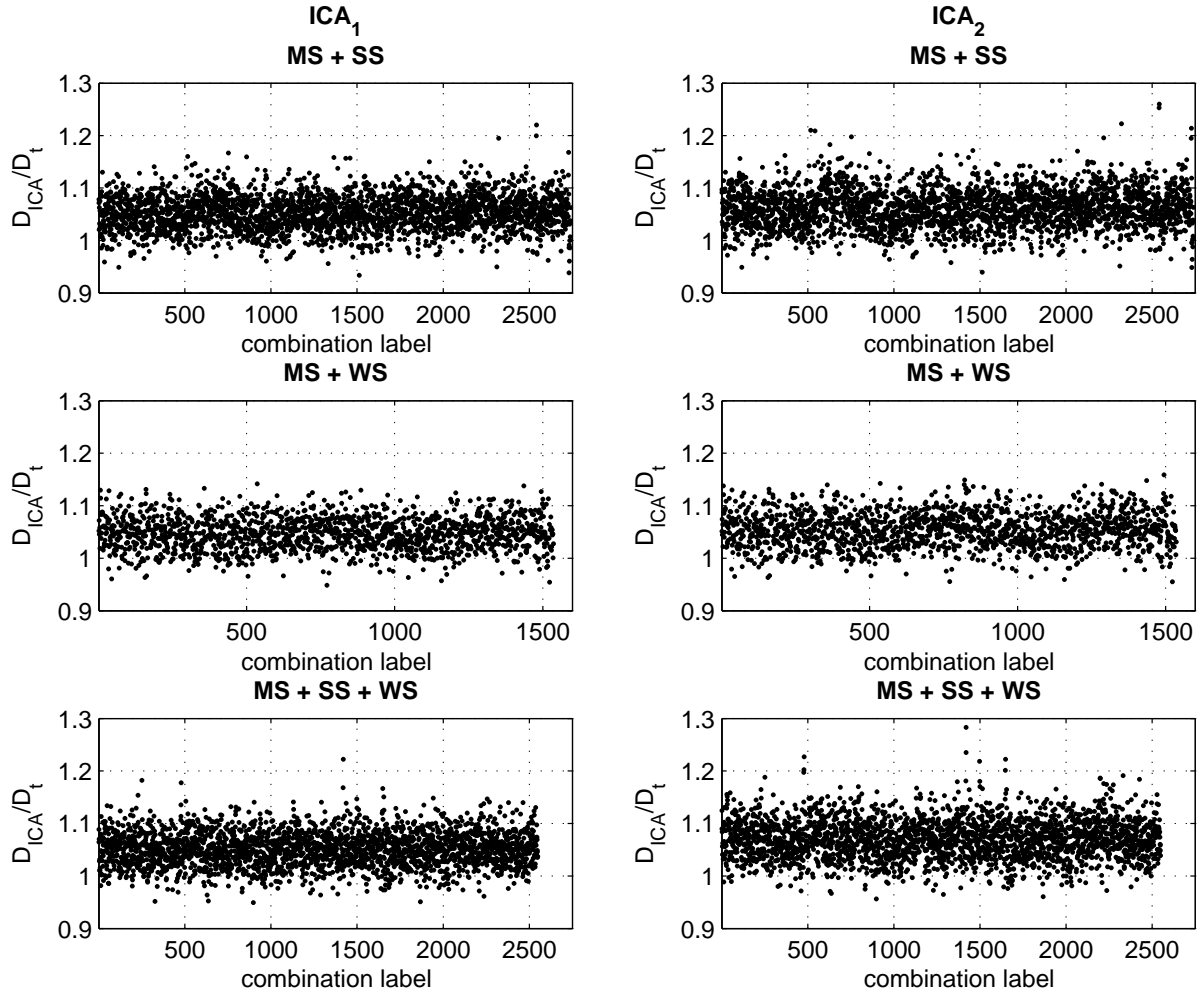


Figure 12: Conservatism level of the two ICA formulas on the sea states database.

Table 10 shows, for the different categories of combinations which have been identified in the metocean database, the following fatigue damages:

- D_t , the total fatigue damage from the reference solution ;
- D_{ICA_1} & D_{ICA_2} , the damages computed by the ICA formulas on the metocean database and their respective ratios to D_t ;
- $D_{ICA_1}^{disc}$ & $D_{ICA_2}^{disc}$, the damages computed by the ICA formulas in connection with the sea states discretised statistics and the respective ratios of those damages to D_t ;

Moreover, table 10 gives D_1 , the damage obtained when the sea states are not partitionned and D_{NB} the damage computed by a narrow band approximation on the response spectra.

The ICA formulas have a relatively small level of conservatism. One has around 2% to 4% conservatism level for the ICA formula in first approximation (*e.g.* ICA_1) in each combination category, while the conservatism level for the ICA formula in second approximation (*e.g.* ICA_2) varies from 2% to 5%. When those formulas are used in connection with the sea states statistics that involve a discretization of the environmental parameters, the conservatism increases up to a level between 10% and 14% for ICA_1 and between 10% and 15% for ICA_2 . Both previous results show that the choice of the discretization bins bring in a large proportion the conservatism of fatigue damage assessment using ICA formula in connection with the sea states statistics. In fact, the bins values were chosen in the middle of the discretization intervals. However, the scatter of the environmental parameters in the discretization intervals are not necessarily symmetric in terms of the middle of the interval. One can expect a reduction of the conservatism

Sea states	Freq. Occ.	D_t	D_{ICA_1}		D_{ICA_2}		$D_{ICA_1}^{disc}$		$D_{ICA_2}^{disc}$		D_1		D_{NB}	
			Value	Ratio \cdot/D_t	Value	Ratio \cdot/D_t	Value	Ratio \cdot/D_t	Value	Ratio \cdot/D_t	Value	Ratio \cdot/D_t	Value	Ratio \cdot/D_t
MS ONLY	15.07%	0.2863	0.2863	100%	0.2863	100%	0.3197	111.67%	0.3197	111.67%	0.2863	100%	0.2980	104.09%
MS+SS	34.08%	0.2542	0.2622	103.14%	0.2630	103.47%	0.2727	107.28%	0.2736	107.64%	0.2110	83.02%	0.2663	104.76%
MS+WS	19.01%	0.0604	0.0626	103.57%	0.0627	103.77%	0.0677	112.04%	0.0678	112.27%	0.0190	31.40%	0.0636	105.26%
MS+SS+WS	31.70%	0.0748	0.0775	103.60%	0.0784	104.79%	0.0849	113.48%	0.0859	114.89%	0.0449	59.97%	0.0790	105.66%
ALL	100%	0.6757	0.6885	101.9%	0.6904	102.17%	0.7450	110.25%	0.7471	110.56%	0.5607	84.46%	0.7069	104.62%

Table 10: Fatigue damages from the metocean database with the approximation methods.

Ref. Solution	ICA_1	ICA_2	ICA_1^{disc}	ICA_2^{disc}	T_1	NB
148	145	145	134	134	178	141

Table 11: Fatigue lifetime from the metocean database with the approximation methods [in years].

level if instead of the middle of discretization intervals, the bins were chosen as the median value of the parameters in those discretization intervals. Nevertheless, one should pay attention in any choice of the bins so that they agree with the exclusion criteria.

Unlike what could be expected, the damage is lower when the sea state are not partitionned. In fact, the RAO depends on the enviromental parameters, therefore, the response spectrum from the environmental parameters of a sea state with several wave systems components can be significantly different from the sum of the response spectra from the environmental parameters of its individual components taken separately. In the actual application, the response spectra from the global environmental parameters appear to be less damaging.

Finally, note that the narrow band approximation of the damage is conservative to a level around 5% which is quite small. This shows that the response spectra have a small frequency bandwidth. The conservatism level when no partition is made on the sea states as well as that of the narrow-band approximation are displayed on figure 13.

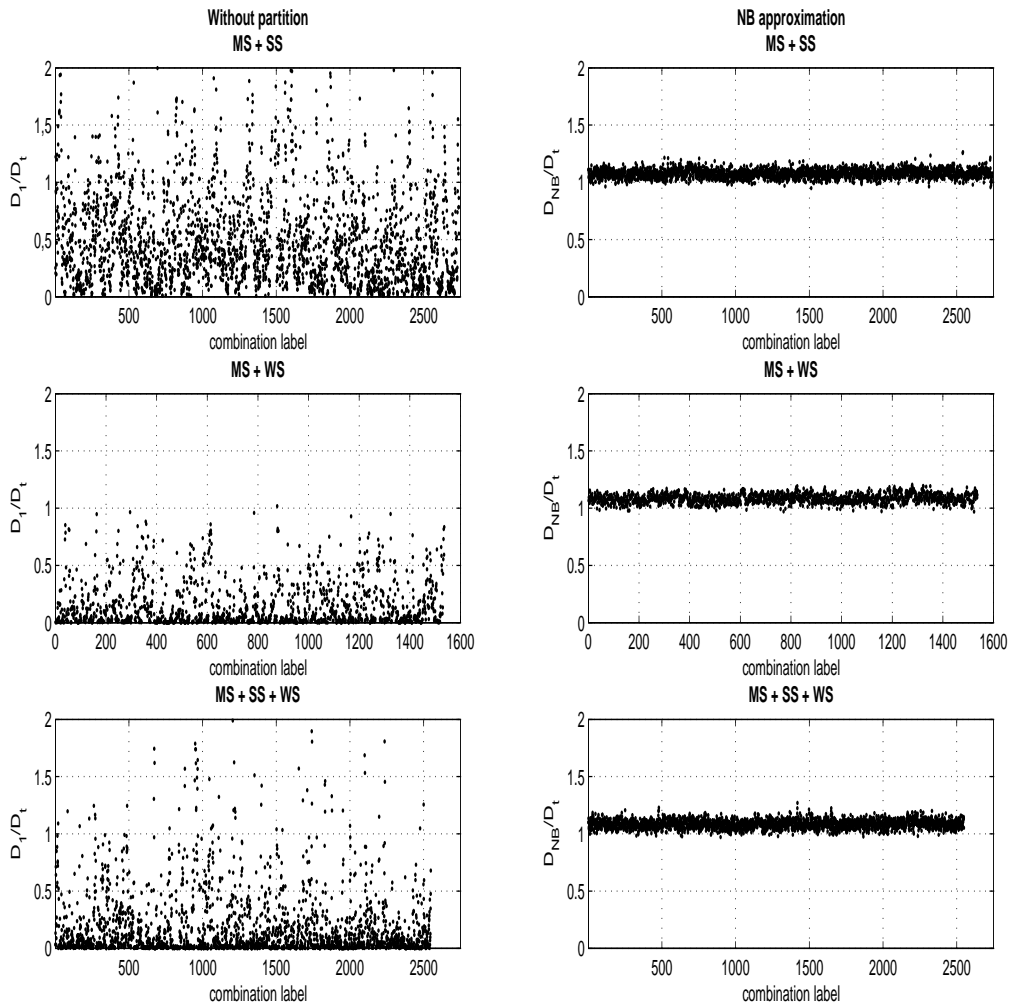


Figure 13: Conservatism level of both no partition and Narrow-Band approximations.

5.2 Damage assessment from the metocean climate description

To assess the total fatigue damage on the design lifetime from a given metocean climate description, the damage produced by all the possible sea states must be computed. Since those sea states are combinations of wave systems with quite different frequency bands, the use of the ICA formulas allows by construction

a significant computational efficiency. The fatigue damage is computed according to two approaches based on ICA formulas :

- ICA-based damage assessment from the wave systems components ;
- ICA-based damage assessment from the response systems components, given by partition of the response spectra to each of the wave systems components.

5.2.1 ICA-based damage assessment from wave systems components damages

Method

In a first approach, ICA formulas are used to compute the damage due to the response of any combination of wave systems components in terms of the damage of those components taken separately. Thus, the mean fatigue damage of the wave systems components are computed first. In the actual application, those damages are computed by the well acknowledged time-domain simulation method. Note that only 312 wave systems components can occur. For each of those components 100 time series are generated from their respective response spectra. One assumed that 100 is large enough to obtain accurate estimates of the mean value of the damage. It could be reduced or increased after a proper analysis of the scatter on the damages samples.

Once those component damages are known, the ICA formulas provide the damages due to each of the possible sea states predicted by the metocean climate description. Then, those damages are weighted by the probabilities of occurrence of their respective sea states and summed to get the expected damage scaled to the design lifetime.

Results & Discussion

The results for this approach are given in tables 12 and 13.

Sea states	Freq. Occ.	D_t	D_{ICA_1}		D_{ICA_2}	
			Value	Ratio \cdot / D_t	Value	Ratio \cdot / D_t
MS ONLY	15.07%	0.2863	0.07	24.45%	0.07	24.45%
MS+SS	34.08%	0.2542	0.2525	99.33%	0.2543	100%
MS+WS	19.01%	0.0604	0.0894	148%	0.0895	148.1%
MS+SS+WS	31.70%	0.0748	0.2309	309%	0.2331	312%
ALL	100%	0.6757	0.6428	95.13%	0.6469	95.74%

Table 12: ICA-based damages from the wave systems components under assumption **(H1)**

Sea states	Freq. Occ.	D_t	D_{ICA_1}		D_{ICA_2}	
			Value	Ratio \cdot / D_t	Value	Ratio \cdot / D_t
MS ONLY	15.07%	0.2863	0.3192	111.50%	0.3192	111.50%
MS+SS	34.08%	0.2542	0.2134	83.93%	0.2143	84.31%
MS+WS	19.01%	0.0604	0.0675	111.72%	0.0676	111.90%
MS+SS+WS	31.70%	0.0748	0.0647	86.50%	0.0653	87.33%
ALL	100%	0.6757	0.6647	98.38%	0.6664	98.63%

Table 13: ICA-based damages from the wave systems components under assumption **(H2)**

The damages provided in each combination category by the ICA-based method reveal especially the effect of the assumptions made on the metocean climate.

Under assumption (H1), one observes that while the damages produced by MS+SS or MS+WS remain stable compared to their respective values obtained from the metocean data, the damages caused by MS only and MS+SS+WS are significantly different. In fact, those last damages are almost exchanged. The damage of MS only decreases strongly to a value close to the magnitude of the reference solution for MS+SS+WS, while the damage of MS+SS+WS increases to a value close to the reference solution

for MS only. This can be explained by the fact that since it is assumed, according to the metocean specifications, that all the main swells observed can be equally combined with other components, the overall sea state significant heights observed for the category MS only in the metocean database are much lower. Therefore, the actual damage produced in this category is lower. On the other hand, from the metocean specifications, a main swell observed alone in the metocean data can also occur in any combination of the three wave systems, which tends to increase the mean significant wave height in that combination category, and hence, makes the associated damage larger. However by chance, the total damage although slightly lower, is still of the same order of magnitude as the reference solution. Finally, note that when one computes the proportions produced by each combination category in the total damage, one obtains 10% for MS only, 37% for MS+SS, 13% for MS+WS and 40% for MS+SS+WS, which agrees with their observed proportions in the lifetime.

Under assumption (H2), the proportions of the damage for the various combination categories with respect to the total damage agree with those of the reference solution. However, the damage is still larger for "MS only" and "MS+WS", while it is lower in the other combination categories. Here also, by chance, the total damage although slightly lower, is still of the same order of magnitude as the reference solution.

5.2.2 ICA-based damage assessment from response systems components damages

In the previous approach, it is implicitly assumed that the response spectrum to any wave system component (which has a unimodal spectrum) is unimodal, which is not necessarily true. Some of those response spectra to single systems exhibit in the actual application more than one peak (Fig 14). In general, the response spectrum to a unimodal sea state may also be a combination of several response systems, for example the quasi-static response to the wave system itself combined with a low-frequency mooring or some resonant response. Hence, in order to make a full use of the ICA approximations, it is more appropriate to apply them, rather than to the damages due to the individual wave systems, to those of the individual response systems. That approach requires to identify all the response systems that can appear in any response spectrum. It is quite obvious, under a linear dynamic assumption, that those response systems are completely given by a partition of the response spectra to the wave systems components.

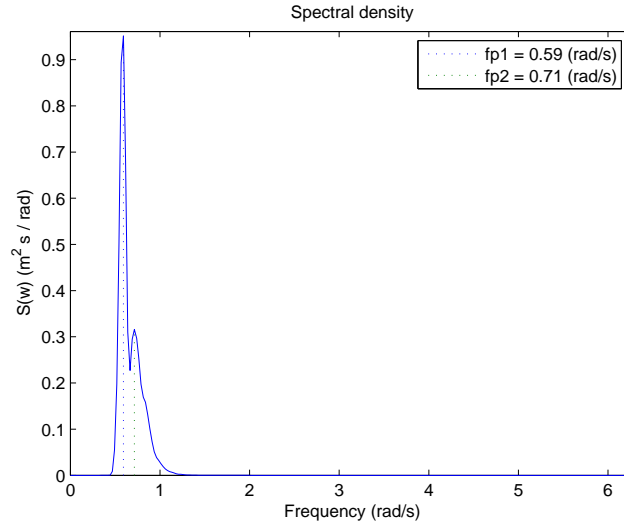


Figure 14: Multimodal response spectrum to a main swell component.

Method

One can define a global procedure for the fatigue damage assessment from the response systems components, as follows. First, let us assume that the metocean climate has been defined and all the possible sea states and their respective probabilities of occurrence are known. To compute the fatigue damage over the lifetime using ICA formulas:

1. one makes a partition of the response spectra to the individual wave systems identified in the metocean database statistic.
2. each obtained response system component is linked to the wave system component it is derived from.
3. The fatigue damage due to each response system spectrum is computed. This may be done by a time-domain simulation method or more efficiently by a spectral formula.
4. For any possible combination of wave systems components, the corresponding combination of response systems components is obtained using the link set up between response systems and wave systems.
5. Then, one recursively applies the ICA formulas to estimate the damages of all the multimodal response spectra. Note that, ICA is applied with single slope damages, then the formulas for double slope damage provide the damage for the double slope S-N curve under consideration.
6. One has to weight those damages with the probabilities of occurrence of the sea states they correspond to and sum them to obtain the expected damage per sea state duration.
7. Finally, that damage is scaled up to the foreseen lifetime to get the total fatigue damage.

Note that the partition method allows to describe the response system spectra with some known spectral shape models (e.g. Triangle, Jonswap...). And for those spectral shapes some parametric formulas for the damage have been deduced from fitting time-domain simulation results in the range of variation of the parameters. Thus, the damage of the response system is directly computed with those parametric formulas (appendix B), which can further accelerate the computations.

In the point 4 of the general procedure for damage assessment, some response system components can overlap or be very close when they are combined (e.g. when their respective peak frequencies are close enough). Therefore, before applying the ICA formula, the overlaps are identified and assembled into one component. The damage of that resulting component can be accurately computed with the combined spectrum approximation, which expresses as:

$$D = N_s \left[\left(\frac{D_h}{N_h} \right)^{\frac{2}{m}} + \left(\frac{D_l}{N_l} \right)^{\frac{2}{m}} \right]^{\frac{m}{2}} \quad (12)$$

Results & Discussion

The results of the damages from the partition of the sea states in the metocean database are shown in table 14. The partitions were made with triangle spectral shapes. That partition underestimates the damages, but it was chosen for its simplicity to illustrate the framework for damage assessment from response systems. One could expect a more accurate approximation with another model, namely Wallops spectral shape, but that one is not yet implemented in the partition software.

Sea states	Freq. Occ.	D_t	D_t^*	
			Value	Ratio \cdot / D_t
MS ONLY	15.07%	0.2863	0.2684	93.75%
MS+SS	34.08%	0.2542	0.2263	89.02%
MS+WS	19.01%	0.0604	0.0548	90.73%
MS+SS+WS	31.70%	0.0748	0.0613	81.95%
ALL	100%	0.6757	0.6108	90.40%

*: on partition with triangle model

Table 14: damage of the partition with triangle model of the response spectra from the metocean database

The results of the ICA-based damage assessment with the response systems are given in the tables 15, 16, 17 and 18. The conclusions concerning the effects of the assumptions made on the metocean climate predictions are the same as those of the previous approach. It is important to note here that these results show that the fully analytical approach, using the ICA formulas and the formulas for the damage from

double slopes S-N curve, performs correctly. That approach provides reasonably conservative values of damages. The approximation (a) of the double slope damage is slightly unconservative but still acceptable, and from approximation (b), which is reasonably conservative (conservatism level between 8% and 17%), the other approximations provide more conservative results.

Sea states	Freq. Occ.	D_t^*	(a)		(b)		(c)		(d)	
			Value	Ratio \cdot/D_t^*						
MS ONLY	15.07%	0.2684	0.0697	25.96%	0.0808	30.11%	0.0873	32.51%	0.0984	36.66%
MS+SS	34.08%	0.2263	0.2123	93.83%	0.2483	109.73%	0.2708	119.68%	0.3068	135.59%
MS+WS	19.01%	0.0548	0.0866	158.12%	0.1005	183.42%	0.1087	198.27%	0.1225	223.58%
MS+SS+WS	31.70%	0.0613	0.1991	324.78%	0.2330	380.06%	0.2544	415.08%	0.2883	470.36%
ALL	100%	0.6108	0.5677	92.95%	0.6626	108.49%	0.7212	118.08%	0.8161	133.61%

Table 15: ICA_1 -based fatigue damages from metocean climate prediction under **(H1)**

Sea states	Freq. Occ.	D_t^*	(a)		(b)		(c)		(d)	
			Value	Ratio \cdot/D_t^*						
MS ONLY	15.07%	0.2684	0.0697	25.96%	0.0808	30.11%	0.0873	32.51%	0.0984	36.66%
MS+SS	34.08%	0.2263	0.2147	94.89%	0.2510	110.90%	0.2742	121.15%	0.3104	137.17%
MS+WS	19.01%	0.0548	0.0869	158.62%	0.1008	183.97%	0.1090	198.96%	0.1229	224.31%
MS+SS+WS	31.70%	0.0613	0.2018	329.15%	0.2359	384.90%	0.2582	421.20%	0.2924	476.95%
ALL	100%	0.6108	0.5731	93.83%	0.6685	109.45%	0.7287	119.30%	0.8241	134.92%

Table 16: ICA_2 -based fatigue damages from metocean climate prediction under **(H1)**

*: on partition with triangle model

Sea states	Freq. Occ.	D_t^*	(a)		(b)		(c)		(d)	
			Value	Ratio \cdot/D_t^*						
MS ONLY	15.07%	0.2684	0.3121	116.27%	0.3615	134.70%	0.3828	142.64%	0.4323	161.07%
MS+SS	34.08%	0.2263	0.1825	80.65%	0.2170	95.91%	0.2416	106.75%	0.2761	122.01%
MS+WS	19.01%	0.0548	0.0624	113.78%	0.0721	131.52%	0.0820	149.65%	0.0917	167.39%
MS+SS+WS	31.70%	0.0613	0.0552	90.03%	0.0638	104.15%	0.0729	118.95%	0.0816	133.07%
ALL	100%	0.6108	0.6121	100.22%	0.7145	116.98%	0.7793	127.59%	0.8817	144.35%

Table 17: ICA_1 -based fatigue damages from metocean climate prediction under **(H2)**

Sea states	Freq. Occ.	D_t^*	(a)		(b)		(c)		(d)	
			Value	Ratio \cdot/D_t^*						
MS ONLY	15.07%	0.2684	0.3121	116.27%	0.3615	134.70%	0.3828	142.64%	0.4323	161.07%
MS+SS	34.08%	0.2263	0.1838	81.23%	0.2185	96.56%	0.2435	107.59%	0.2782	122.91%
MS+WS	19.01%	0.0548	0.0626	114.19%	0.0723	131.97%	0.0823	150.25%	0.0921	168.04%
MS+SS+WS	31.70%	0.0613	0.0559	91.17%	0.0646	105.40%	0.0740	120.64%	0.0827	134.88%
ALL	100%	0.6108	0.6144	100.58%	0.7170	117.38%	0.7826	128.13%	0.8852	144.93%

Table 18: ICA_2 -based fatigue damages from metocean climate prediction under **(H2)**

*: on partition with triangle model

6 Summary: Proposed procedure and practical performance

Most of the studies reported in the previous sections have first been carried out with the concern of validating a procedure through its results, and putting aside computational performance issues until one could be confident with the method itself. Indeed, many problems were encountered and solved before a general procedure could be chosen. We present hereafter the procedure that was eventually retained.

After that choice, optimization of the procedure became much easier, and was carried out using a number of algorithms and methods that are also presented. It is noteworthy that the largest gains were in fact obtained when converting the computer programs from Matlab to a procedural language more suited to scalar calculations, here Fortran 95. We now believe that the fatigue design in a multiple wave systems loading climate can be carried out without any obvious computational performance penalty when compared to the conventional "narrow-band single system sea state" approach. In the final version, 312 wave components are identified to span the database. They can be combined in 1,901,009 ways to provide realistic sea states. The response to each of those 312 wave components is then computed using the directional RAOs and represented with one, two or three of 441 distinct unimodal "response components". The corresponding computational effort is comparable to considering 312 sea states in a conventional unimodal sea state fatigue study. In an actual study, many of those sea states would even be neglected as they are known not to contribute to the structure's fatigue.

Calculation and combination of up to nine (3 wave systems \times 3 peaks for each response) damages into each of the 1,901,009 possible sea states and summation with the appropriate occurrence probabilities of those possible sea states now requires less than 15 seconds on a powerful PC.

6.1 Procedure

1. Wave spectra partition and discretization
2. Determination of the wave systems combinations probabilities of occurrence
3. Calculation of the responses to the wave systems
4. Responses partition and discretization
5. Calculation of the damages and other characteristics of the response systems
6. Combination within each possible sea state (i.e. each wave systems combination)
7. Summation with the probabilities of occurrence

The two first steps of the above procedure are preliminary to the fatigue design, they correspond to characterizing the wave climate of the region of interest with a high level of details with respect to the energy distribution over the direction and frequency ranges, and to joint probabilities of occurrence. They are probably now the most difficult steps given that measurements and hindcasts were often not made with such a refined description in mind. It was not in the scope of the present study to improve them, but they should be the highest priority topic to consider for further research.

The third step, calculation of the responses to individual wave systems, does not significantly differ from current engineering practice.

The fourth one is more unusual, and may still require some improvements. For instance, partitioning software packages were developed for directional wave spectra, using conventional parametric models for unimodal wave spectra that may not be very well suited to scalar stress spectra. We would also like to draw attention to the fact that high-frequency tail behaviour is much more secondary for responses than for wave spectra, and can be easily dealt with, for instance using the separation method studied in Appendix F.

Using the unimodal formulas of Appendix B, the fifth step is rather straightforward. In the case of a two slope S-N curve, see Appendix C, the characteristics of the response to a given wave system need to comprehend the first seconds of the autocorrelation function to compute ρ and ϕ to use the formulas that we suggest. Since autocorrelation functions add up when spectra are added, that is also a simple point to deal with.

Iterative application of the ICA combination formulas at step six may imply a large number of individual response systems. Some of them may exhibit a good deal of frequency overlapping and little

difference in the peak frequency. We thus suggest to run them through preliminary merging with the combined spectrum method (for damage, $D = (D_1^{2/k} + D_2^{2/k})^{k/2}$) when the peak frequencies differ by less than 10 or 20%. The remaining systems will then be separated enough to apply the ICA formulas at their best range of operation. In case of a two slope S-N curve, the corresponding damage should be approximated for each possible sea state at this stage rather than on the accumulated damage over the structure lifespan, since the assumptions that we use include stationarity.

6.2 Performance

A number of performance issues were encountered along the study. The main ones are evaluation of the $F(k, \alpha, \beta, \eta_s)$ functions, especially in the context of two slope S-N curves, and avoidance of simulations or other lengthy calculations for each combination of systems.

6.2.1 Fast evaluation of F functions

To speed up evaluation of the $F(k, \alpha, \beta, \eta_s)$ functions that are directly linked to the k^{th} -order statistical moments of a Rice(η_s) distribution raised to some power, the first point is to get rid of the separation into two domains induced by two slope S-N curves. The method described in Appendix C allows to remove the dependency of F on the threshold between the two slopes, and thus for each of the k values of the S-N curves slopes given in the specifications (one or two slopes, plus the value 1 for computation of the reduction factor k_a), F only depends on a restricted function $F_r(\beta, \eta_s)$ multiplied by a simple expression of α . Since F_r is well behaved over the unit square in (β, η_s) , we suggest furthermore to tabulate it on a grid of, say, step 0.01 and then to evaluate it via linear interpolation between the closest grid values.

6.2.2 Avoidance of lengthy calculations for each combination

Combination parameters can be evaluated from spectral moments. Since spectral moments add up in the combination, they need only be computed for the response components, thus in small numbers. Similarly, autocorrelation functions add up in the combination, so their first few seconds can be calculated for each response component and stored, then a simple ratio of added terms provides the autocorrelation at $\frac{T_{02}}{2}$ to obtain ρ and ϕ .

7 Conclusion

In this study, our main purpose was to validate the use of the ICA formulas that were introduced earlier on an industrial design application. The retained application concerned the hull girder of an FPSO in a West Africa location subjected to a linear dynamic response due to wave bending moment. The results of the study reveal that ICA formulas provide reasonably conservative results and that most of the conservatism comes from the discretization choices. Those formulas were also simply implemented with an eventual high performance in that real application.

During this analysis some problems were highlighted. They concern firstly the adaptation of the various features introduced to the use of double-slopes S-N curves. A satisfactory solution was eventually found. The other underlined difficulty was raised by the definition of a probabilistic model for the operational sea states according to the metocean specifications. The model with full independence of wave systems yields statistical properties highly different from those of the metocean database. The model with independence within each type of combination provides significant improvement, but is still not fully satisfactory. Further research is needed on that point. In addition, partition software needs to be adapted to deal with response systems rather than wave systems in a swift operational manner.

Nevertheless, that study and the good behaviour it revealed for the ICA formula allows to consider that a global framework for fatigue design of offshore structure subjected to multimodal loading spectra is now available to design engineers.

References

- [1] D. Benasciutti and R. Tovo. Comparison of spectral methods for fatigue analysis of broad-band random processes. *Probabilistic Engineering Mechanics*, 21:287–299, 2006.
- [2] Bureau Veritas. *Fatigue strength of welded ship structure*, 1998. Ref. NI 393.
- [3] Z. Gao and T. Moan. Fatigue damage under combined high and low frequency gaussian load processes considering a two-slope sn curve. In *Applications of Statistics and Probability in Civil Engineering*, 2007.
- [4] N.E. Huang, S.R. Long, C.-C. Tung, Y. Yuen, and L. Bliven. A unified two-parameter wave spectral model for a general sea state. *J. Fluid Mechanics*, 112:203–224, 1981.
- [5] W. Huang and T. Moan. Fatigue under combined high and low frequency loads. In *Proceedings of 25th International Conference on Offshore Mechanics and Arctic Engineering*, 2006.
- [6] ITTC. Report of the specialist committee on waves. In *Proceedings of 15th 23rd ITTC*, volume II, pages 505–551, 2002.
- [7] G. Jiao and T. Moan. Probabilistic analysis of fatigue due to gaussian load processes. *Probabilistic Engineering Mechanics*, 5(2):76–83, 1990.
- [8] M. A. Kerbiriou, M. Prevosto, C. Maisondieu, A. Babarit, and A. Clément. Influence of an improved sea-state description on a wave energy converter production. In *Proceedings of 26th International Conference on Offshore Mechanics and Arctic Engineering*, volume 12, 2007.
- [9] G. Lindgren and J. Rydén. Transfer-function approximations of the rainflow filter. *Mechanical Systems and Signal Processing*, 16(6):979–989, 2002.
- [10] A. Mansour and R. eds. Ertekin. Report of technical committee i.1 – environment. In *Proceedings of 15th ISSC*, volume 1, 2003.
- [11] M. A. Miner. Cumulative damage in fatigue. *Journal of Applied Mechanics*, 12:A–159, 1945.
- [12] A. Naess. The joint crossing frequency of stochastic processes and its application to wave theory. *Applied Ocean Res.*, 7(1):35–50, 1985.
- [13] A. Naess. On the distribution of crest-to-trough wave heights. *Ocean Engineering*, 12:221–234, 1985.
- [14] M. Olagnon and Z. Guédé. Rainflow fatigue analysis for loads with multimodal power spectral densities. *Marine Structures*, pages 160–176, 2008.
- [15] V. Quiniou. Pazflor project - metocean design criteria. Technical report, TOTAL, 2006.
- [16] V. Quiniou, M.-A. Hoche, M. François, R. Nerzic, A. Ledoux, and M. Orsero. Recent breakthroughs in the analysis of total e&p angola block 17 wind/wave/current records and their impact on floating structures design. In *Proceedings of XVth Deep Offshore Technology Conf.*, 2003.
- [17] S. O. Rice. Mathematical analysis of random noise. *Bell Systems Technical Journal*, pages 24–25, 1945.
- [18] I. Rychlik. A new definition of the rainflow counting method. *International Journal of Fatigue*, 9:119–21, 1987.

A Iterative Component Addition formulas

The Iterative Component Addition formulas is a set of two analytical formulas which allow to compute the fatigue damage due to a multimodal loading (*i.e.* with a multimodal spectrum) in terms of the damages of its components taken separately. Initially meant to deal with bimodal loading spectra, those formulas may be iteratively applied to loading spectra with more than two peaks. Those formula have been proposed by Olagnon & Guédé (2008) [14].

A.1 Damage of bi-modal loading spectra

Let us consider a random signal $x(t)$ with a bi-modal power spectral density $W(\omega)$. That signal is assumed to represent the stress field or an equivalent stress at a critical point in the mechanical structure under study where fatigue damage needs to be estimated. The bi-modal power spectral density is regarded as the sum of two unimodal spectra, denoted $W_h(\omega)$ for the one with the highest peak frequency and $W_l(\omega)$ that with the lowest peak frequency. We will need the assumption that the low frequency signal is narrow-band, we will however not impose any assumption on the bandwidth of the high frequency signal. The spectra $W_h(\omega)$ and $W_l(\omega)$ correspond to the random signals $x_h(t)$ and $x_l(t)$ respectively and we have:

$$\begin{aligned} W(\omega) &= W_h(\omega) + W_l(\omega) \\ x(t) &= x_h(t) + x_l(t) \end{aligned}$$

The two Iterative Component Addition formulas, denoted ICA_1 & ICA_2 , aim at estimating the rainflow fatigue damage of the signal $x(t)$ from the damages of its high and low frequencies components. They are based on a partition of the set of local extrema (*i.e.* turning points) of the global signal $x(t)$ (see figure 15). Those turning points can be partitionned into two separate subsets \mathcal{A} and \mathcal{B} :

- subset \mathcal{B} : set of maxima and minima of local extrema between two successive up- to down-zero-crossings and down- to up- respectively of the low-frequency signal $x_l(t)$. Negative maxima and positive minima are forced to zero, which is a conservative move.
- subset \mathcal{A} : set of all the remaining turning points.

The subset \mathcal{B} produces the largest rainflow ranges, while the subset \mathcal{A} is responsible for the smallest ones. From the mathematical formulation of the rainflow counting [18], both subsets are shown to be stable by rainflow counting. The mathematical formulation of the rainflow counting is schematically explained on the figure 16. Thus, the damage of the global signal $x(t)$ is the simple sum of the damages of the subsets \mathcal{A} and \mathcal{B} taken separately:

$$D = D_{\mathcal{A}} + D_{\mathcal{B}} \quad (13)$$

The damages $D_{\mathcal{A}}$ and $D_{\mathcal{B}}$ will be then expressed respectively in terms of the high-frequency component damage D_h and the low-frequency component damage D_l . For that, let us introduce the following notations :

$$\begin{aligned} \beta_l &= \frac{N_l}{N_s} & \beta_h &= \frac{N_h}{N_s} \\ \eta &= \frac{\lambda_{s,2}}{\sqrt{\lambda_{s,0}\lambda_{s,4}}} & \eta_h &= \frac{\lambda_{h,2}}{\sqrt{\lambda_{h,0}\lambda_{h,4}}} \\ \alpha &= \sqrt{\frac{\lambda_{h,0}}{\lambda_{s,0}}} \end{aligned}$$

η and η_h are the irregularity factors of the signal $x(t)$ and $x_h(t)$ respectively.

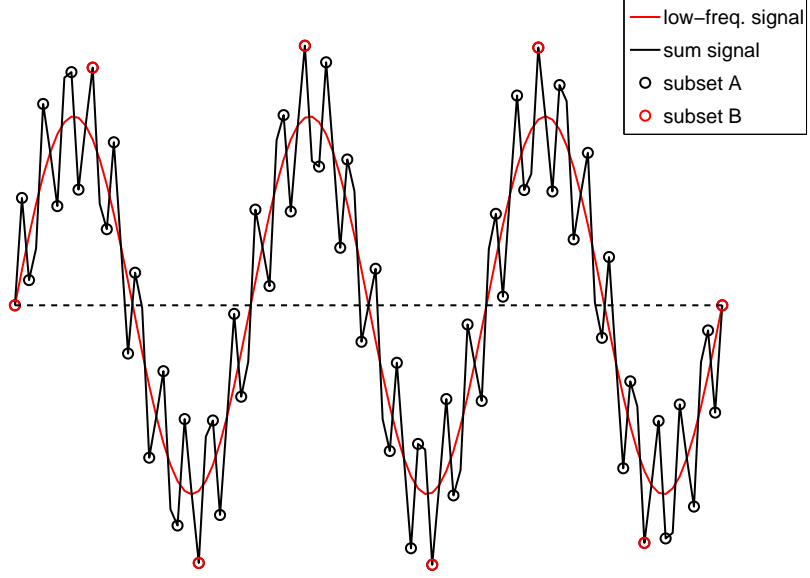


Figure 15: Partition of the set of turning points.

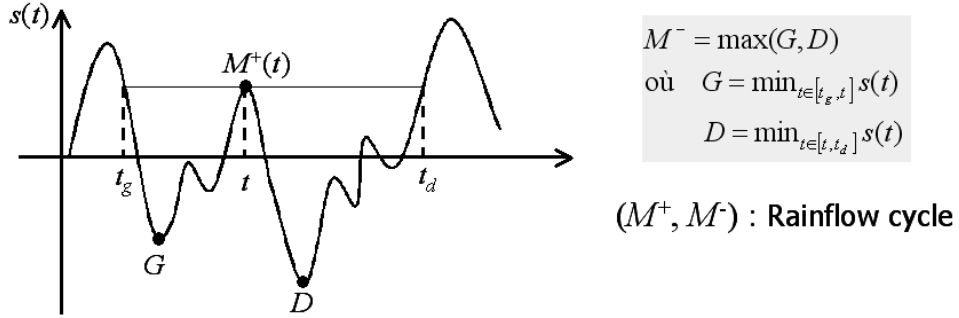


Figure 16: Mathematical formulation of Rainflow counting.

A.1.1 Damage associated to subset \mathcal{A}

The damage of subset \mathcal{A} reads:

$$D_{\mathcal{A}} = \frac{N_{\mathcal{A}}}{K} \int_0^{\infty} S_{\mathcal{A}}^m p(S_{\mathcal{A}}) dS_{\mathcal{A}}$$

Now, let us express $D_{\mathcal{A}}$ in terms of D_h , the damage of the high-frequency component. The number of rainflow cycles in subset \mathcal{A} , $N_{\mathcal{A}}$, can be expressed in terms of the number of rainflow cycles in the high-frequency component by:

$$N_{\mathcal{A}} = N_s - N_l = \frac{N_s - N_l}{N_s} \frac{N_s}{N_h} N_h = \frac{1 - \beta_l}{\beta_h} N_h \quad (14)$$

A range $S_{\mathcal{A}}$ is reduced compared to S_h , the corresponding range of the high-frequency component, due to the addition of the low frequency component. It may even disappear if the slope of the low-frequency component is large at that location. Let $k_{\mathcal{A}} = (\overline{S_{\mathcal{A}}}/\overline{S_h})$, then $S_{\mathcal{A}}$ is approximated by $k_{\mathcal{A}} \cdot S_h$. Having noted that the mean value of the rainflow ranges of the global signal can be written from the means in subsets \mathcal{A} and \mathcal{B} as:

$$\overline{S} = \frac{N_{\mathcal{A}} \overline{S_{\mathcal{A}}} + N_l \overline{S_{\mathcal{B}}}}{N_s}$$

the parameter $k_{\mathcal{A}}$ is given by:

$$k_{\mathcal{A}} = \frac{\overline{S_{\mathcal{A}}}}{\overline{S_h}} = 1 - \frac{\beta_l}{1 - \beta_l} \frac{\overline{S_{\mathcal{B}}} - \overline{S_h}}{\overline{S}} \quad (15)$$

In the previous equation, only $\overline{S_{\mathcal{B}}}$ is unknown, the remaining variables can be computed. To ensure a conservative estimate a lower bound of $\overline{S_{\mathcal{B}}}$ must be used. An approximation of $\overline{S_{\mathcal{B}}}$ will be given in the next section.

Finally, the rainflow ranges in subset \mathcal{A} , scaled by $k_{\mathcal{A}}$, are assumed to have the same distribution as those of the high-frequency component which leads to the equality $p(S_{\mathcal{A}})dS_{\mathcal{A}} = p(S_h)dS_h$. Therefore, we have:

$$D_{\mathcal{A}} = \frac{N_{\mathcal{A}}}{K} \int_0^{\infty} S_{\mathcal{A}}^m p(S_{\mathcal{A}}) dS_{\mathcal{A}} = \frac{1 - \beta_l}{\beta_h} k_{\mathcal{A}}^m \frac{N_h}{K} \int_0^{\infty} S_h^m p(S_h) dS_h,$$

which yields the following relation :

$$D_{\mathcal{A}} = \frac{1 - \beta_l}{\beta_h} k_{\mathcal{A}}^m D_h \quad (16)$$

A.1.2 Damage associated to subset \mathcal{B}

The damage of subset \mathcal{B} reads:

$$D_{\mathcal{B}} = \frac{N_{\mathcal{B}}}{K} \int_0^{\infty} S_{\mathcal{B}}^m p(S_{\mathcal{B}}) dS_{\mathcal{B}}$$

Now, the issue is to express the damages $D_{\mathcal{B}}$ in terms of D_l , the low-frequency component damage. Under the narrow-band assumption for low-frequency component, the damage associated to the low-frequency component reads:

$$D_l = \frac{N_l}{K} (2\sqrt{2\lambda_{0,l}})^m \Gamma\left(1 + \frac{m}{2}\right)$$

which leads to:

$$\frac{N_l}{K} = \frac{D_l}{(2\sqrt{2\lambda_{0,l}})^m \Gamma\left(1 + \frac{m}{2}\right)}$$

Having noted that by definition $N_{\mathcal{B}} = N_l$, the expression of N_l/K can be substituted into $D_{\mathcal{B}}$ and we get:

$$D_{\mathcal{B}} = \frac{\int_0^{\infty} S_{\mathcal{B}}^m p(S_{\mathcal{B}}) dS_{\mathcal{B}}}{(2\sqrt{2\lambda_{0,l}})^m \Gamma\left(1 + \frac{m}{2}\right)} D_l$$

To compute that damage, the distribution of $S_{\mathcal{B}}$ needs to be known. Note that, by definition, $S_{\mathcal{B}}$ amplitude is twice the excursion of the largest extremum among the positive local maxima that are found between two successive minima of the low-frequency signal $x_l(t)$. Keeping in mind that we are trying to obtain a conservative estimate of the damage, two approximations are suggested for the distribution of $S_{\mathcal{B}}$. Both approximations use the fact that the local maxima of a standard gaussian process follow a Rice distribution [17], which is given by:

$$\begin{aligned} \text{PDF. } f(s) &= \frac{1}{\sqrt{2}} \left[\sqrt{\frac{1-\eta}{\pi}} e^{-\frac{s^2}{2(1-\eta^2)}} + \frac{\eta s}{\sqrt{2}} e^{-\frac{s^2}{2}} \operatorname{erfc}\left(-\frac{\eta s}{\sqrt{2(1-\eta^2)}}\right) \right] \\ \text{CDF. } \mathcal{F}(s) &= \frac{1}{2} \left[\operatorname{erfc}\left(-\frac{s}{\sqrt{2(1-\eta^2)}}\right) - \eta e^{-\frac{s^2}{2}} \operatorname{erfc}\left(-\frac{\eta s}{\sqrt{2(1-\eta^2)}}\right) \right] \end{aligned}$$

Approximation $\mathcal{Y}_1(S)$: This approximation intends to be close to the real distribution of $S_{\mathcal{B}}$. It assumes that the local extrema in subset \mathcal{B} are independent (which is a conservative assumption) and

the number of local maxima between two successive minima of the low-frequency signal is fixed to its average value. The distribution of the positive local maxima of the global signal is:

$$\mathcal{F}_p(S) = \frac{\mathcal{F}(S) - \mathcal{F}(0)}{\mathcal{F}(\infty) - \mathcal{F}(0)} = \frac{2\mathcal{F}(S) + \eta - 1}{\eta + 1}$$

and the mean number of those maxima between two successive minima of $x_i(t)$ is:

$$n_p = \frac{\eta + 1}{2\beta_l}$$

Thus the first approximation reads:

$$\mathcal{Y}_1(S) = \mathcal{F}^{n_p}(S) \text{ and } y_1(S) = \frac{d\mathcal{Y}_1}{dS} = n_p f \mathcal{F}^{n_p-1}(S) \quad (17)$$

Approximation $\mathcal{Y}_2(S)$: This approximation is a definitely conservative option. It suggests that S_B are the largest possible local maxima of the global signal. Having noted that the mean number of local maxima between two successive minima of the low-frequency signal is $N_s/N_l = 1/\beta_l$, it is equivalent to say that S_B belong to the upper $1/\beta_l$ -fractile of the distribution of the maxima of $x(t)$. Thus, the second approximation reads:

$$\mathcal{Y}_2(S) = 1 - \frac{1}{\beta_l} (1 - \mathcal{F}(S)) \text{ and } y_2(S) = \frac{f(S)}{\beta_l} \text{ for } S \geq \delta_2$$

where $\delta_2 = \max\left(0, \mathcal{F}^{-1}\left(1 - \frac{N_l}{N_s}\right)\right) = \max(0, \mathcal{F}^{-1}(1 - \beta_l))$

Now, let us denote:

$$Y_i = \int_0^\infty S^m y_i(S) dS \text{ with } i = 1, 2$$

we obtain finally:

$$D_B = \frac{Y_i}{\sqrt{2(1 - \alpha^2)^m} \Gamma(1 + \frac{m}{2})} D_l \quad (18)$$

At this stage, one can make use of the approximation of the distribution of S_B to estimate $\overline{S_B}$ needed in the expression of k_A in equation (15). A first attempt to approximate $\overline{S_B}$ is to use the distribution $\mathcal{Y}_1^*(S)$, same as $\mathcal{Y}_1(S)$ but not restricted to positive maxima, *i.e.* replacing n_p with $\frac{1}{\beta_l}$, which is thought to be close to the real distribution of S_B . When with this approximation the factor k_A is not in its correct interval $[0, 1]$, one can still use the distribution $\mathcal{Y}_1(S)$ replacing in the expression of \mathcal{F} and \mathcal{F}_p , the irregularity factor η , by the high-frequency component one η_h . This way we get a lower estimate for $\overline{S_B}$. If again the factor k_A is not in its correct interval $[0, 1]$, this time one can replace η by zero. This way, $\mathcal{Y}_1(S)$ is computed with a gaussian peak distribution, leading to an even lower estimate. If none of these solutions work, one has to set k_A to 1.

A.2 Damage of loading spectra with more than two peaks

When a loading spectrum with more than two peaks is considered, the formula for bi-modal spectra is applied iteratively starting from the spectrum component with the highest peak frequency. This explains the name of these formulas as "Iterative Component Addition".

Let us consider a multimodal loading spectrum W with more than two components W_i , sorted in ascending order of their peak period (*i.e.* in descending order of their peak frequency) :

$$W = \sum_{i=1}^n W_i, \quad n > 2$$

The damage of the bi-modal spectrum $W_1 + W_2$, is computed first with the formulas (16) & (18). Then the next high-frequency component W_3 is added to the previous spectrum. The resulting spectrum $W_3 + (W_1 + W_2)$ is treated as a bi-modal one, with its high frequency component set to $(W_1 + W_2)$, and its damage is again computed with the formulas (16) & (18). In this case, the high-frequency damage is the damage of $(W_1 + W_2)$ computed previously. Note that, one can treat a multimodal spectrum as a high-frequency component since no restriction is made on the band width of the high-frequency component in the application of the formulas (16) & (18) ; only the low-frequency component is assumed narrow-banded. Thus, the previous procedure is repeated until one reaches the last component W_n .

B Parametric Damage for Unimodal Spectra

B.1 Introduction

The purpose of the global study is to validate a methodology for robust and cost-effective evaluation of fatigue damage for the design of marine structures, in the case of multiple loading systems (for instance, wind sea, several swells and even responses at natural frequencies). It is as such a development of some questions raised in the “Joint Probabilities & Response Based Design” project [16].

In the previous phases of the study, we compared the performance of combination methods based on the standard deviation, zero-crossing frequency, spectral bandwidth and induced rainflow damage of each component taken in isolation. In order to speed up computations, the rainflow damage induced by a given component need not be computed by simulations, but can be derived from the parameters of a spectral model fitted to that component.

Formulas such as the Wirsching and the Dirlik one allow to take into account spectral bandwidth. However, if one considers parametric shape families for the spectra, a more straightforward way is to make damage depend on the shape parameter of the family rather than on the spectral moments. We provide here formulas for the Jonswap, Wallops, Triangle and power-tail families.

B.2 Spectral shapes

When dealing with sea state climate, an important point is to be able to provide reasonably accurate and detailed models of the spectral energy contents of the wave field. That is necessary because dynamic responses dominate the design process for most of the structures presently developed for oil and gas production offshore, and those responses cannot be accurately computed from significant wave height and dominant or zero-crossing period only.

It is nevertheless completely unpractical to try to extrapolate design conditions from the collection of the spectra observed at a given location if the spectra are described as energy values on a fine frequency-direction grid. The idea is thus to characterize spectra by a small number of parameters from which the whole spectral shape can then be precisely reconstructed.

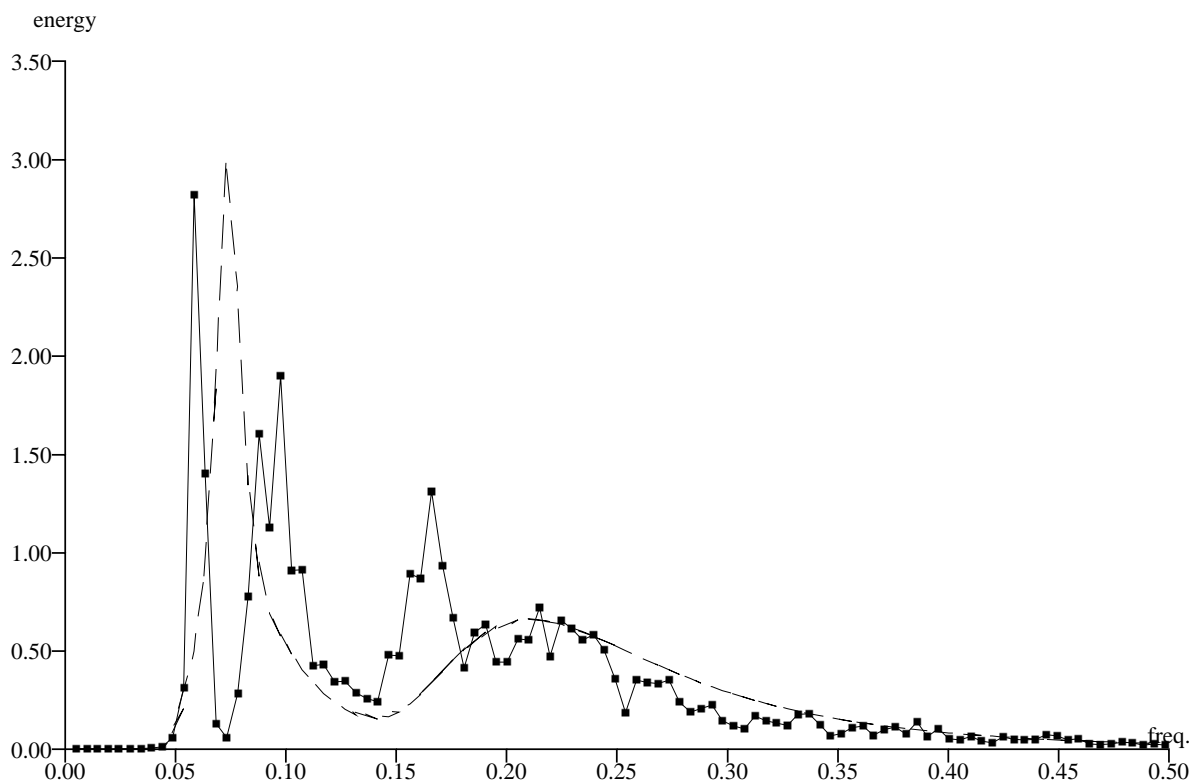


Figure 17: A spectrum with 3 swell components and its conventional model as the sum of two Jonswap

Several studies, see for instance the review in the 2003 ISSC report [10], have shown the limitations of conventional spectral shapes when it comes to swell.

Figure 17 shows how inadequate the Jonswap shape may be for a West Africa spectrum with several swell components. On first examination, it appears clearly that a model for such a spectrum must be able to take into account two, three peaks or more.

A pragmatic consequence is that each peak of the spectrum should be modeled separately, allowing for a relatively large number of independent spectral peaks (for instance, three different swells and one wind sea).

The impact of this partitioning of the spectra into several wave components can significantly improve the accuracy of the computed responses (see for instance Quiniou-Ramus *et al* (2003) [16]). However, the climate statistics and the choice of design sea states become much more complex. Still, a partitioning of the spectrum into several individual wave systems allows to take into account the physical reality of swell coming from different generating storms in various remote locations, and to study those separately. That relies on the assumption that the individual responses to simultaneous wave systems are sufficiently independent for the corresponding peaks in the response spectra to be dealt with separately also. When that is not the case, one should definitely try to construct a “response systems climate” and apply similar methods to it, rather than to the wave systems one.

In any case, a first step is to construct parametric models for individual wave (or response) systems and a method that is suited to representing most if not all of the spectra at the location of interest as the combination of those models. A second step is to allow to carry out climate statistics on those parameters, so as to enable design analyses of structures with respect to fatigue. A last issue is to apply statistical reconstruction methods to such parametric descriptions so as to obtain the joint probabilities of occurrence together with the fatigue damage calculations.

Appendix A. of the Waves report of the 23rd ITTC [6] gives the most commonly used parametric models for wave spectra. Assuming that the same families of spectra can be used for the responses, the

rainflow damage intensity for such a spectrum and a S-N curve slope of k can be computed directly from the narrow-band approximation:

$$D_{NB} = C \frac{1}{T_z} \left(2\sqrt{2} \frac{H_s}{4} \right)^k \Gamma \left(1 + \frac{k}{2} \right) \quad (19)$$

$$D_{NB} = C \sqrt{\frac{M_2}{M_0}} \left(2\sqrt{2} \sqrt{M_0} \right)^k \Gamma \left(1 + \frac{k}{2} \right) \quad (20)$$

$$(21)$$

by using a reduction factor to take into account bandwidth. This reduction factor depends only on the spectral shape, since the time and the amplitude scales are taken into account in the narrow-band approximation, and thus only on the shape parameter of the model. Previous authors have suggested formulas depending on the spectral moments.

Full description of the Wirsching and Dirlik formulas can be found, for instance, in *Benasciutti & Tovo* [1].

Wirsching (or Wirsching-Light) formula states:

$$D_{Wirsching} = D_{NB} (a(k) + (1 - a(k))(1 - \epsilon)^{b(k)}) \quad (22)$$

$$a(k) = 0.926 - 0.033k \quad (23)$$

$$b(k) = 1.587k - 2.323 \quad (24)$$

$$(25)$$

with ϵ the usual bandwidth parameter defined by:

$$\epsilon = \sqrt{1 - \frac{\lambda_2^2}{\lambda_0 \lambda_4}} \quad (26)$$

Dirlik formula is:

$$D_{Dirlik} = D_{NB} \frac{\nu_{24}}{\nu_{02}} \left(D_1 \left(\frac{Q}{\sqrt{2}} \right)^k \frac{\Gamma(1+k)}{\Gamma(1+k/2)} + D_2 |R|^k + D_3 \right) \quad (27)$$

$$\nu_{24} = \sqrt{\frac{\lambda_4}{\lambda_2}} \quad (28)$$

$$\nu_{02} = \sqrt{\frac{\lambda_2}{\lambda_0}} \quad (29)$$

$$\eta = \sqrt{1 - \epsilon^2} \quad (30)$$

$$= \frac{\nu_{02}}{\nu_{24}} \quad (31)$$

$$x_m = \frac{\lambda_1}{\lambda_0} \sqrt{\frac{\lambda_2}{\lambda_4}} \quad (32)$$

$$D_1 = \frac{2(x_m - \eta^2)}{1 + \eta^2} \quad (33)$$

$$Q = 1.25D_1 \quad (34)$$

$$R = \frac{\eta - x_m - D_1^2}{1 - \eta - D_1 + D_1^2} \quad (35)$$

$$D_2 = \frac{1 - \eta - D_1 + D_1^2}{1 - R} \quad (36)$$

$$D_3 = 1 - D_1 - D_2 \quad (37)$$

$$(38)$$

Yet, when a spectral shape from a given parametric family is given, spectral moments seem an unnecessary intermediate stage, sometimes difficult to estimate robustly, and it would be more convenient to relate the factor to the family parameter itself (γ for the Jonswap family, λ for the Wallops, etc.). Assuming k in the range 2 to 5, we determined empirical formulas for the damage reduction as a function of the shape (bandwidth) parameter in those spectral families.

B.3 Jonswap spectral shape

For conditions that are current in the North Sea, and more generally in medium or high latitudes, common spectral models have been developed: the Pierson-Moskowitz one,

$$\alpha \frac{g^2}{(2\pi)^5} f^{-5} e^{-\frac{5}{4} \left(\frac{f}{f_p}\right)^{-4}} \quad (39)$$

that is often found more convenient under the form recommended by the ISSC:

$$0.11087 \frac{H_s^2}{T_z^4} f^{-5} e^{-0.44336 \frac{f^{-4}}{T_z^4}} \quad (40)$$

and the one that was obtained by modifying it to represent the more narrow-banded sea-states of the North Sea in the JONSWAP project after which it was named:

$$\alpha \frac{g^2}{(2\pi)^5} f^{-5} e^{-\frac{5}{4} \left(\frac{f}{f_p}\right)^{-4}} \gamma^{\exp\left(-\frac{\left(1-\frac{f}{f_p}\right)^2}{2\sigma^2}\right)} \quad (41)$$

with σ set to 0.07 for the ascending part of the spectrum ($f < f_p$) and 0.09 for the descending part ($f \geq f_p$).

We suggest the empirical formula:

$$D_{Jonswap}(\gamma) = D_{NB}(1 - \max(0.0, 0.0103 \ln(k)(5 - \ln(\gamma)))) \quad (42)$$

for the reduction factor of the Jonswap spectrum family in the γ range 1 to 15.

Based on the comparison with 2920 simulations of 3 hours sea states with $T_{02} = 10$ and $H_s = 4.$, this formula provides mean biases and errors as displayed in table 19. It may be noted that typical aleatory variability for that number of simulations is about 0.3%, and typical maximum difference over the considered range of γ and k about 1.3%.

Formula	bias (%)	RMS Error (%)	Max underest.(%)	Max overest.(%)
This report	0.5	0.6	0.4	1.6
Wirsching	-3.1	3.8	5.8	3.0
Dirlik (1)	3.3	3.4	-	5.5
Dirlik (2)	2.4	2.6	-	5.0

Table 19: Comparison of formulas to simulation over the range γ 1 to 15 and k 1 to 5

In the same table, we show the comparison with the Wirsching formula, and with the Dirlik formula estimated in two manners: (1) with the fourth spectral moment computed from the spectral shape, and (2) with the fourth spectral moment estimated from the observed irregularity factor in the simulations.

Given the cut-off frequency problems and the lack of numerical robustness in the calculation of the fourth spectral moment λ_4 , its empirical value obtained from the number of local extrema and the number of zero-crossings in the signal gives better results than the one calculated from the theoretical spectral shape. Both cases of the Dirlik approximation are better than the Wirsching one. However, the proposed formula is definitely superior to the Dirlik one, and simpler to compute.

B.4 Wallops spectral shape

In the original paper [4], the Wallops spectrum is defined as:

$$\beta \frac{g^2}{f_p^5} \left(\frac{f}{f_p}\right)^{-q} e^{-\frac{q}{4} \left(\frac{f}{f_p}\right)^{-4}} \quad (43)$$

We will use here the form that appears in the Ochi-Hubble double peak spectrum:

$$K \frac{H_s^2}{T_z^4} \left(\frac{f_p}{f}\right)^{4\lambda+1} e^{-\frac{4\lambda+1}{4} \left(\frac{f_p}{f}\right)^4} \quad (44)$$

with $4\lambda + 1 = q$.

We suggest the empirical formula for the damage reduction:

$$D_{Wallops}(\lambda) = D_{NB} \left(1 - \max \left(0, \frac{5k+2}{300} \frac{\lambda^{\frac{\ln(k)}{3}}}{\lambda^{\frac{4}{3}}} \right) \right) \quad (45)$$

in the λ range 0.8 to 8. It should be noted that for λ less than 1, the fourth spectral moment is not finite and thus the Wirsching and Dirlik formulas cannot apply. Damage, as shown by Rychlik, can however be finite with an infinite fourth spectral moment. The above formula is empirical and can still be used, though caution is required since damage is highly dependent on the cut-off frequency, as shown in the previous parts of this study.

Based on the same comparison with 2920 simulations of 3 hours sea states as previously, this formula provides mean biases and errors displayed in table 20.

Formula	bias (%)	RMS Error (%)	Max underest.(%)	Max overest.(%)
This report, λ 0.8-8	0.0	0.3	1.7	2.9
This report, λ 1-8	0.0	0.3	0.7	0.7
Wirsching, λ 1-8	3.7	4.4	2.8	7.6
Dirlik (1), λ 1-8	-0.2	0.8	1.0	8.6
Dirlik (2), λ 1-8	-0.2	0.6	1.0	4.3

Table 20: Comparison of formulas to simulation over the range λ 0.8 to 8 and k 1 to 5

Again, the proposed formula is better than the Wirsching or Dirlik ones, and simple to compute.

B.5 Triangle Spectral shape

Swell peaks are much narrower than the wind sea peaks that may be observed in the North Sea. In average, they will be all the more narrow as the swell generation occurs very remotely. Modeling such narrow peaks by a Jonswap shape implies to have γ take much higher values than those in the commonly used range of 1 to 7. Very high values of γ for swell are somewhat in contradiction with the construction of the Jonswap shape, where that parameter is used to reflect the non-saturation of a fetch-limited wind sea whereas swell corresponds to the part of energy that propagated onto the location of observation, and they lead to a risk of unnoticed numerical accuracies in the practical computations. Similarly, high values of λ in the Wallops model narrow the peak, but do not cut-off the tail of the spectrum.

Because the propagation is not supposed to provide energy outside of a finite frequency interval, and in order to keep the complexity of the fitting and reconstruction processes within reasonable limits, a triangle shape was proposed, and devised in a way recalled in Appendix D of the report on Phase II.

For the sake of simplicity, the triangle was chosen within the triangular family of triangles extending from $\frac{\mu-1}{\mu}f_p$ to $\frac{\mu}{\mu-1}f_p$ and parameterized by the value μ :

$$\begin{aligned} S(f) &= \frac{2\mu(\mu-1)}{2\mu-1} \frac{H_s^2}{16f_p} \left(\mu \frac{f}{f_p} - (\mu-1) \right) & \frac{\mu-1}{\mu}f_p < f < f_p \\ S(f) &= \frac{2\mu(\mu-1)}{2\mu-1} \frac{H_s^2}{16f_p} \left(\mu - (\mu-1) \frac{f}{f_p} \right) & f_p < f < \frac{\mu}{\mu-1}f_p \\ S(f) &= 0 & elsewhere \end{aligned}$$

Spectral moments are given by:

$$m_p = \frac{H_s^2}{16} f_p^p \frac{2(\mu^{p+1} - (\mu-1)^{p+1})(\mu^{p+2} - (\mu-1)^{p+2})}{(p+1)(p+2)(2\mu-1)\mu^p(\mu-1)^p} \quad (46)$$

and thus

$$\begin{aligned} m_0 &= \frac{H_s^2}{16} \\ m_1 &= \frac{H_s^2}{16} f_p \left(1 + \frac{1}{3\mu(\mu-1)} \right) \\ m_2 &= \frac{H_s^2}{16} f_p^2 \left(1 + \frac{1}{3\mu(\mu-1)} \right) \left(1 + \frac{1}{2\mu(\mu-1)} \right) \\ m_4 &= \frac{H_s^2}{16} f_p^4 \left(1 + \frac{1}{\mu(\mu-1)} + \frac{1}{5\mu^2(\mu-1)^2} \right) \left(1 + \frac{1}{\frac{3}{4}\mu(\mu-1)} + \frac{1}{3\mu^2(\mu-1)^2} \right) \end{aligned}$$

$$\begin{aligned}
Q_p &= \frac{2}{M_0^2} \int_0^\infty f S^2(f) df \\
&= \frac{4\mu-2}{3}
\end{aligned}$$

The reduction from narrow-band damage can be computed using the empirical formula:

$$D_{Triangle}(\mu) = D_{NB}(1 - \max(0, (0.0116k - 0.0085) * (1 - \ln(\ln(\mu)))))) \quad (47)$$

Based on the same comparison with 2920 simulations of 3 hours sea states as previously, this formula provides mean biases and errors displayed in table 21.

Formula	bias (%)	RMS Error (%)	Max underest.(%)	Max overest.(%)
This report	0.0	0.4	1.3	1.8
Wirsching	-1.4	1.9	4.7	2.5
Dirlik (1)	0.2	0.4	2.6	1.6
Dirlik (2)	0.2	0.9	3.3	1.3

Table 21: Comparison of formulas to simulation over the range μ 1.5 to 15 and k 1 to 5

On the opposite from what is observed for a Jonswap or Wallops spectrum, for a triangle shape where there is no cut-off frequency problem and where the spectral moments can be calculated in closed-form, the theoretical value gives better results than the estimated one. Again, the proposed formula is better than the Wirsching or Dirlik ones, and simpler to compute.

B.6 Power or Log-Triangle Spectral shape

An attractive idea is to model separately the main body and the tail of the spectrum. The tail of the spectrum decreasing with power p can then be represented by a triangle in log coordinates:

$$\begin{aligned}
S(f) &= 0 & f < f_p \\
S(f) &= \frac{H_s^2}{16f_p} (p-1) \left(\frac{f}{f_p}\right)^{-p} & f \geq f_p
\end{aligned}$$

Spectral moments are given by:

$$m_i = \frac{H_s^2}{16} f_p^i \frac{p-1}{p-i-1} \quad (48)$$

and thus

$$\begin{aligned}
m_0 &= \frac{H_s^2}{16} \\
m_1 &= \frac{H_s^2}{16} f_p \frac{p-1}{p-2} \\
m_2 &= \frac{H_s^2}{16} f_p^2 \frac{p-1}{p-3} \\
m_4 &= \frac{H_s^2}{16} f_p^4 \frac{p-1}{p-5}
\end{aligned}$$

$$\begin{aligned}
Q_p &= \frac{2}{M_0^2} \int_0^\infty f S^2(f) df \\
&= p-1
\end{aligned}$$

The reduction from narrow-band damage can be computed using the empirical formula:

$$D_{Power}(p) = D_{NB}(1 - e^{-0.032(0.6p-10k+105)}) \quad (49)$$

Based on the same comparison with 2920 simulations of 3 hours sea states as previously, this formula provides mean biases and errors displayed in table 22. It may be noted that the Wirsching and Dirlik formulas are affected by the non-robustness of spectral moments estimation, especially for slowly decreasing spectral tails.

Formula	bias (%)	RMS Error (%)	Max underest.(%)	Max overest.(%)
This report	0.0	0.4	0.6	1.4
Wirsching	1.9	2.6	2.9	6.4
Dirlik (1)	-2.1	2.9	13.4	6.4
Dirlik (2)	-4.6	6.3	14.5	2.8

Table 22: Comparison of formulas to simulation over the range p 5.1 to 10 and k 1 to 5

Summary

The formulas are summarised hereafter for $1 < k \leq 5$:

Jonswap	$\alpha \frac{g^2}{(2\pi)^5} f^{-5} e^{-\frac{5}{4} \left(\frac{f}{f_p}\right)^{-4}} \gamma \exp\left(-\frac{\left(1-\frac{f}{f_p}\right)^2}{2\sigma^2}\right)$	$\sigma = 0.07$ for $f < f_p$ $\sigma = 0.09$ for $f \geq f_p$	$D(\gamma) = D_{NB}(1 - \max(0, 0.0103 \ln(k)(5 - \ln(\gamma))))$	$1 \leq \gamma \leq 15$
Wallops	$K \frac{H_s^2}{T_z^4} \left(\frac{f_p}{f}\right)^{4\lambda+1} e^{-\frac{4\lambda+1}{4} \left(\frac{f_p}{f}\right)^4}$		$D(\lambda) = D_{NB}\left(1 - \max\left(0, \frac{5k+2}{300} \frac{\lambda \frac{\ln(k)}{3}}{\lambda^{\frac{4}{3}}}\right)\right)$	$0.8 \leq \lambda \leq 8$
Triangle	$\frac{2\mu(\mu-1)}{2\mu-1} \frac{H_s^2}{16f_p} \left(\mu \frac{f}{f_p} - (\mu-1)\right)$ $\frac{2\mu(\mu-1)}{2\mu-1} \frac{H_s^2}{16f_p} \left(\mu - (\mu-1) \frac{f}{f_p}\right)$ 0	$\frac{\mu-1}{\mu} f_p < f < f_p$ $f_p < f < \frac{\mu}{\mu-1} f_p$ elsewhere	$D(\mu) = D_{NB}(1 - \max(0, (0.0116k - 0.0085) * (1 - \ln(\ln(\mu)))))$	$1.5 \leq \mu \leq 15$
Powertail	0 $\frac{H_s^2}{16f_p} \frac{1}{p} \left(\frac{f}{f_p}\right)^{-p}$	$f < f_p$ $f \geq f_p$	$D(p) = D_{NB}(1 - e^{-0.032(6p-10k+105)})$	$5 < p \leq 10$

C Parametric Damage for Double slope S-N curve

C.1 Introduction

The Palmgren-Miner hypothesis together with a linear Wöhler S-N curve of slope $-k$ imply that each cycle of range S in the loading history creates some elementary fatigue damage $\frac{S^k}{K}$ in the structural detail of interest, and that failure occurs when accumulated damage is about 1.

The rules of Classification Societies often require to consider a double-slope S-N curve, *i.e.*

$$\begin{aligned} d_{k_1 k_2}(S) &= \frac{1}{K S_0^{k_2 - k_1}} S^{k_2}, & S \leq S_0 \\ &= \frac{1}{K} S^{k_1}, & S \geq S_0 \end{aligned}$$

$$\begin{aligned} s &= \frac{S}{2\sigma} \\ s_0 &= \frac{S_0}{2\sigma} \\ d_{k_1 k_2}(s) &= \frac{1}{K s_0^{k_2 - k_1}} (2\sigma)^{k_1} s^{k_2}, & s \leq s_0 \\ &= \frac{1}{K} (2\sigma)^{k_1} s^{k_1}, & s \geq s_0 \end{aligned}$$

With respect to a single slope S-N curve where the cumulated damage is just the k^{th} moment of the statistical distribution of ranges, the double-slope definition introduces significant additional complexity due to the threshold value. For instance, the effect of multiplying the load signal by a constant value C is a straightforward multiplication by C^k for a single slope damage, but much more complex in the double-slope case where ranges are then moved from one side of the threshold to the other.

Gao and Moan ([3]) have been able to verify that combination formulas could still be used with reasonable accuracy when the loading signal is the combination of two narrow-band Gaussian processes. In practice, that assumption is more restrictive than one could expect. On one hand, many encountered narrow-band signals are so narrow that the Gaussian assumption is no longer fully valid. The Rayleigh distribution used for ranges in those cases shows a large excess of high amplitude cycles with respect to reality, and the k_1 - and k_2 -order statistical moments of the actual distributions of the cycles are no longer in the same proportions as for a Rayleigh.

On the other hand, one may need to combine components that are not all narrow-band, for instance at the last stages when using the ICA method with more than two components, and the distribution of the rainflow counted cycles of a broadband signal differs significantly from a Rayleigh, showing a large excess of very small cycles.

We aim here at finding ways to estimate the double slope rainflow damage, in a slightly conservative manner, by combining the single slope damages and we will assume that the loading signal is a gaussian process with variance σ^2 .

We will mainly investigate the case where $k_1 = 3$ and $k_2 = 5$, but other values of these slopes can be treated in a similar fashion. We consider that we know (from the ICA method for multimodal power spectra, see Appendix A, from semi-empirical formulas such as Wirsching, Dirlik, or the ones proposed in Appendix B for unimodal ones) how to compute the damage for a S-N curve with single slope k_1 or k_2 .

C.2 Double-slope damage computation

The damage density can be computed as:

$$\begin{aligned} D_{35} &= \frac{\nu_{24}}{K s_0^5} (2\sigma)^5 \int_0^{s_0} s^5 p(s) ds + \frac{\nu_{24}}{K} (2\sigma)^3 \int_{s_0}^{\infty} s^3 p(s) ds \\ &= D_{5l} + D_{3u} \end{aligned} \tag{50}$$

One may thus try to find best estimates for each of the terms. Conventionally, such estimates rely on the narrow bandwidth approximation, and their quality and degree of conservatism or non-conservatism cannot be guaranteed for wide-band loading signals. However, as we will discuss further, the narrow-band approximation is in all cases a sensible one for the largest ranges of a process, even when it is broad-band. We thus prefer the following formula:

$$\begin{aligned} D_{35} &= \frac{\nu_{24}}{K s_0^5} (2\sigma)^5 \int_0^{\infty} s^5 p(s) ds - \frac{\nu_{24}}{K s_0^5} (2\sigma)^5 \int_{s_0}^{\infty} s^5 p(s) ds + \frac{\nu_{24}}{K} (2\sigma)^3 \int_{s_0}^{\infty} s^3 p(s) ds \\ &= D_5 - D_{5u} + D_{3u} \end{aligned} \tag{51}$$

The above formula takes a negative D_{5u} and a positive D_{3u} correction to D_5 . It should be used when slope 5 gives the major contribution to the damage. The negative correction term compensates for the damage of the ranges above the threshold, that are counted with exponent 3 by the positive correction term and should thus be removed from the count with exponent 5.

In order to be able to compute those corrections easily and conservatively, one can use a best approximation for D_5 , an upper bound for D_{3u} , and a best approximation or a lower bound for D_{5u} . Those corrections should be sought in the form of functions of D_3 and D_5 and of S_0 and of the spectral parameters (moments). As stated in the introduction, D_5 (and D_3) can be estimated using the ICA or some other method.

If a best approximation is used for D_{5u} (or $D_{3u} = D_3 - D_{3l}$), then the final result is likely but not guaranteed to be conservative, whereas if a lower bound is used, the result is definitely conservative but may be overly so.

C.3 Approximations

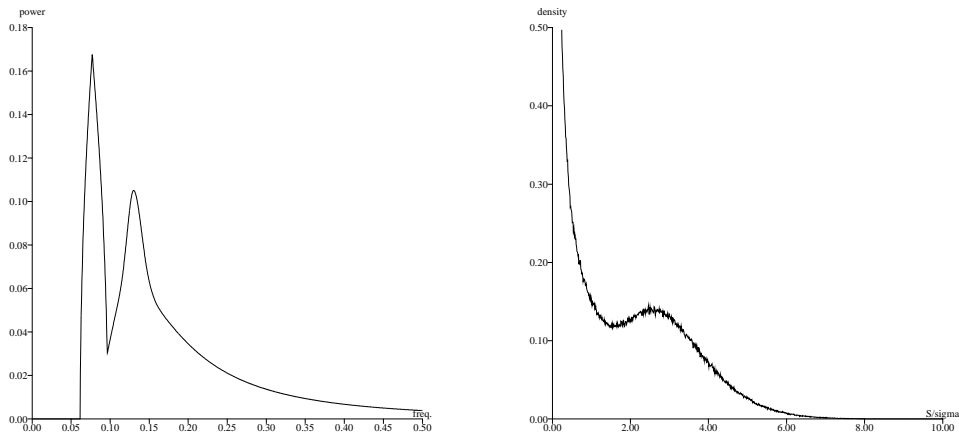


Figure 18: Power spectrum (left) and rainflow ranges density (right) of the loading signal used for illustration

For the sake of illustration, we use in the following a spectrum made of a triangle at 13 seconds representing the response to swell and a Jonswap with $\gamma = 3$ at 7.7 seconds representing that to wind sea, as shown on figure 18. It can be seen that the ranges density is not globally close to a Rayleigh distribution, and that is all the more true when further components (peaks) are added to the load power spectral density.

The incomplete Gamma functions can thus not be used directly to estimate the proportions of damage coming from above and below the threshold as could be if the loading was narrow-banded.

C.3.1 Damage of largest ranges D_{ku}

Rainflow-filtering with a threshold at the S-N curve angle point allows to extract the rainflow ranges above that threshold. The essential point in this section is that considering the S_0 -rainflow-filtered process of the turning points of the load history and assuming that S_0 is sufficiently large, we can approximate it by S_0 -rainflow-filtering the history obtained by the zero-crossing counting method. Though it may be difficult to find an explicit expression for it, we can assume as in [9] that the remaining turning points are

the turning points of a “phantom” gaussian process. Since the latter phantom process is narrow-band, we can use a Rayleigh model for the distribution of its turning points whereas we could not for the original one.

We then have

$$\frac{D_{ku}}{D_k} \approx Q\left(\frac{k}{2} + 1, \frac{s_0^2}{2}\right) \quad (52)$$

where Q is the upper regularized Gamma function and D_k^* is the overall damage of the phantom zero-crossing process.

C.3.2 D_{ku}

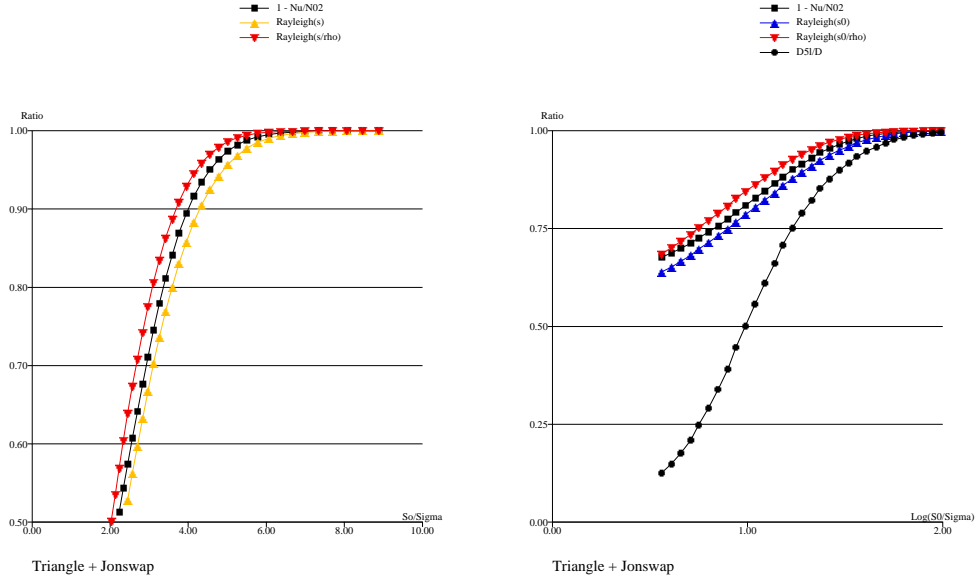


Figure 19: Cumulative distribution of largest rainflow ranges and Rayleigh approximation

For a narrow-band process, it is well-known that the min-max counting is unconservative with respect to rainflow, i.e. that it provides a lower bound to the rainflow damage, whereas the doubled turning-points amplitudes (excursions from the mean), or the narrow-band approximation counting is always conservative with respect to rainflow, as shown by Rychlik (1993).

Considering zero-crossing cycles or waves with a narrow-band spectrum, the min-max amplitudes can be derived from the doubled turning-points amplitudes using a reducing ratio ρ that depends on the value $r\left(\frac{T}{2}\right)$ of the normalized autocorrelation function at half the dominant (here, zero-crossing) period [13, 12].

$$\rho = \sqrt{\frac{1 - r\left(\frac{T}{2}\right)}{2}}$$

We know that $r\left(\frac{T}{2}\right)$ is negative, so a definite lower bound for ρ is $\frac{1}{\sqrt{2}}$ and then

$$D_{ku} \geq Q\left(\frac{k}{2} + 1, t_0\right) 2^{-\frac{k}{2}} D_k$$

Applying that ratio to the rainflow amplitudes instead of the doubled turning-points amplitudes guarantees also a lower bound to the rainflow damage. However, that lower bound may be too coarse, and

thus provide results that are too conservative. For instance, for a unimodal shape, empirical relationships are:

$$\begin{aligned}
\rho_{Jonswap} &= 0.9 + 0.025 \text{Log}(\gamma) \\
\rho_{Wallops} &= 0.9 + 0.050 \text{Log}(\lambda) \\
\rho_{Triangle} &= (\text{Log}(\text{Log}(1 + \mu)))^{0.03} \\
\rho_{Powertail} &= (\text{Log}(\text{Log}(p)))^{0.096}
\end{aligned}$$

and thus $\rho > 0.9$ as soon as $\gamma > 1$ (Jonswap), $\lambda > 1$ (Wallops), $\mu > 1.75$ (Triangle) or $p > 4.25$ (Powertail).

A better approximation for ρ is obtained by computing the auto-correlation function by applying inverse Fourier transform to the (combined in case of multimodal) spectrum. The auto-correlation function can also be computed directly on the time-signal when that signal is obtained by a time-domain simulation.

It should however be noted that if the spectrum is very narrow, the process may no longer be gaussian (it can be close to a noisy sinewave, for instance), and ρ will not provide a sufficient reduction to account for the modelling bias. We thus advise to restrain ρ to a maximum value of 0.95 or not accept $r\left(\frac{T}{2}\right)$ to be lower than -0.8 so as to bypass this modelling difficulty.

Denoting N_u the number of ranges above S_0 , it can be seen on Figure 19 that the distribution of the largest rainflow ranges is indeed between that of the doubled amplitudes and of the min-max (crest-trough) ranges of the phantom process, which are Rayleigh distributed and in a number of N_{02} corresponding to the zero-crossing period of the process.

The bounding might loose its validity if the threshold is not sufficiently high and if the distribution of ranges thus diverts too much from a Rayleigh. Yet, for practical applications, we would not expect that threshold to be less than twice the standard deviation of the loading signal, *i.e.* the number of ranges below the threshold not less than twice the number of ranges above it. As can be seen on figure 19, damage is in the proportion 20%/80% for slopes 5 and 3 respectively when that threshold value is used. From the above considerations about min-max, rainflow and doubled-peaks amplitudes, the following bounding can be derived for sufficiently large ranges:

$$\frac{s}{\rho} e^{-\frac{1}{2}\left(\frac{s}{\rho}\right)^2} \leq p(s|s > s_0) \leq s e^{-\frac{1}{2}s^2} \tag{53}$$

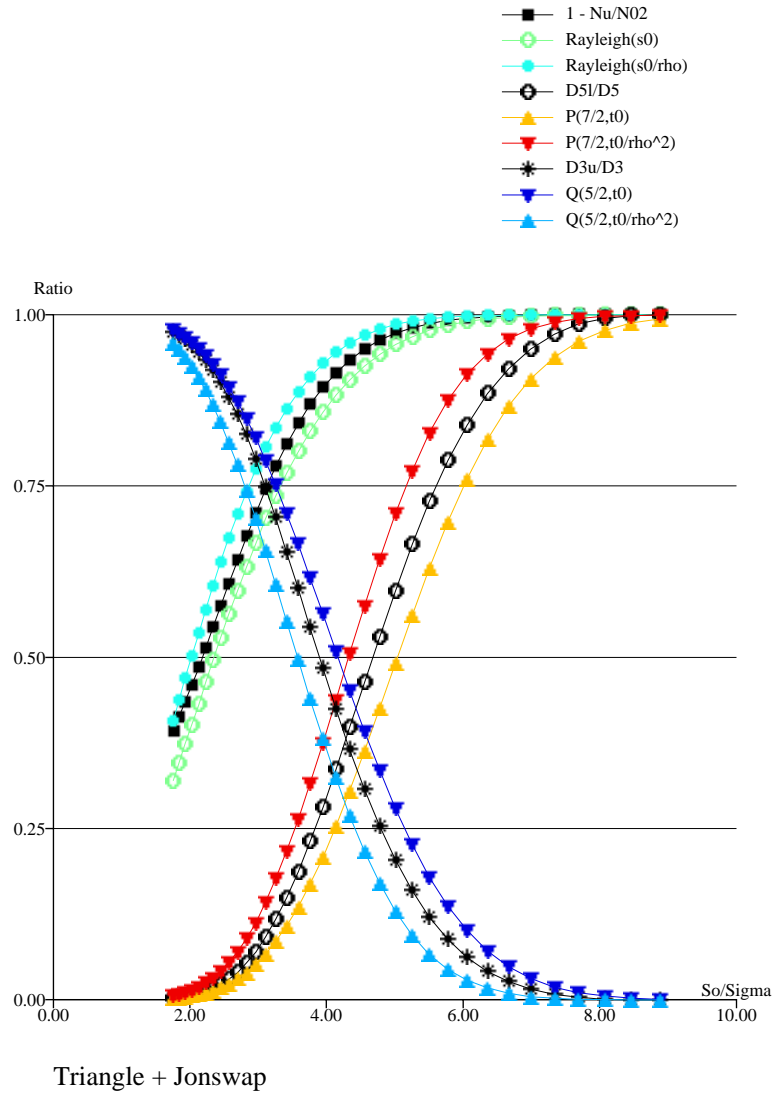


Figure 20: Application of the formulas in 52 and 53 to the practical example with slopes 3 and 5

We can also derive an approximation for $p(s|s > s_0)$ by taking the mid-point of the arguments to the exponential:

$$p(s|s > s_0) \approx \frac{s}{\phi} e^{-\frac{1}{2}\left(\frac{s}{\phi}\right)^2} \quad (54)$$

with

$$\begin{aligned} \frac{1}{\phi^2} &= \frac{1}{2} \left(\frac{1}{\rho^2} + 1 \right) \\ \phi &= \sqrt{\frac{2-2r\left(\frac{r}{2}\right)}{3-r\left(\frac{r}{2}\right)}} \end{aligned}$$

Thus,

$$\begin{aligned}
D_{ku} &\gtrsim Q\left(\frac{k}{2} + 1, \frac{s_0^2}{2\rho^2}\right) D_k \\
D_{ku} &\approx Q\left(\frac{k}{2} + 1, \frac{s_0^2}{2\phi^2}\right) D_k \\
D_{ku} &\lesssim Q\left(\frac{k}{2} + 1, \frac{s_0^2}{2}\right) D_k
\end{aligned} \tag{55}$$

C.4 Estimates for total damage - Summary

Taking the above estimates and bounds into the equations, we obtain:

$$\begin{aligned}
D_{35} &\approx D_5 P\left(\frac{7}{2}, \frac{t_0}{\phi^2}\right) + D_3 Q\left(\frac{5}{2}, \frac{t_0}{\phi^2}\right) \\
&\lesssim D_5 P\left(\frac{7}{2}, \frac{t_0}{\rho^2}\right) + D_3 Q\left(\frac{5}{2}, \frac{t_0}{\phi^2}\right) \\
&\lesssim D_5 P\left(\frac{7}{2}, \frac{t_0}{\phi^2}\right) + D_3 Q\left(\frac{5}{2}, t_0\right) \\
&< D_5 P\left(\frac{7}{2}, \frac{t_0}{\rho^2}\right) + D_3 Q\left(\frac{5}{2}, t_0\right)
\end{aligned}$$

More generally:

$$\begin{aligned}
D_{k_1 k_2} &\approx D_{k_2} P\left(\frac{k_2}{2} + 1, \left(\frac{S_0}{2\phi\sigma\sqrt{2}}\right)^2\right) + D_{k_1} Q\left(\frac{k_1}{2} + 1, \left(\frac{S_0}{2\phi\sigma\sqrt{2}}\right)^2\right) & (a) \\
&\lesssim D_{k_2} P\left(\frac{k_2}{2} + 1, \left(\frac{S_0}{2\rho\sigma\sqrt{2}}\right)^2\right) + D_{k_1} Q\left(\frac{k_1}{2} + 1, \left(\frac{S_0}{2\phi\sigma\sqrt{2}}\right)^2\right) & (b) \\
&\lesssim D_{k_2} P\left(\frac{k_2}{2} + 1, \left(\frac{S_0}{2\phi\sigma\sqrt{2}}\right)^2\right) + D_{k_1} Q\left(\frac{k_1}{2} + 1, \left(\frac{S_0}{2\sigma\sqrt{2}}\right)^2\right) & (c) \\
&< D_{k_2} P\left(\frac{k_2}{2} + 1, \left(\frac{S_0}{2\rho\sigma\sqrt{2}}\right)^2\right) + D_{k_1} Q\left(\frac{k_1}{2} + 1, \left(\frac{S_0}{2\sigma\sqrt{2}}\right)^2\right) & (d)
\end{aligned} \tag{56}$$

where Q is the regularized upper Gamma function and $P = 1 - Q$ the regularized lower Gamma function.

ρ and ϕ were defined from the value $r\left(\frac{T_{02}}{2}\right)$ of the normalized autocorrelation function of the loading signal at half the zero-crossing period:

$$\begin{aligned}
\rho &= \sqrt{\frac{1 - r\left(\frac{T_{02}}{2}\right)}{2}} \\
\phi &= \sqrt{\frac{2 - 2r\left(\frac{T_{02}}{2}\right)}{3 - r\left(\frac{T_{02}}{2}\right)}}
\end{aligned}$$

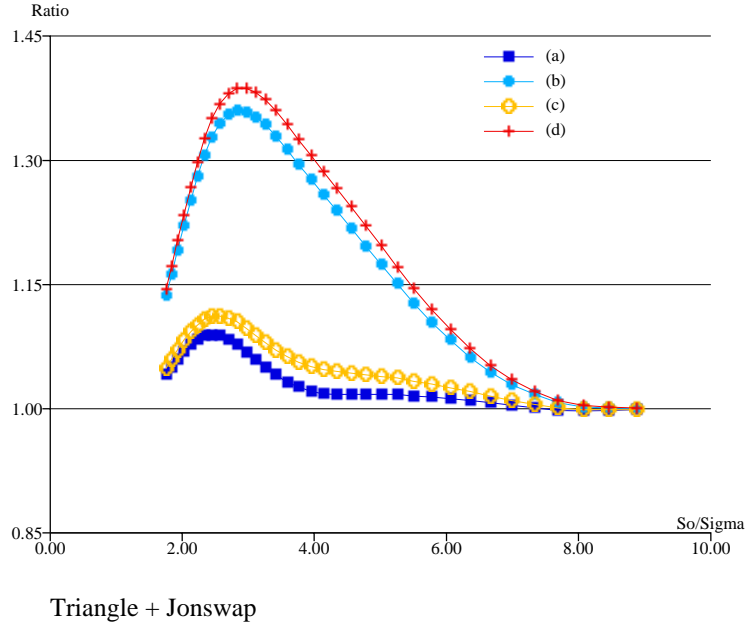


Figure 21: Levels of conservatism of formulas in 56 in the practical example

The results are displayed on figure 21. We recommend to use formula (d) to ensure conservatism, especially since the actual loading processes may divert somewhat from the Gaussian process model and since high order moments are very sensitive to such differences.

C.5 Application to the full computation

Let us consider the FPSO case of the study. In that case, the field data consists of 8040 sea states, 6825 of which are multimodal. The corresponding response spectra (Vertical Wave Bending Moment at midship) have been modelled by combinations of triangles on one hand, and of Jonswap spectra on the other. Triangles represent narrow-band components at all times, whereas Jonswap spectra are often wide-band when they model the part of the response that corresponds to wind sea action.

For each sea state, the double slope and single slope damages have been computed by simulating 50 3-hour histories. Figure 22 compares the total damages summed up over the whole database obtained by recombining the single slope damages in each sea state according to formulas in (56) to the total damage computed directly with a double slope S-N curve. In the study, the SCF had to be exaggerated to 4 in order to make fatigue significant, resulting in a value of $\frac{S_0}{\sigma}$ of about 6 when considering a global σ for the set of sea states actually contributing to fatigue.

The afore-mentioned limitation of $r\left(\frac{T_{02}}{2}\right)$ to -0.8 has been applied. If it were not, the triangle modeling especially would lead to a great deal of conservatism, up to 5 times, because of the overestimation of the large low frequency (swell response) amplitudes by a Rayleigh distribution.

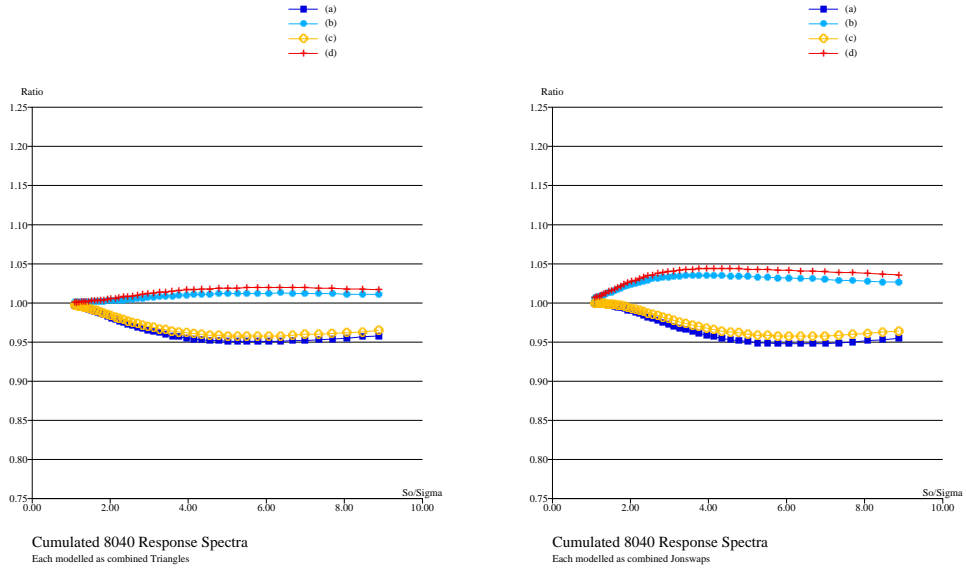


Figure 22: Application of formulas in (56) to the field data in a West Africa climate case (left: Triangles, right: Jonswaps)

One might wonder if the formulas in 56 could be applied at the last stage of the computation only, with an overall averaged value of $r\left(\frac{T_{02}}{2}\right)$. From the tests that we made, we obtain very high levels of conservatism, up to more than 5 for $\frac{S_0}{\sigma}$ between 4 and 6: the overall (non-stationary) process, even when time-scaled with the local T_{02} so as to enable computation of $r\left(\frac{T_{02}}{2}\right)$, is too far from the Gaussian process assumption to be suited to the use of the formulas as such.

C.6 Conclusions

As can be seen on figure 22, it is possible to estimate a double slope S-N curve damage from the single slope ones with reasonable conservatism using the value of the normalized autocorrelation function of the loading signal at half the zero-crossing period and the regularized upper and lower Gamma functions. This allows to use combination formulas such as the ICA one in a double slope S-N curve case just as if the S-N curve had a single slope.

D Response spectra partition

Each response spectrum is partitioned into several "systems" fitted to Triangle or Jonswap spectral shape; The partition involves the following steps:

1. *Systems isolating*: This first step consists in extracting the distinct components of the response spectrum. The method used for this process is the watershed method which treats a 2D spectrum like a reversed topography. The peaks in an upside-down directional spectrum are then found by following the paths of strongest gradient leading to a same point. The Matlab routine watershed is used. Since the response spectrum is a frequency (1D) spectrum, the preliminary step consists in creating a fake 2D spectrum from the response spectrum. Next, watershed image segmentation algorithm is applied to identify the systems composing the spectra.
2. *Systems grouping*: Because of the sensitivity of the extraction method, all the isolated spectral components are not consistent wave systems and can be regarded as noise. Next stage of analysis consists in gathering meaningless components into physically valid wave systems. The used method states that two spectral components are merged if they satisfy two separate conditions about the gaps between the peak frequencies and the peak frequency directions. The overlapping is taken into account in the next steps of the analysis, by computing the cross-influence of the components. Every extracted subset of the spectrum can then be considered as an isolated response system. The 3 peaks with the most energy are kept for the analysis.
3. *Systems fitting*: The aim is to fit the response spectrum with a Jonswap shape, either by minimizing the square error between the original spectrum and the fit, or by fitting of a triangle shape fit is given either by minimizing the square error between the original spectrum and the fit. An example

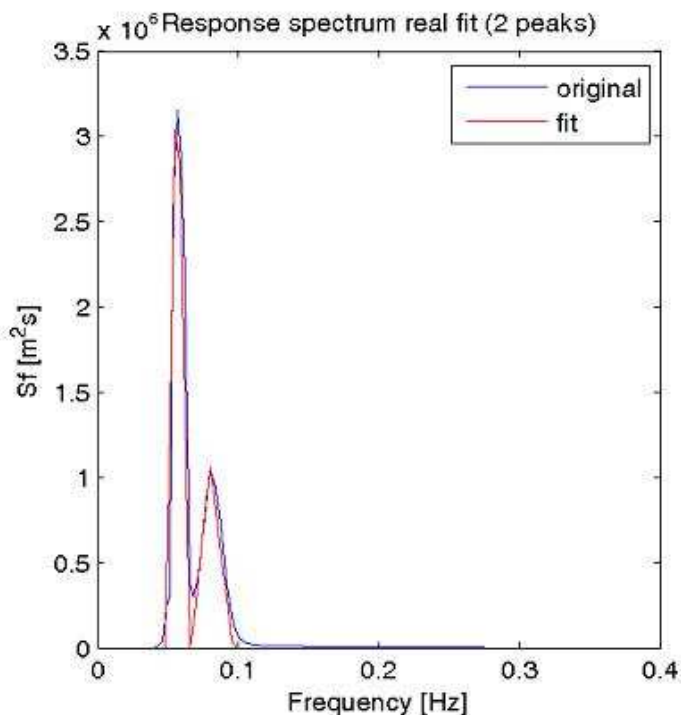
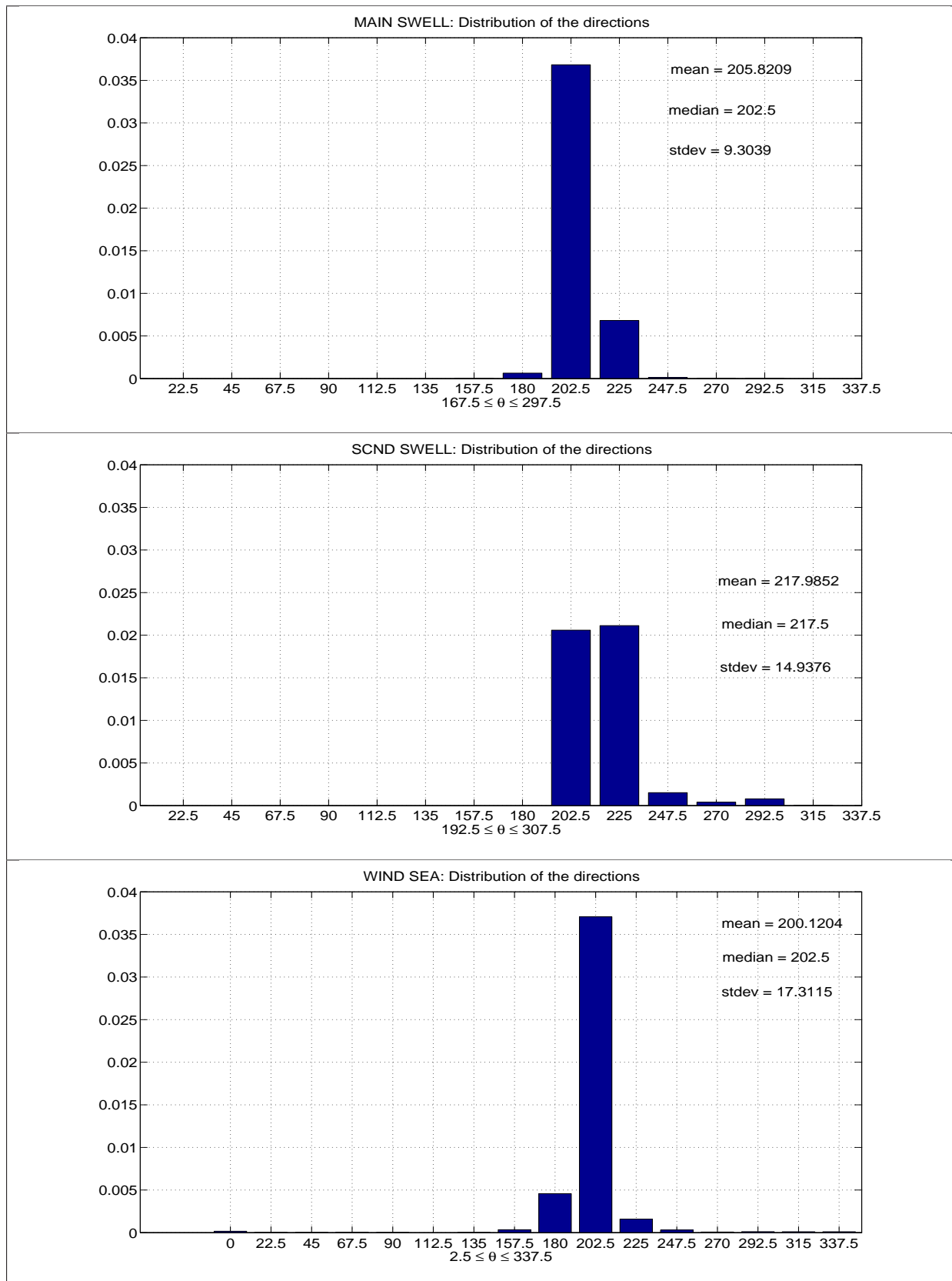


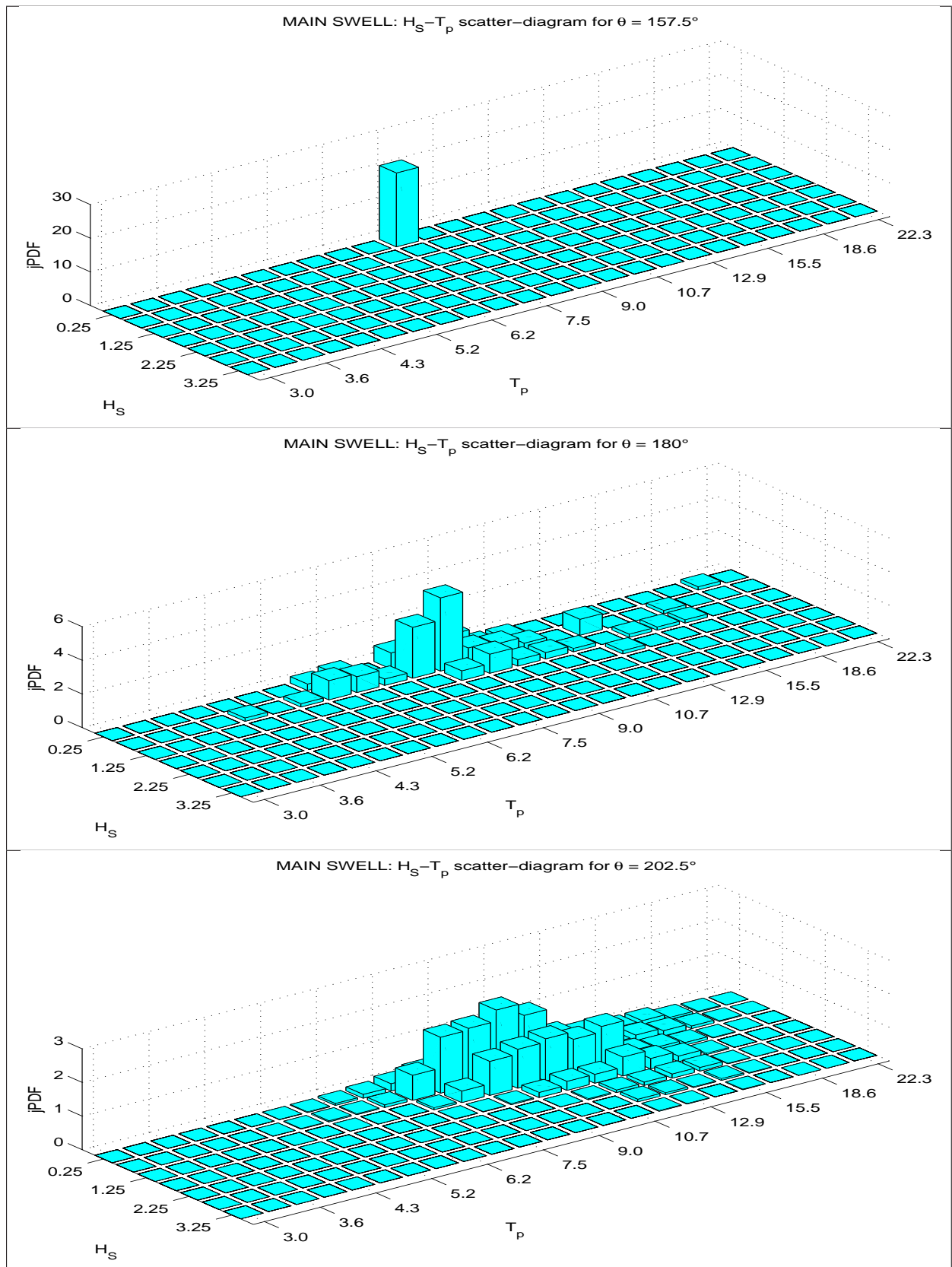
Figure 23: Girassol real spectra response (original and fit)

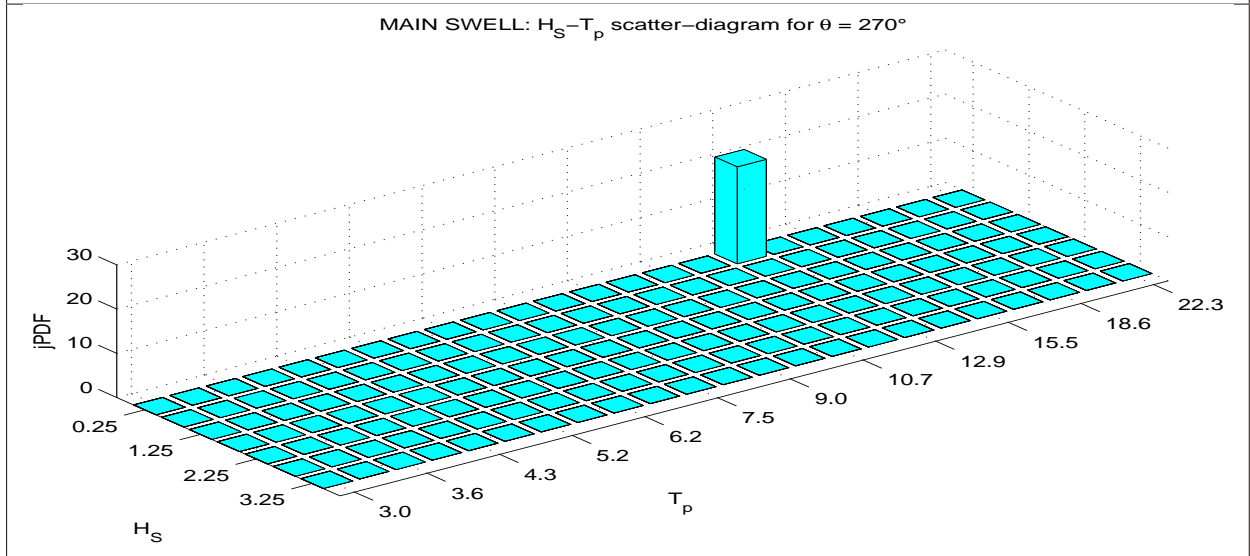
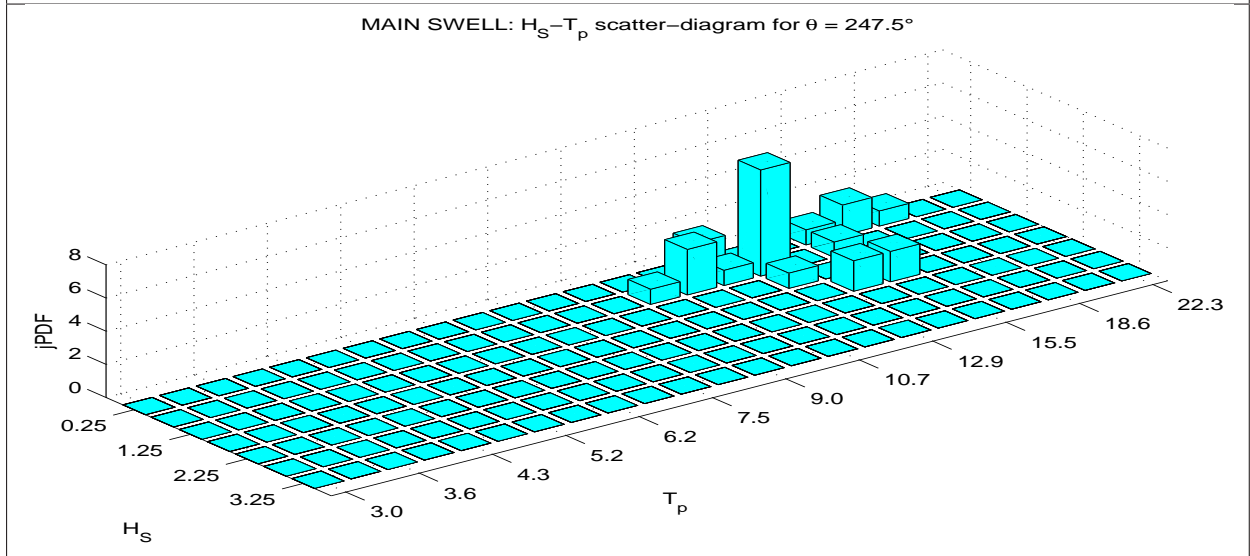
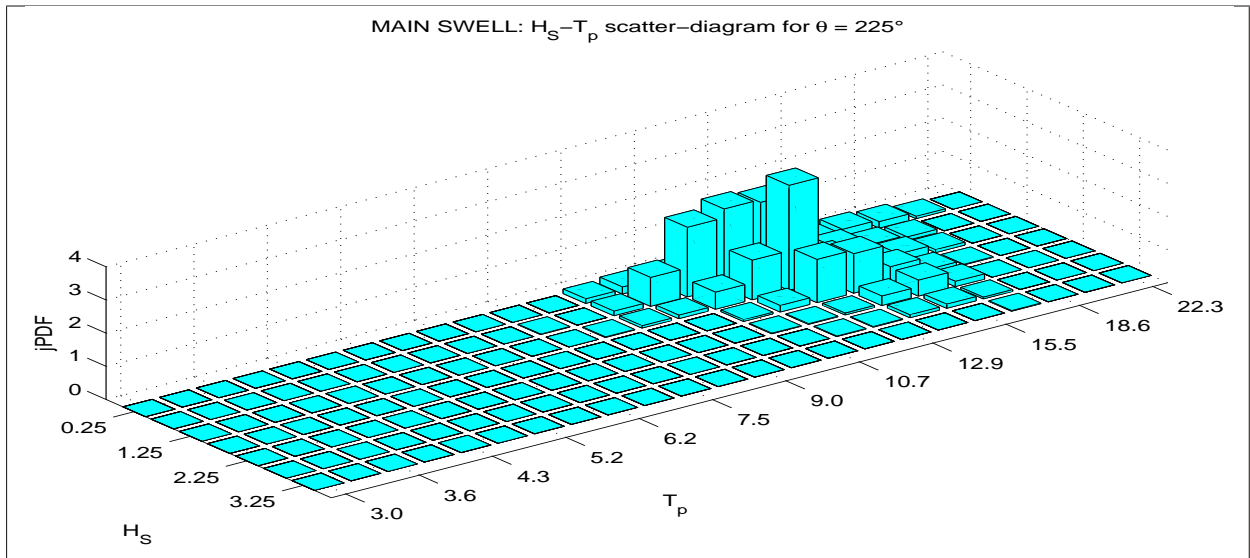
E Joint distribution of spectral parameters

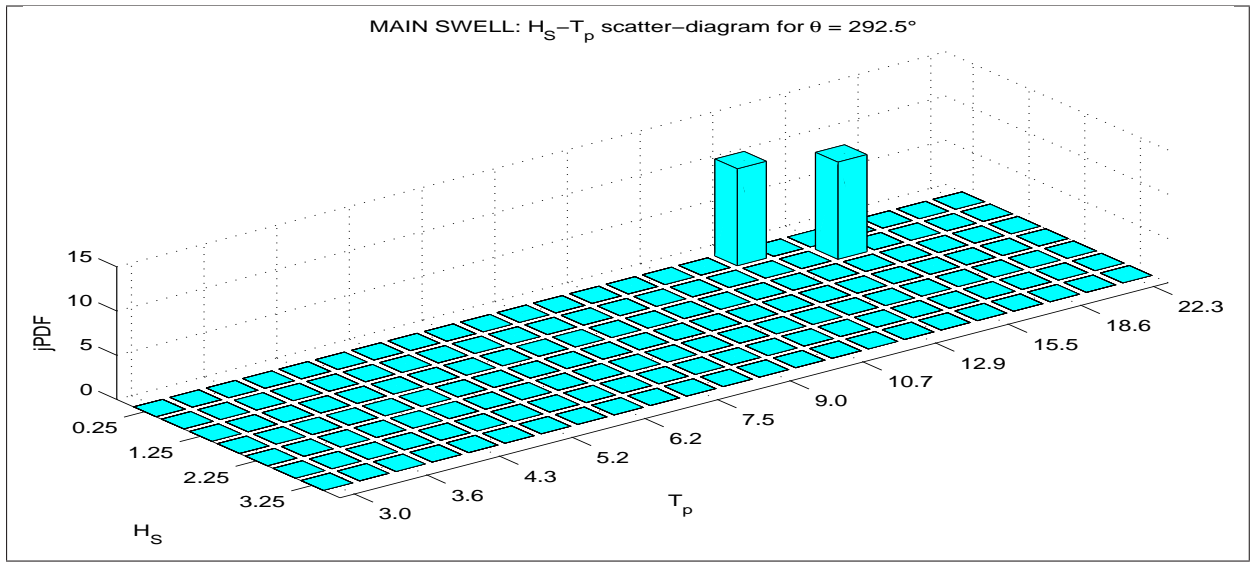
Distribution of the directions



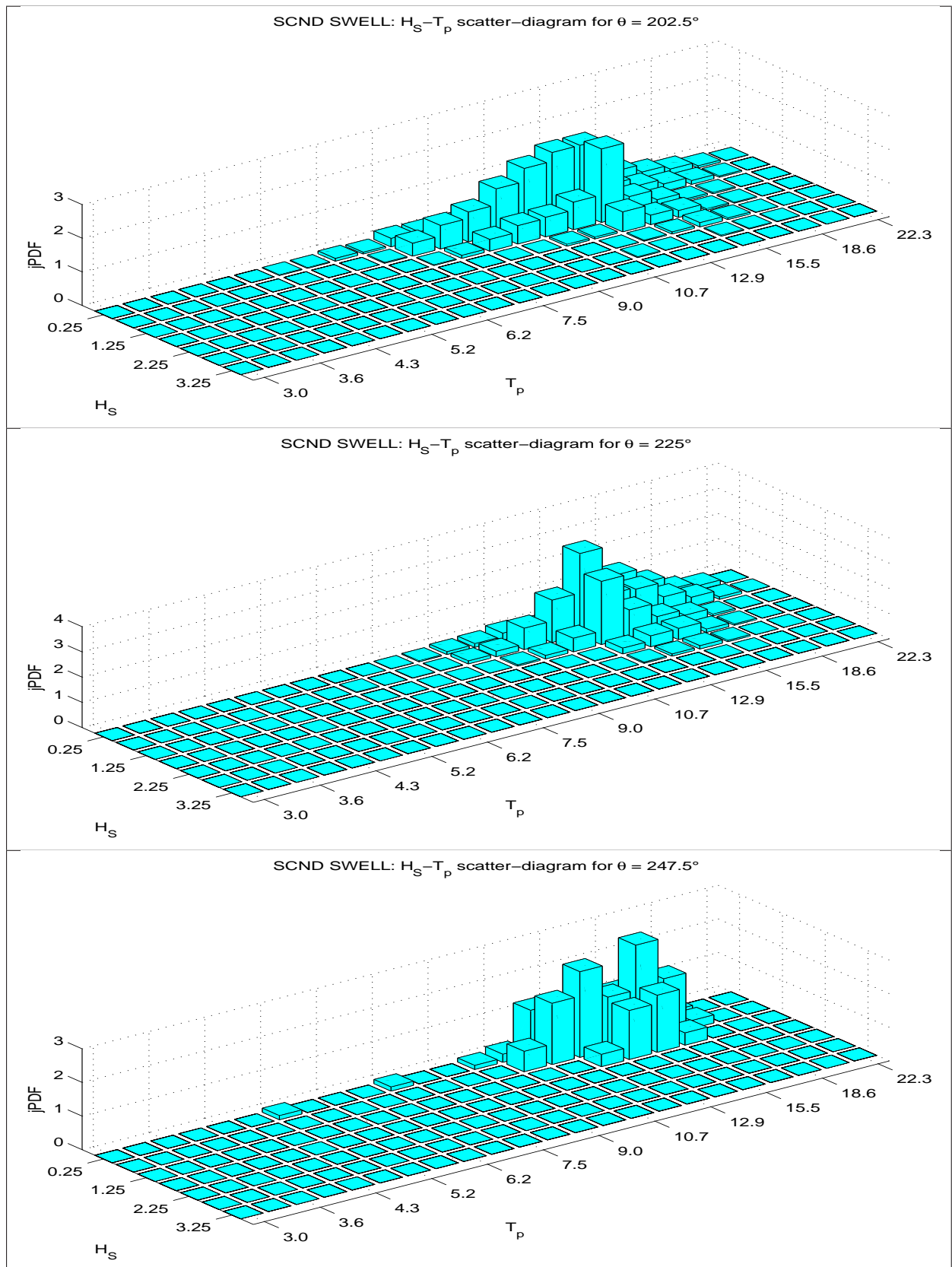
Directional $H_S - T_p$ scatter diagrams for Main Swell

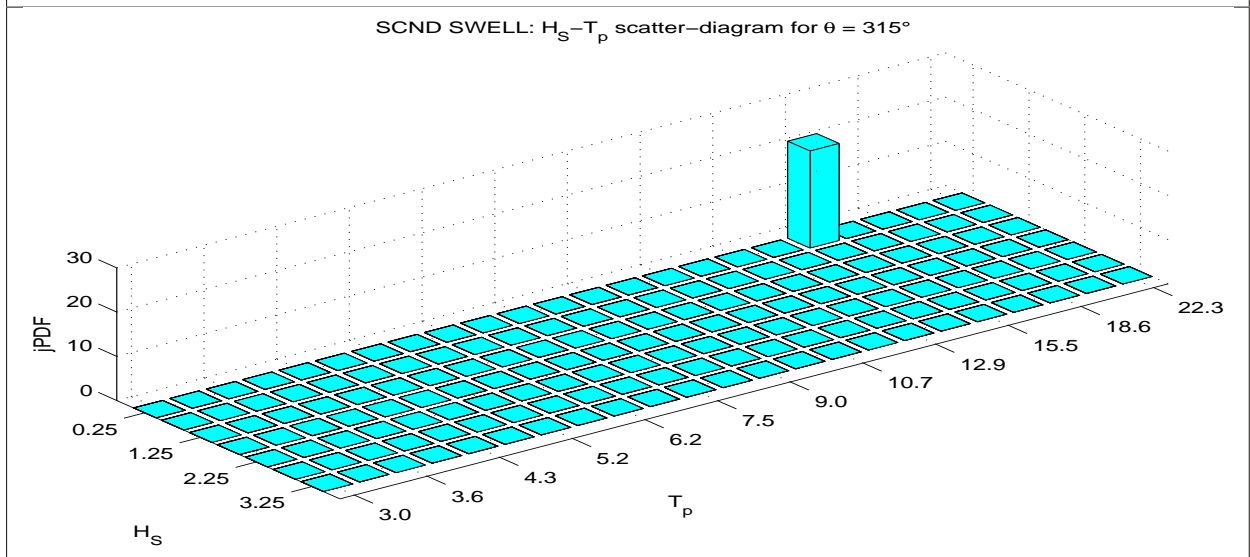
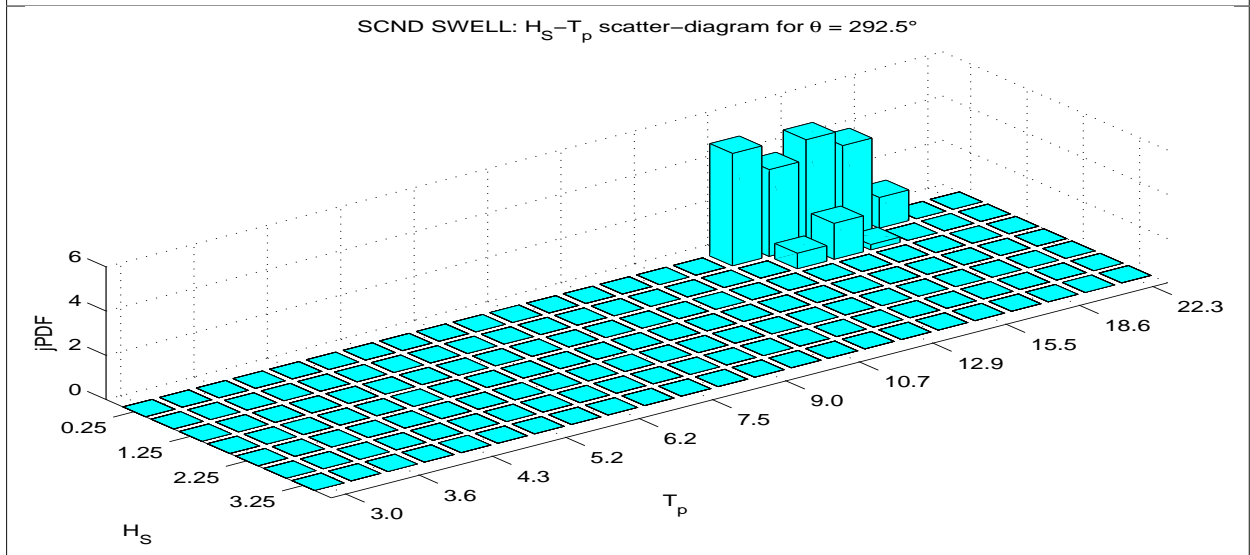
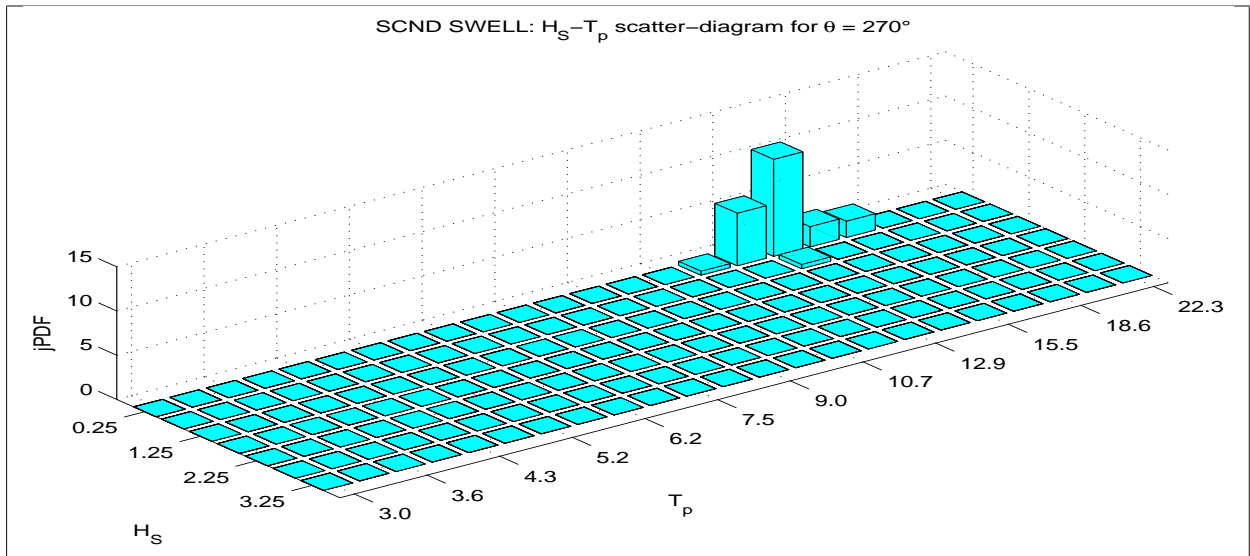




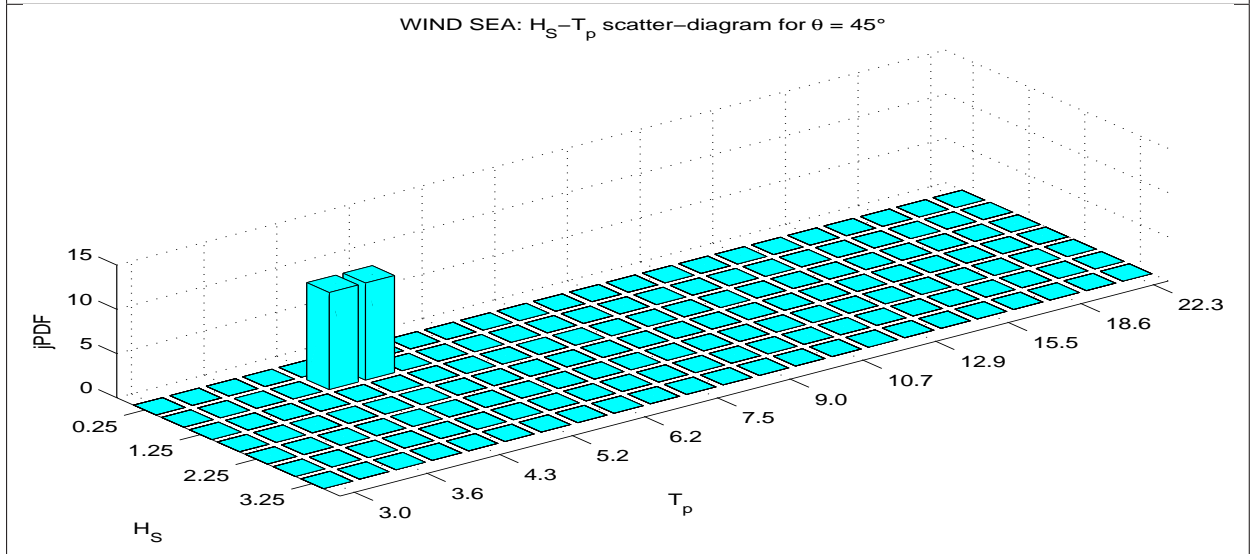
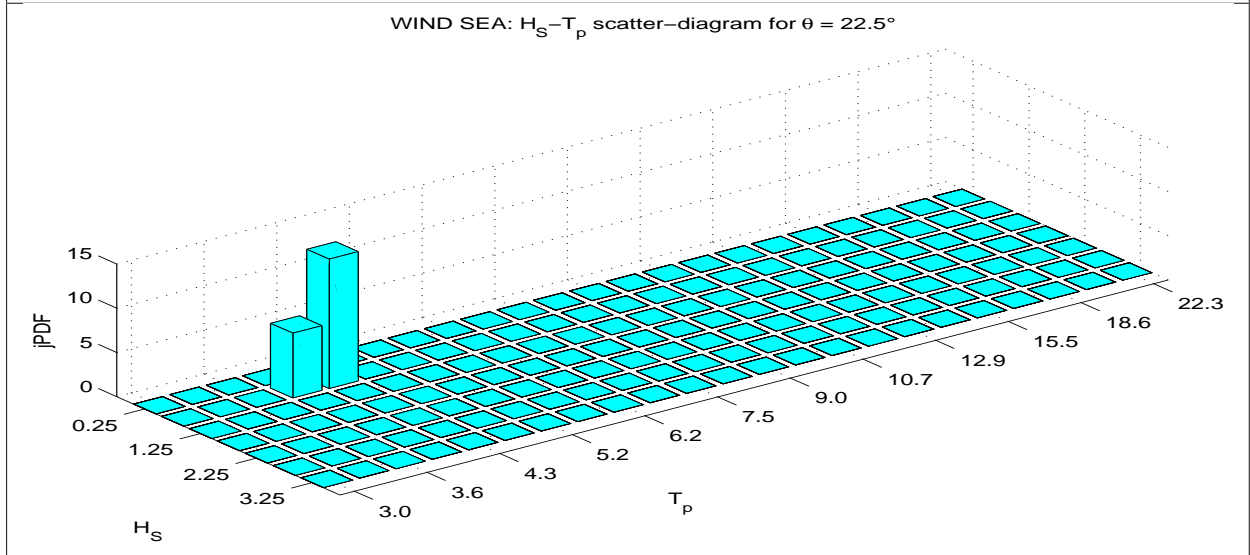
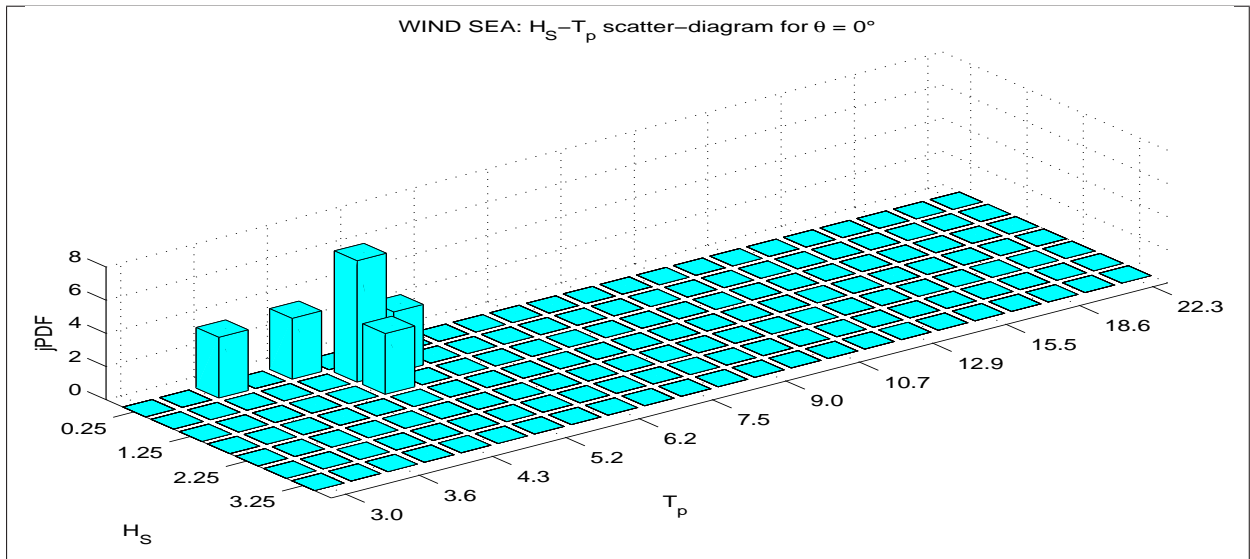


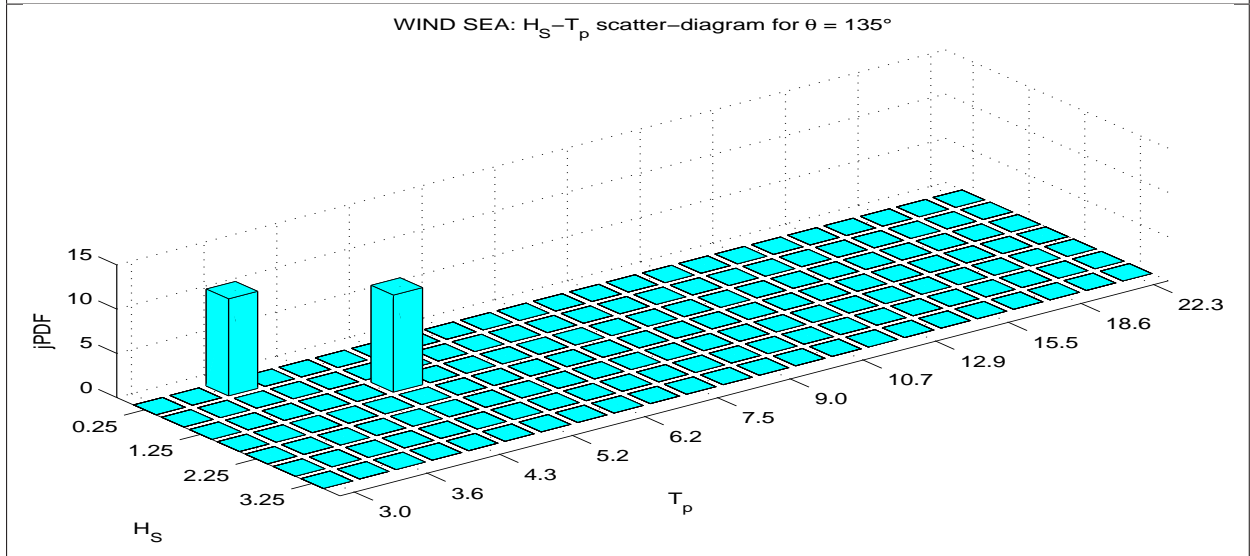
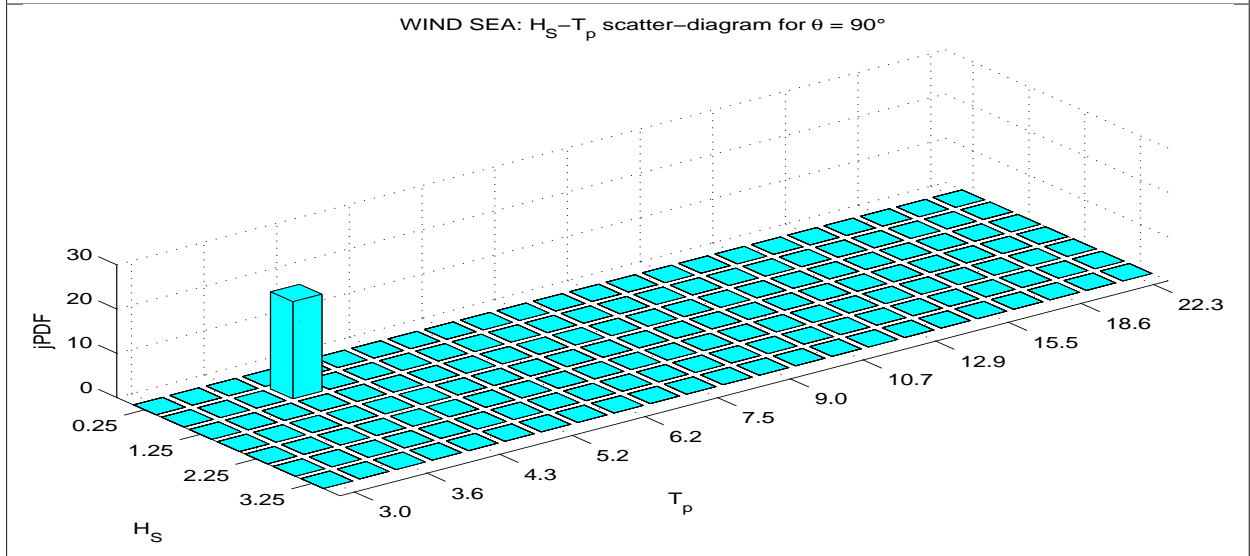
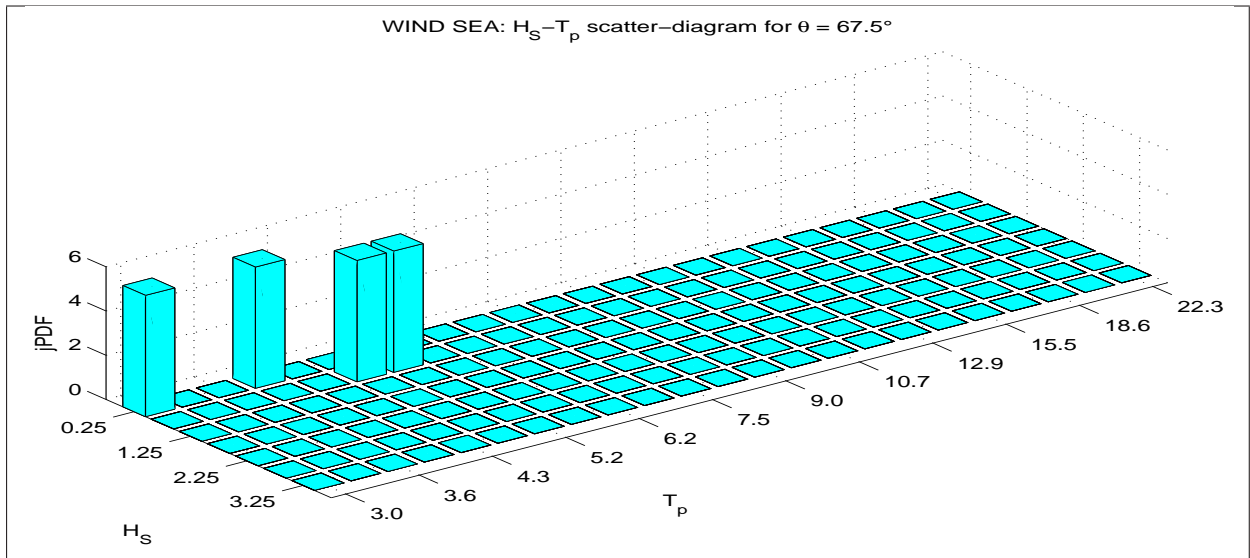
Directional $H_S - T_p$ scatter diagrams for Secondary Swell

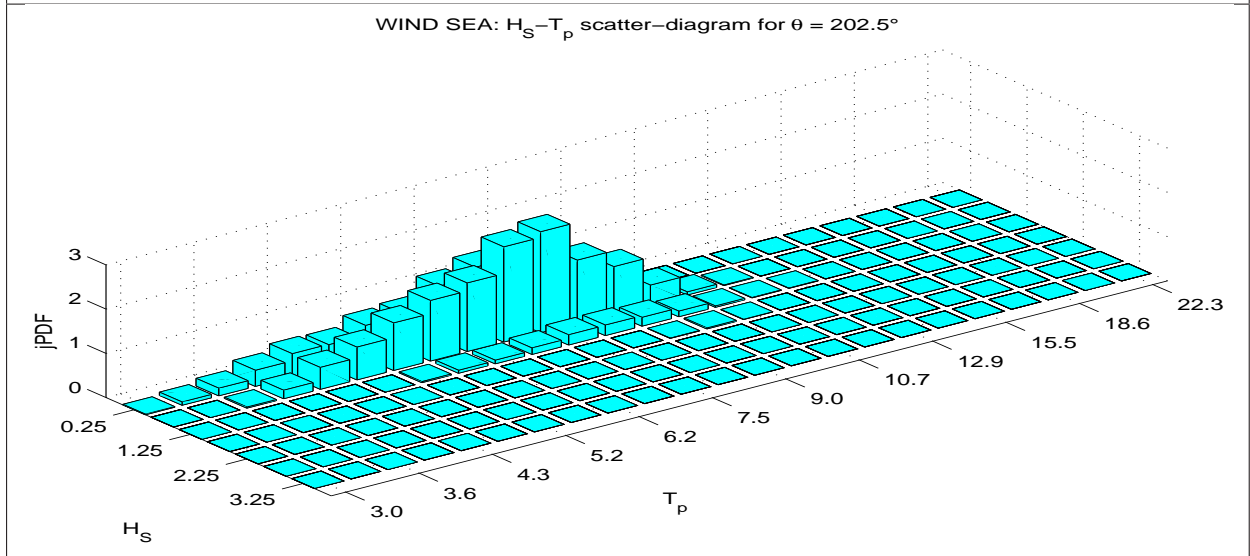
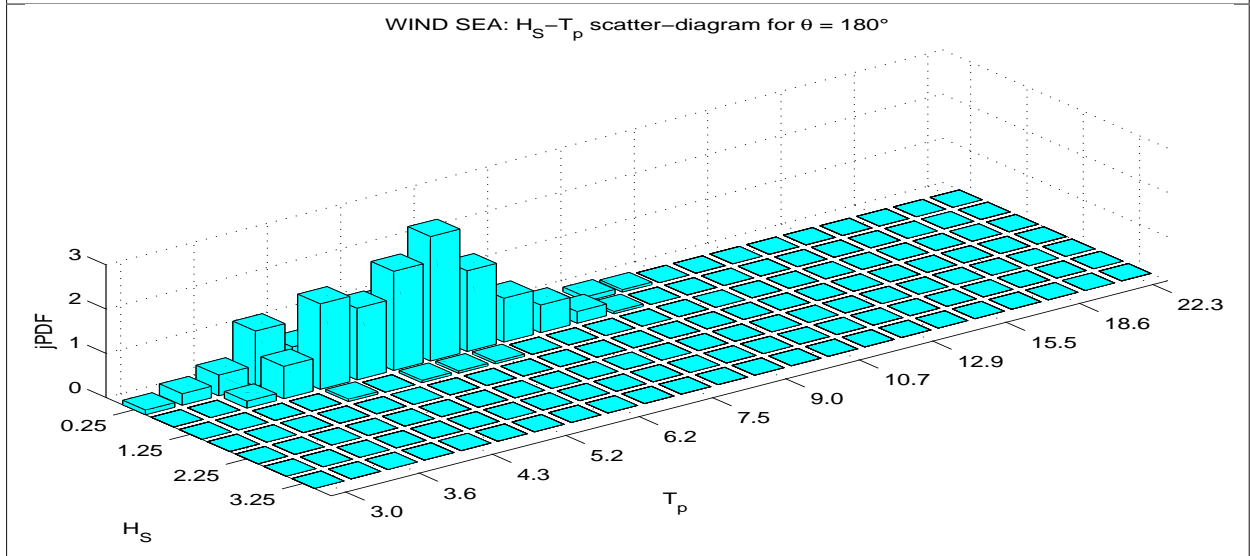
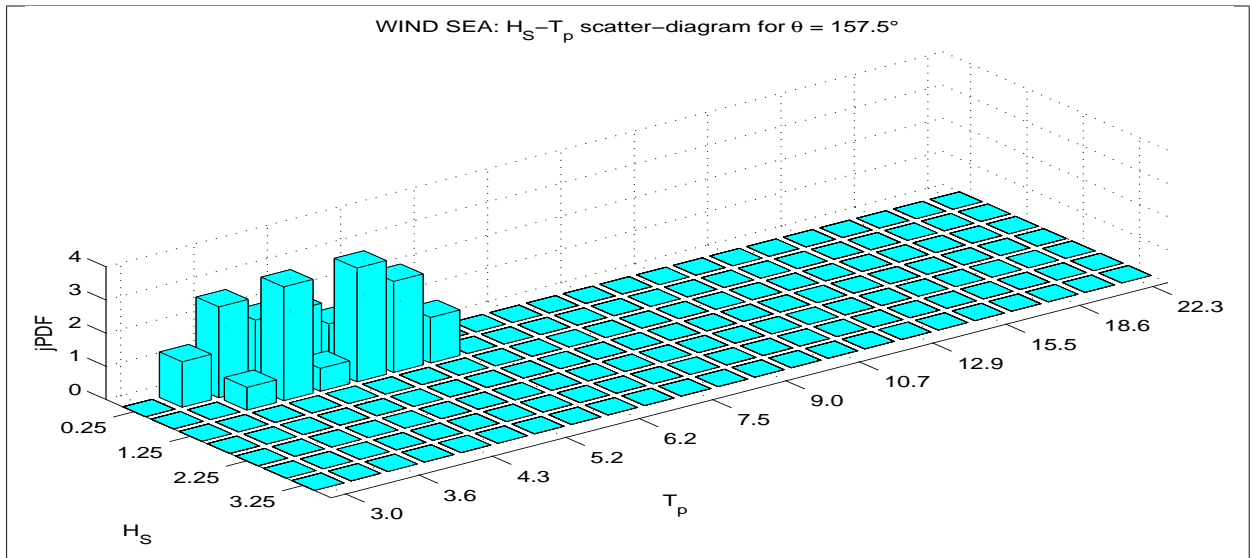


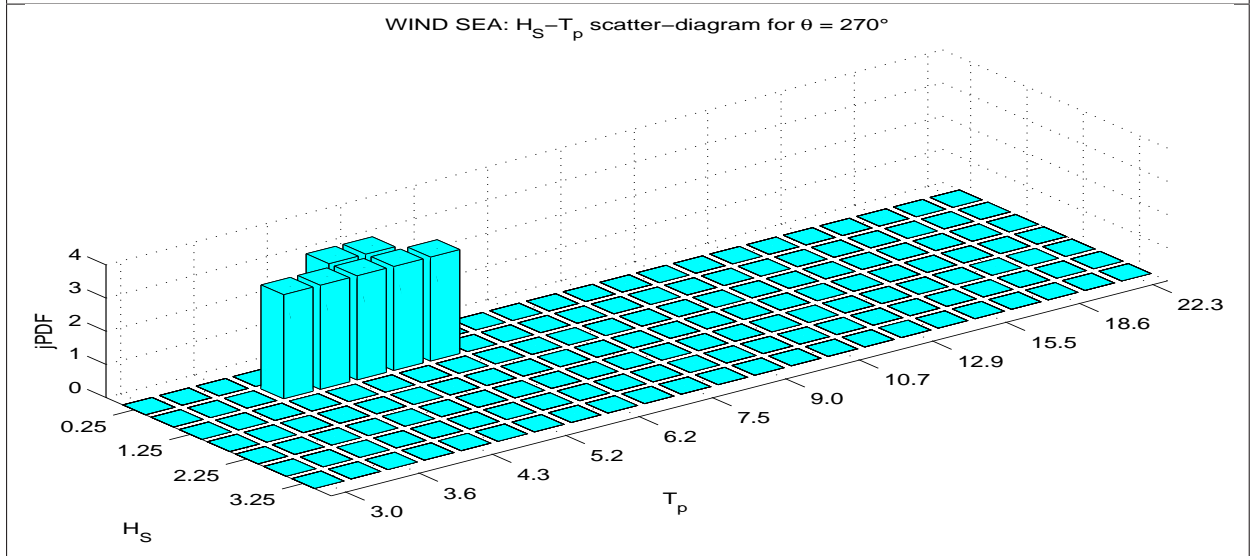
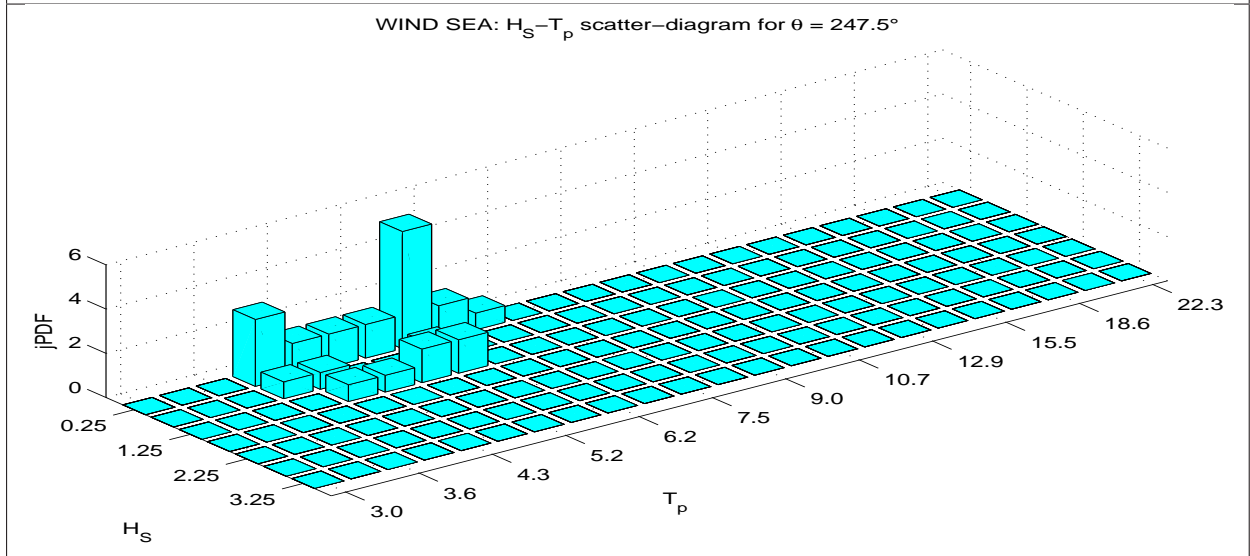
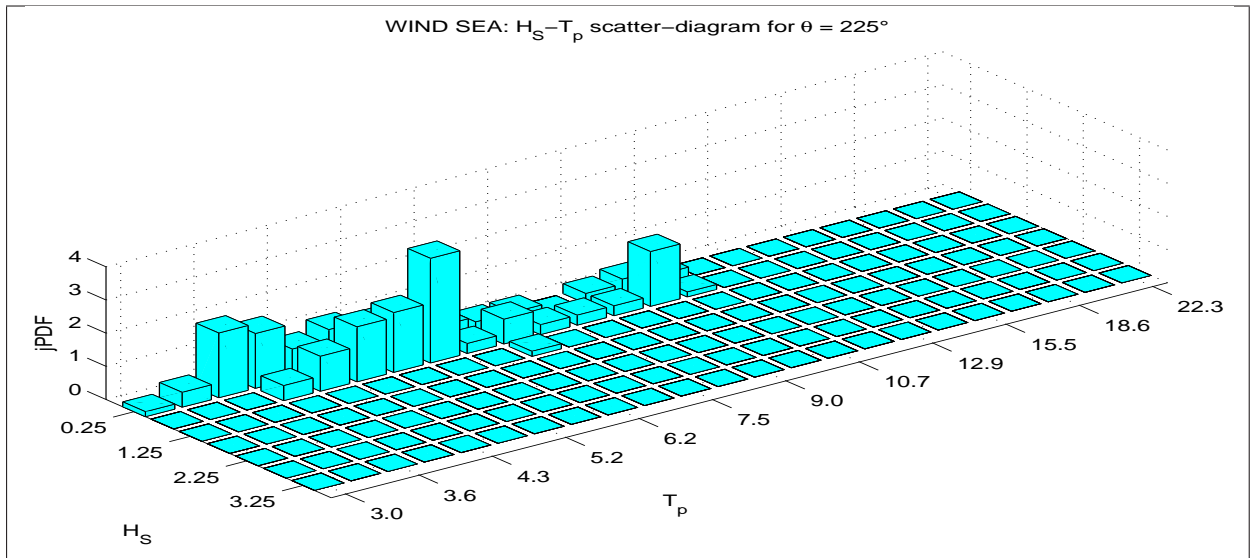


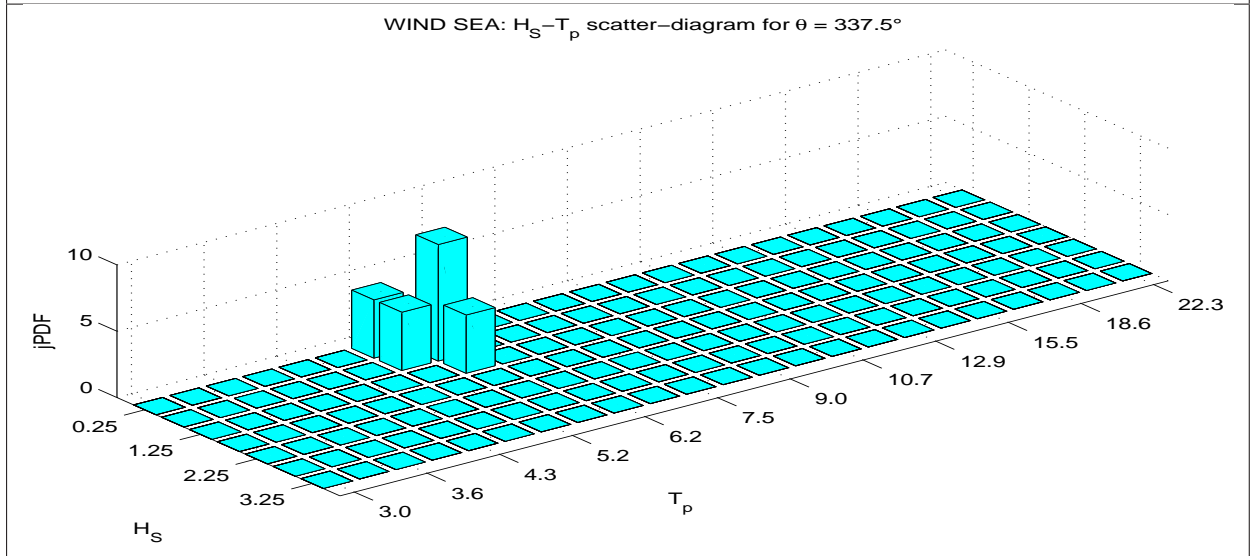
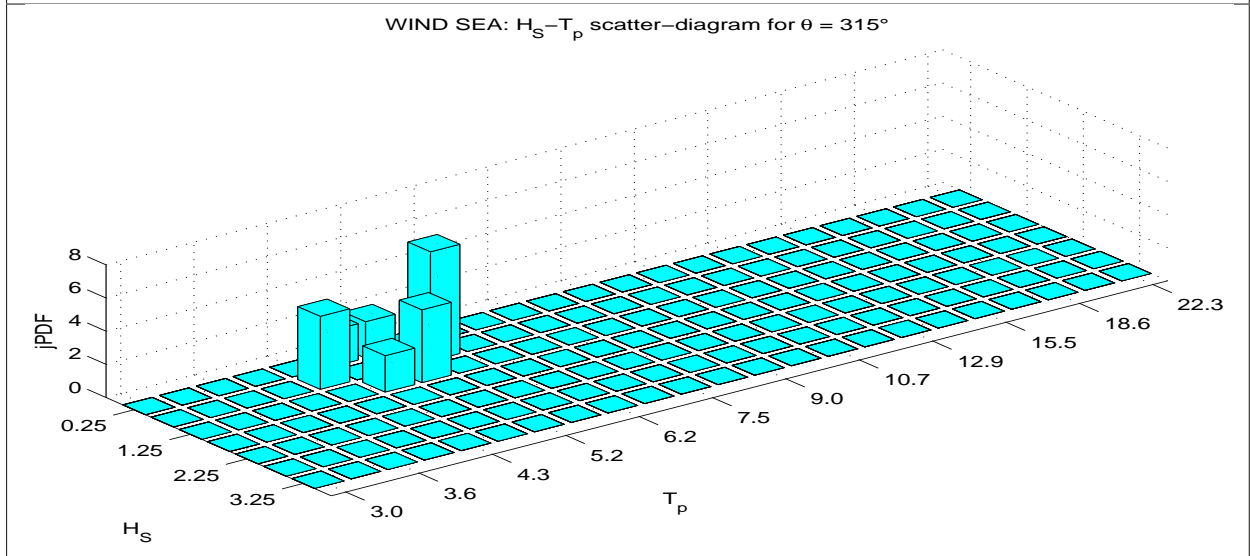
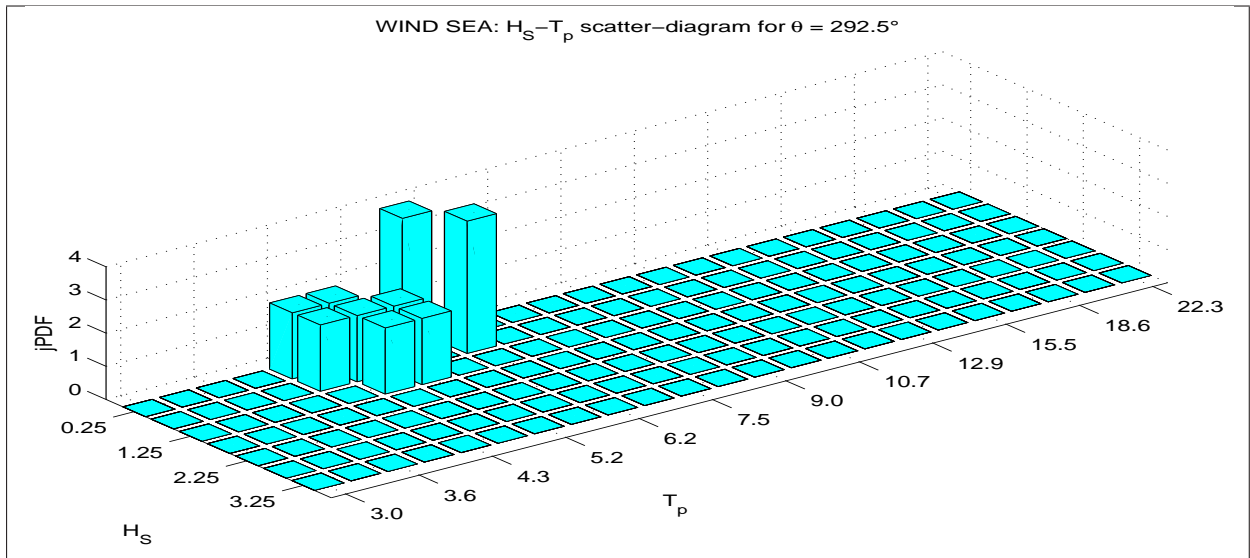
Directional $H_S - T_p$ scatter diagrams for Wind sea











F Effect of separating spectrum tail from body

F.1 Introduction

The purpose of the global study is to validate a methodology for robust and cost-effective evaluation of fatigue damage for the design of marine structures, in the case of multiple loading systems (for instance, wind sea, several swells and even responses at natural frequencies). It is as such a development of some questions raised in the “Joint Probabilities & Response Based Design” project [16].

In the previous phases of the study, we compared the performance of combination methods based on the standard deviation, zero-crossing frequency, spectral bandwidth and induced rainflow damage of each component taken in isolation. The ICA method that we introduced accepts components with main periods rather close to each other without significantly degrading the results. An idea suggested by Michel François is then to deal with spectra with fat tails by separating as two components the body of the spectrum, and the part of its tail where the structural RAO is imposing a higher slope onto this spectrum. The spectrum is then made of a truncated Wallops or Jonswap spectrum, and of a Power spectrum as defined in a previous report of this study.

We provide here the figures showing the performance of the ICA method in this procedure.

F.2 Jonswap + tail spectral shape

The studied spectrum is defined as follows:

$$S_l(f) = \alpha \frac{g^2}{(2\pi)^5} f^{-5} e^{-\frac{5}{4} \left(\frac{f}{f_p}\right)^{-4}} \gamma^{\exp\left(-\frac{\left(1-\frac{f}{f_p}\right)^2}{2\sigma^2}\right)}, \quad f \leq f_0$$
$$S_h(f) = \beta \left(\frac{f}{f_0}\right)^{-p} \quad f \geq f_0$$

with σ set to 0.07 for the ascending part of the spectrum ($f < f_p$) and 0.09 for the descending part ($f \geq f_p$), and α, β such that $S_l(f_0) = S_h(f_0)$ and $H_s = 4\sqrt{m_0}$.

For the practical study, parameters were chosen as:

- $T_p = 7\text{s}$
- $T_0 = 2.5\text{s}$
- $H_s = 4\text{m}$
- $\gamma = 1, 2, 3$
- $p = 5, 6$

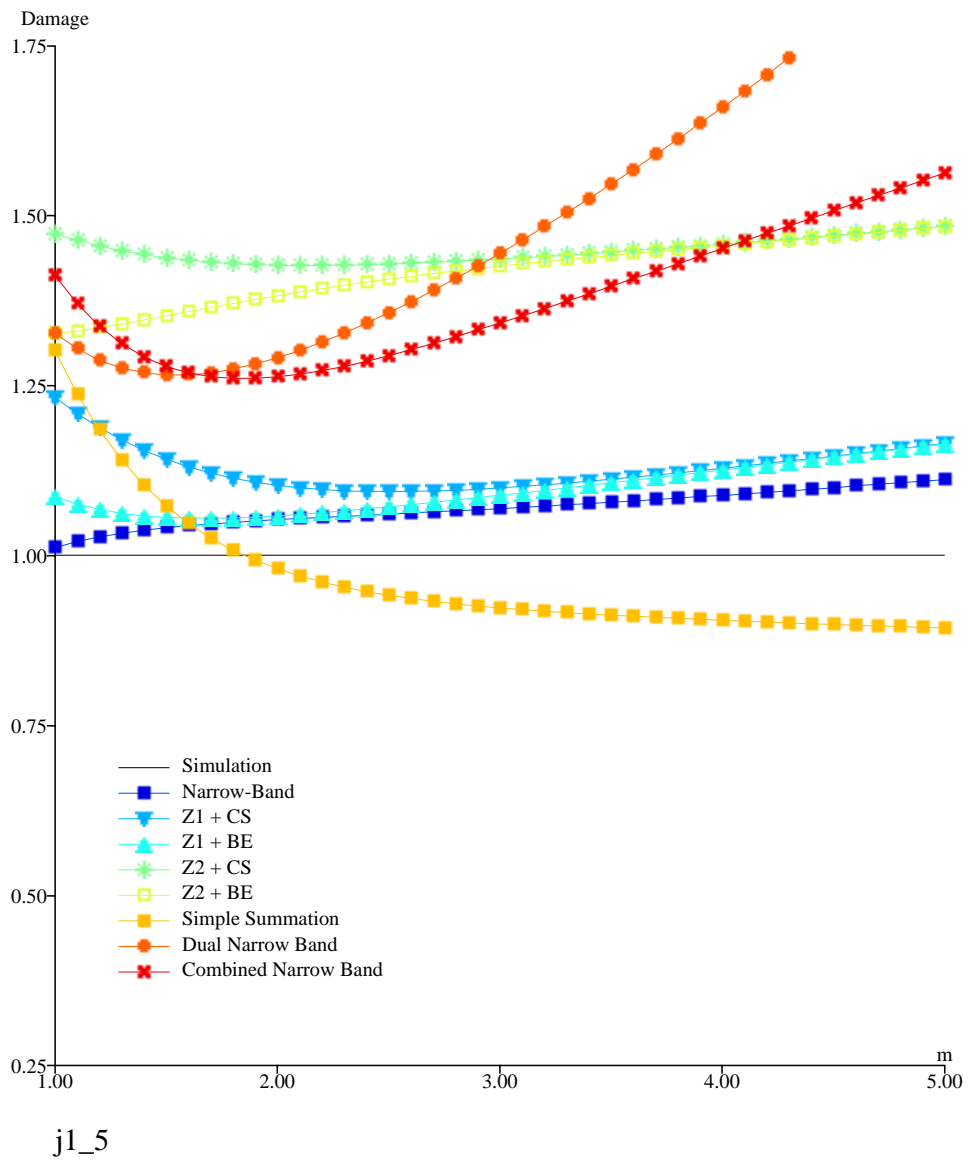


Figure 24: Comparison of the various methods for $\gamma = 1$ and $p = 5$

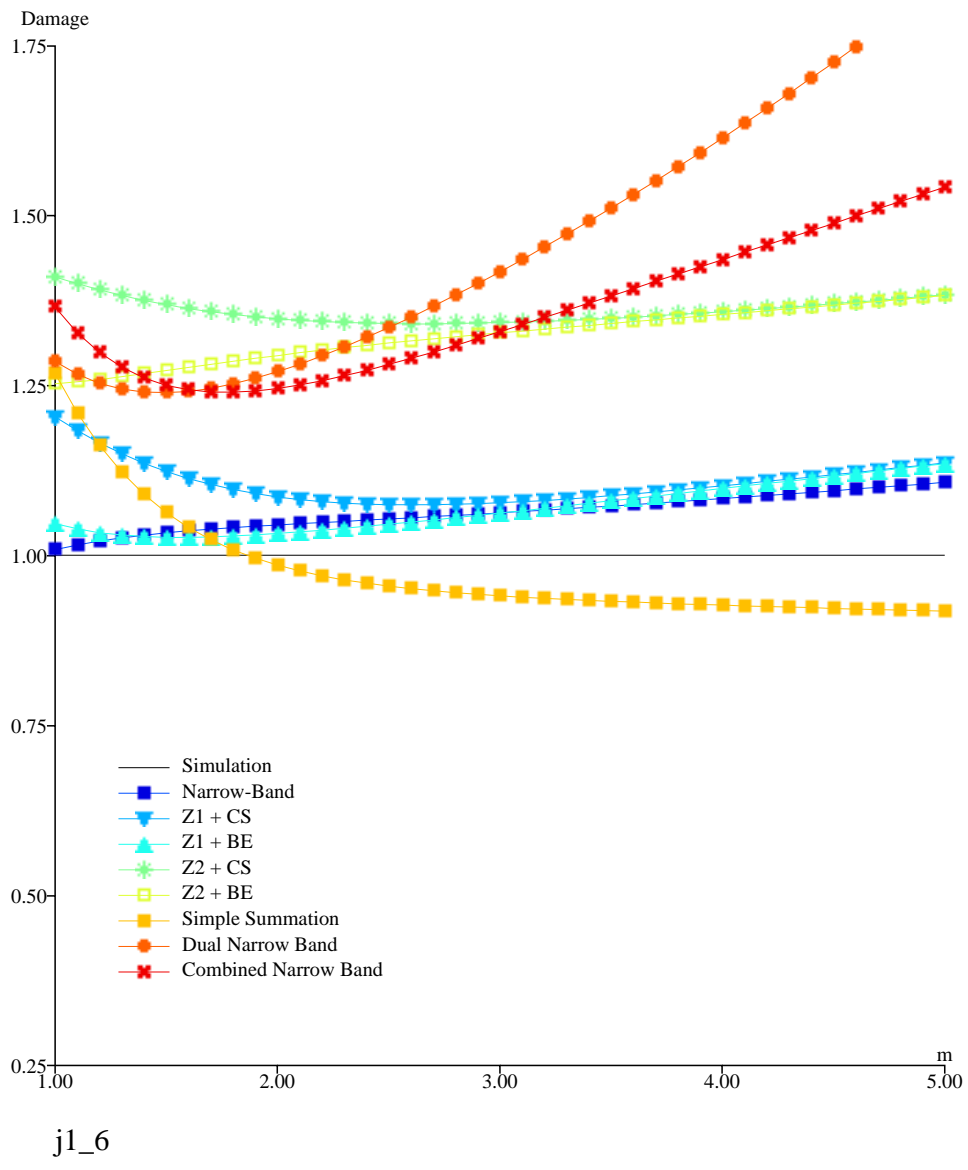


Figure 25: Comparison of the various methods for $\gamma = 1$ and $p = 6$

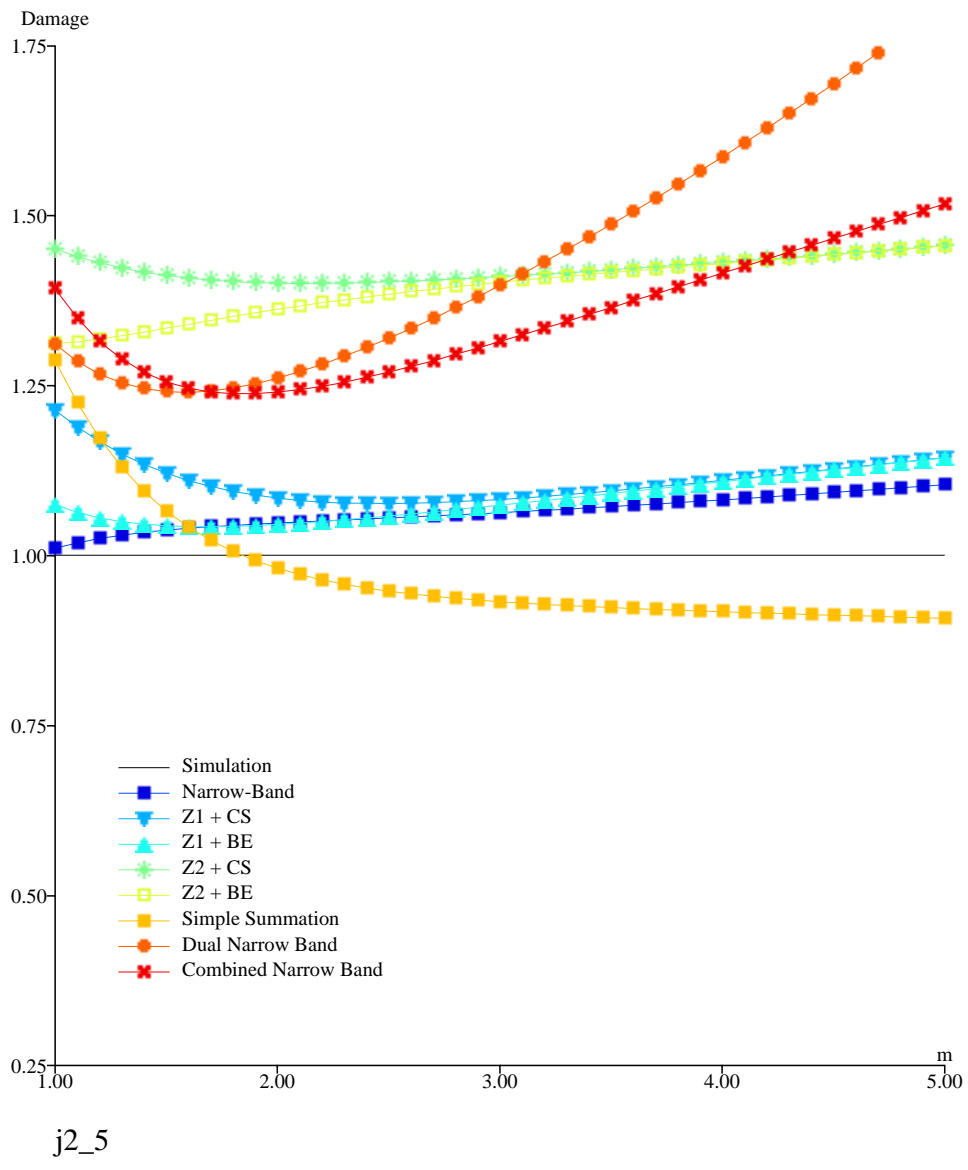


Figure 26: Comparison of the various methods for $\gamma = 2$ and $p = 5$

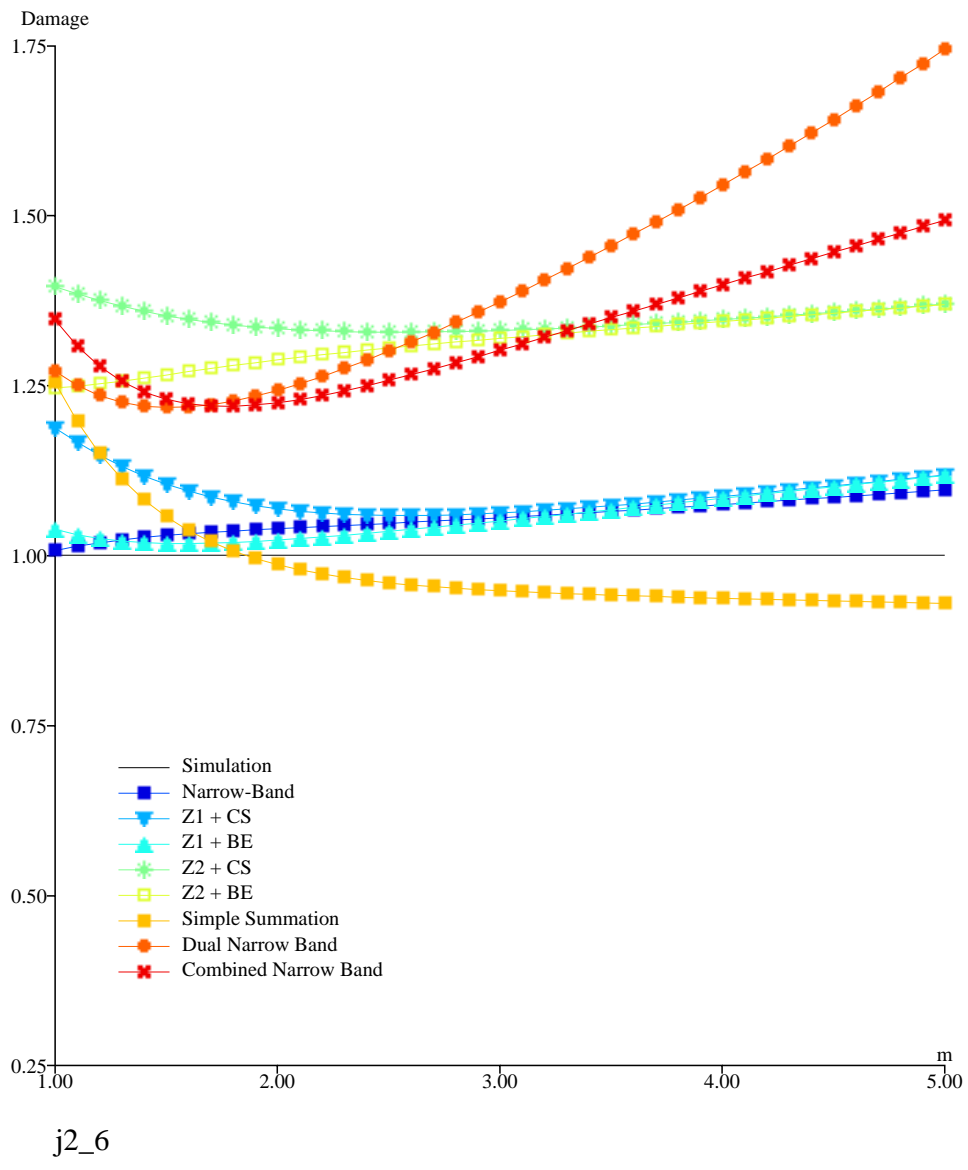


Figure 27: Comparison of the various methods for $\gamma = 2$ and $p = 6$

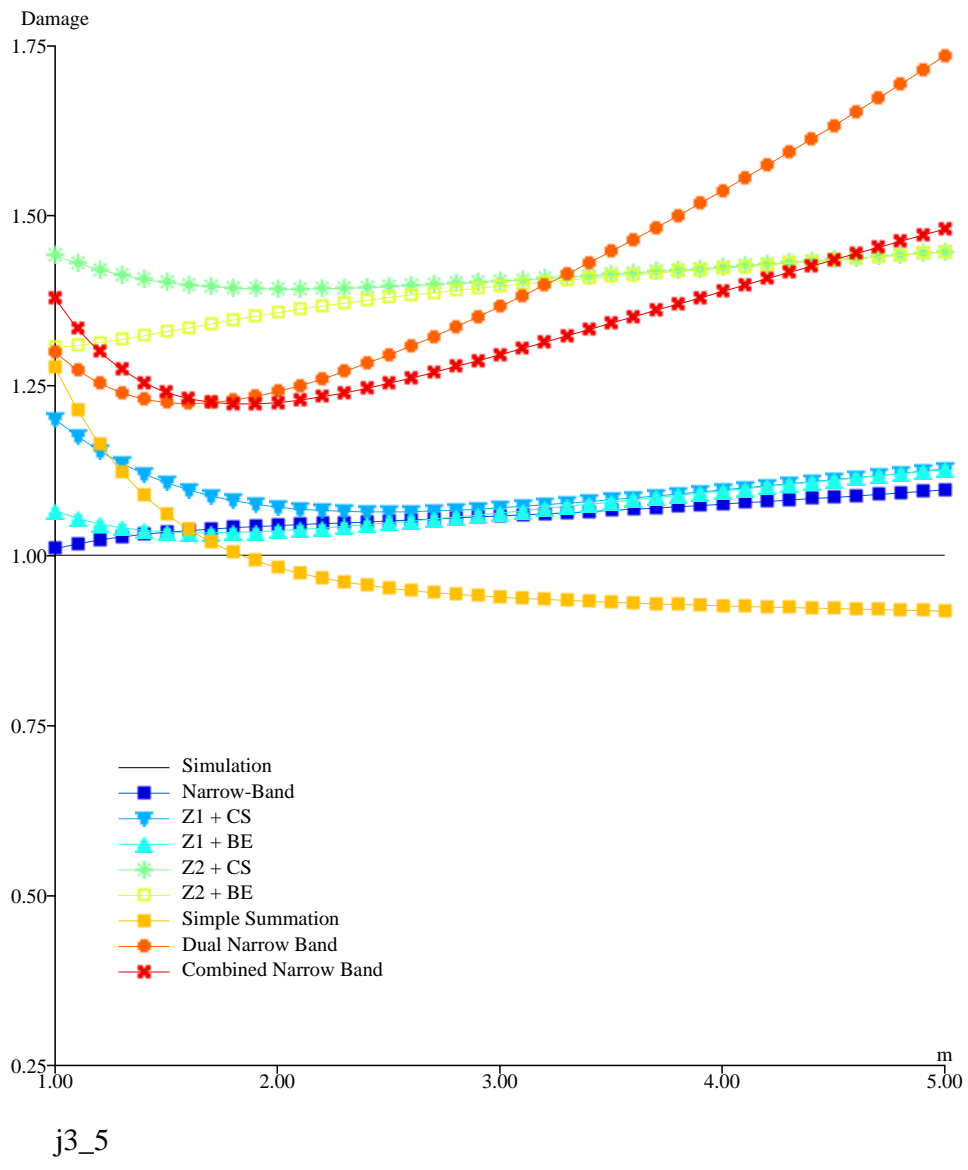


Figure 28: Comparison of the various methods for $\gamma = 3$ and $p = 5$

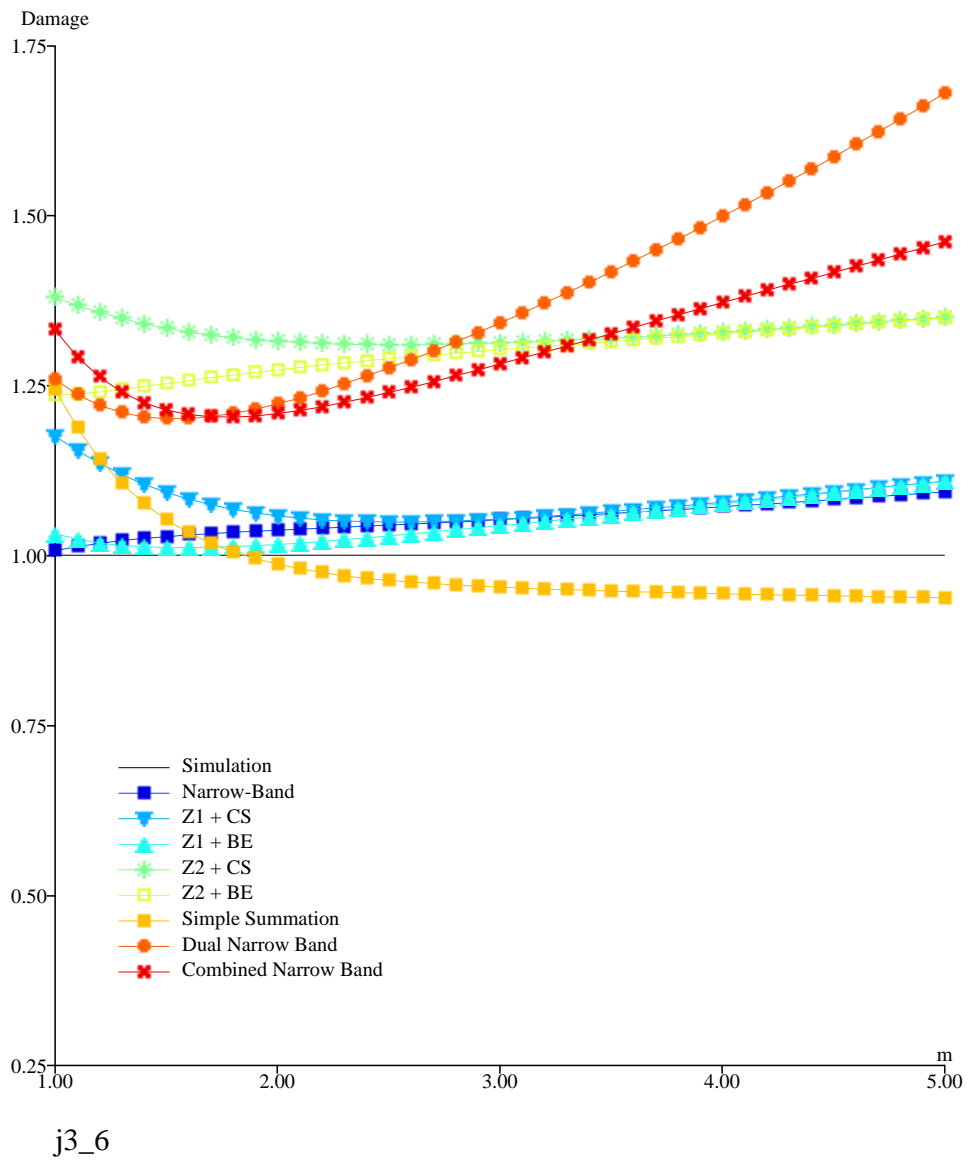


Figure 29: Comparison of the various methods for $\gamma = 3$ and $p = 6$

F.3 Wallops + tail spectral shape

We will use here the following spectrum:

$$S_l(f) = \alpha \frac{H_s^2}{T_z^4} \left(\frac{f_p}{f} \right)^{4\lambda+1} e^{-\frac{4\lambda+1}{4} \left(\frac{f_p}{f} \right)^4}, \quad f \leq f_0$$
$$S_h(f) = \beta \left(\frac{f}{f_0} \right)^{-p}, \quad f \geq f_0$$

with α, β such that $S_l(f_0) = S_h(f_0)$ and $H_s = 4\sqrt{m_0}$.

For the practical study, parameters were chosen as:

- $T_p = 7\text{s}$
- $T_0 = 2.5\text{s}$
- $H_s = 4\text{m}$
- $\lambda = 0.5, 0.75, 1.25, 1.75$
- $p = 5, 6$

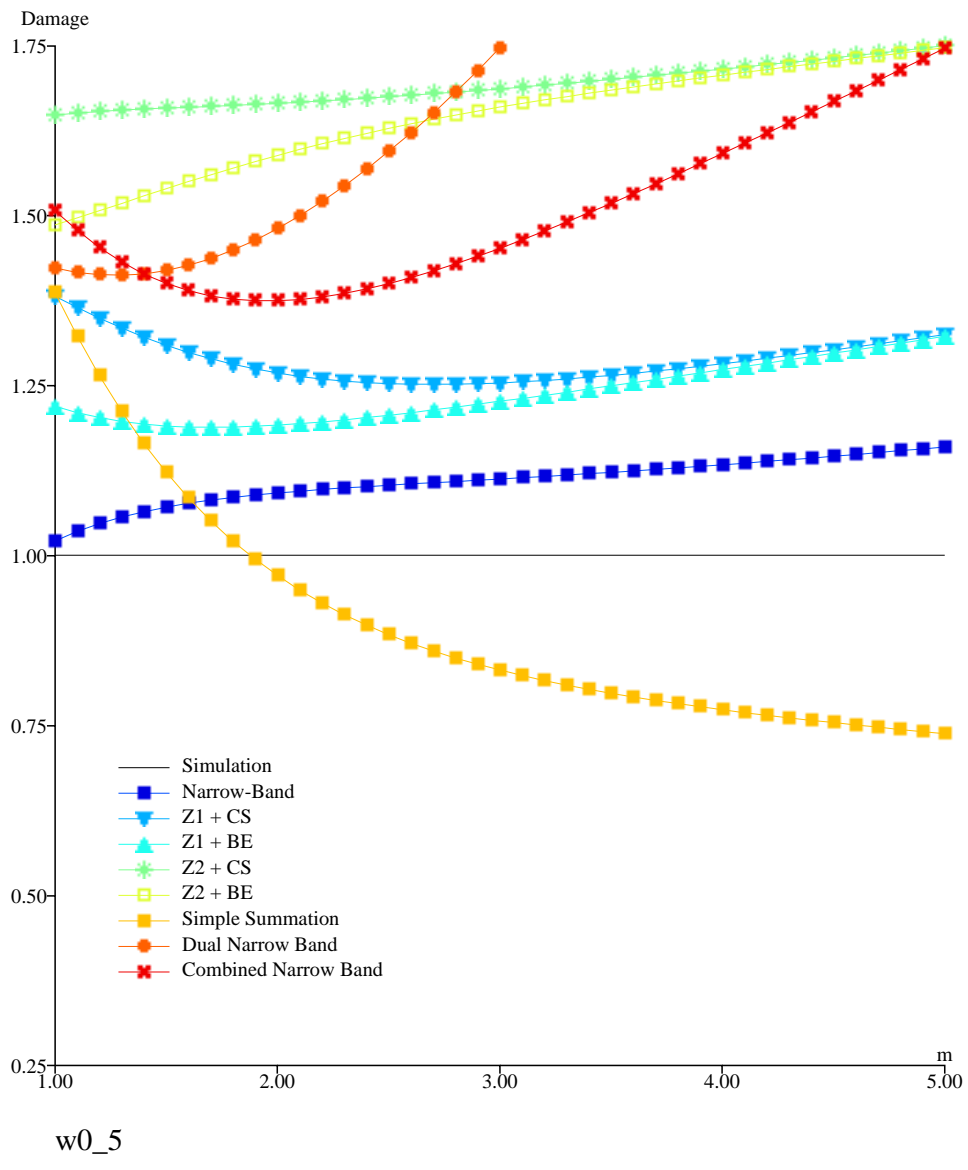


Figure 30: Comparison of the various methods for $\lambda = 0.5$ and $p = 5$

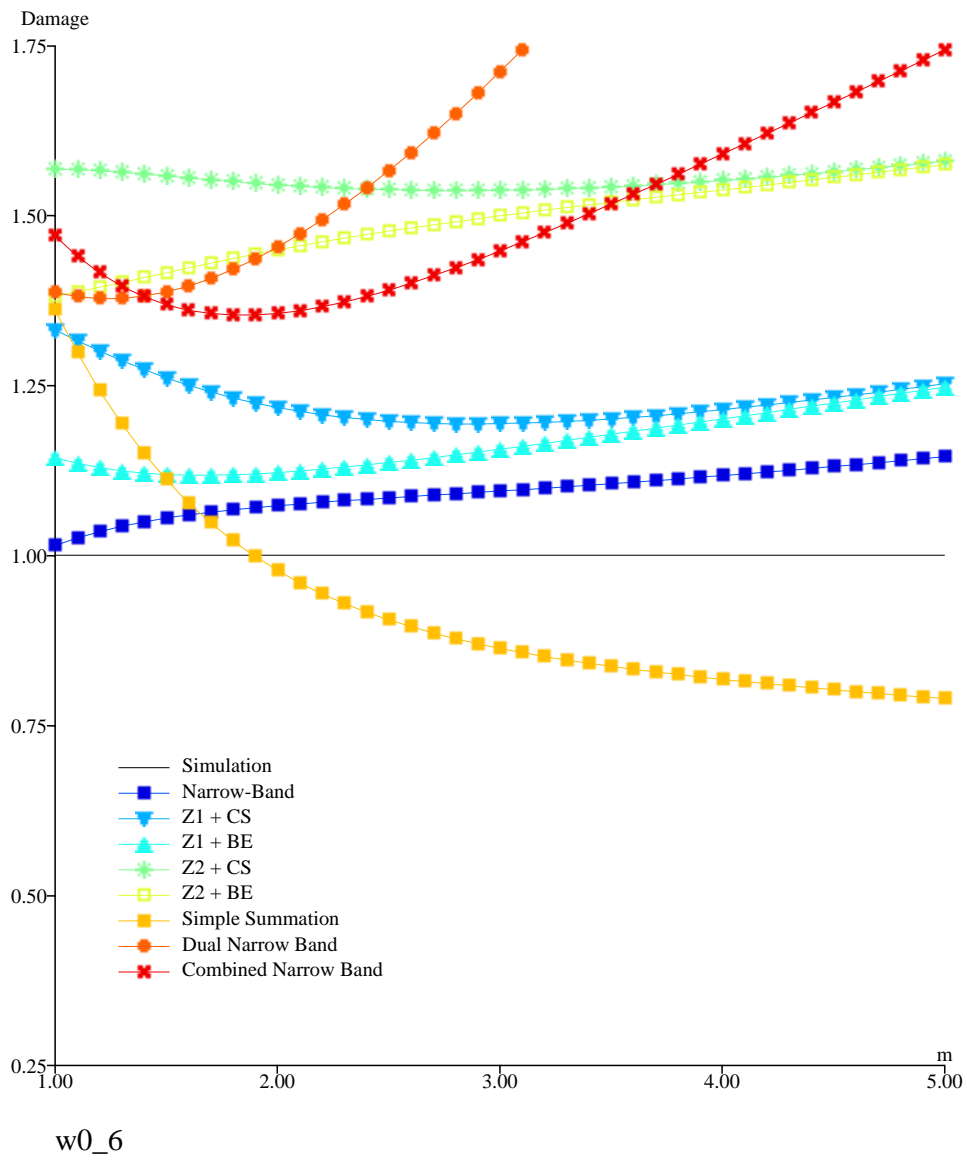


Figure 31: Comparison of the various methods for $\lambda = 0.5$ and $p = 6$

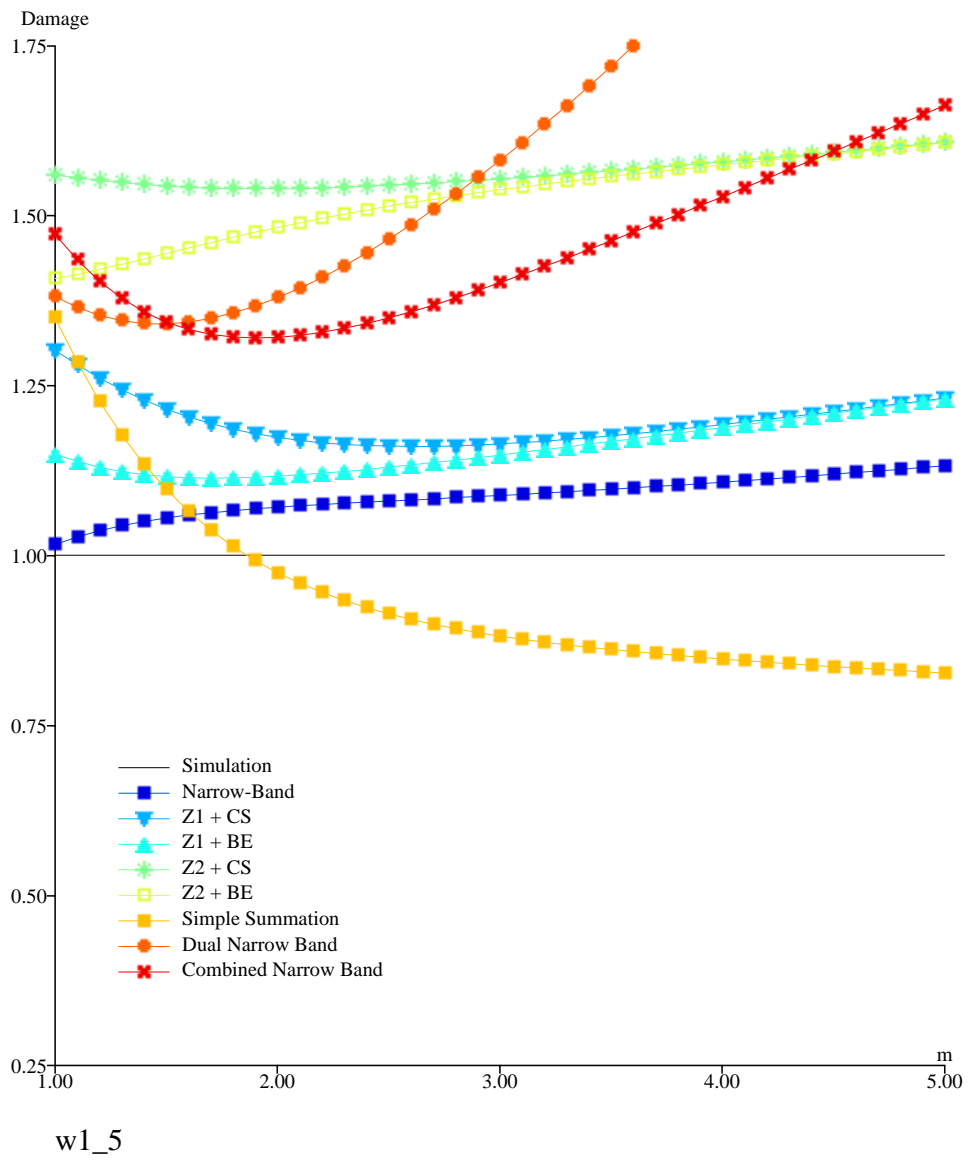


Figure 32: Comparison of the various methods for $\lambda = 0.75$ and $p = 5$

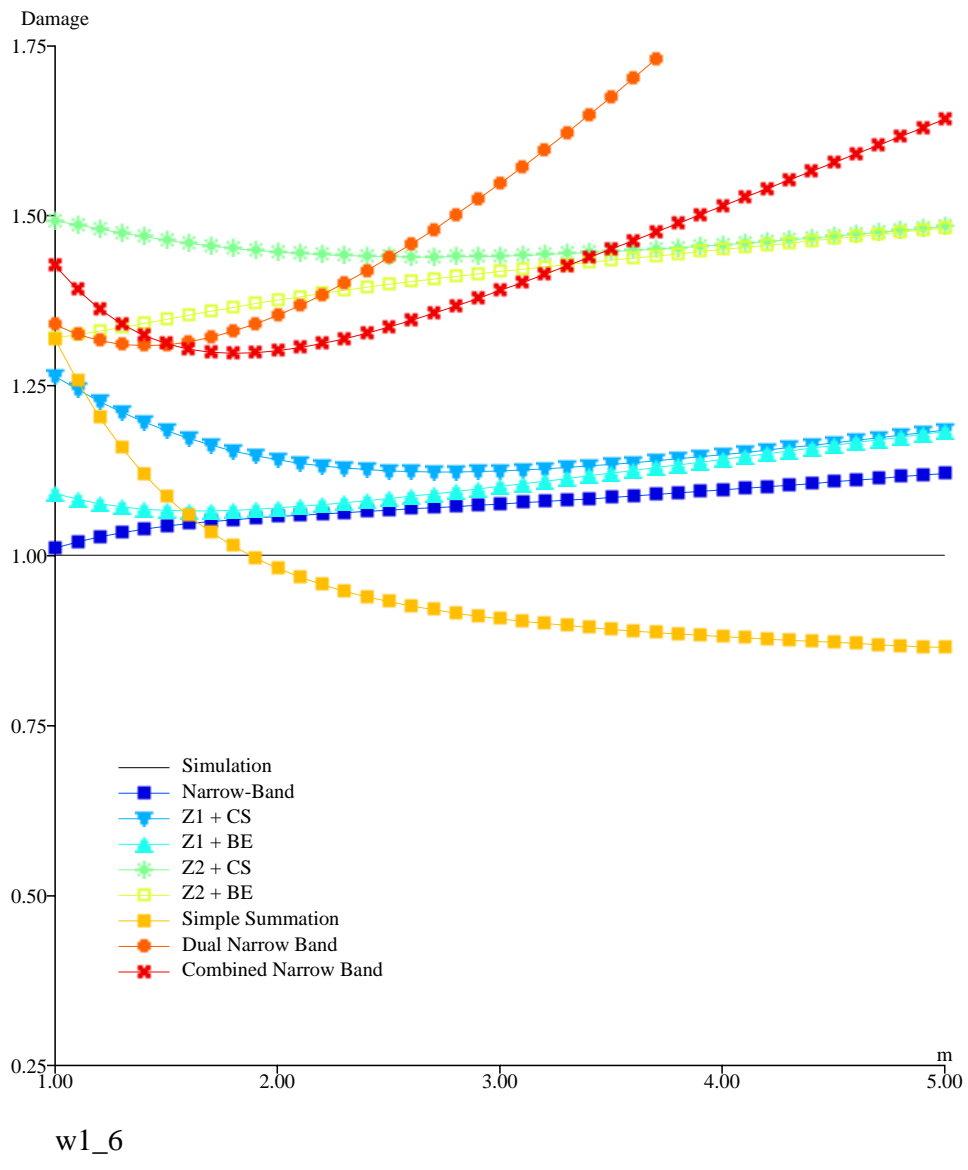


Figure 33: Comparison of the various methods for $\lambda = 0.75$ and $p = 6$

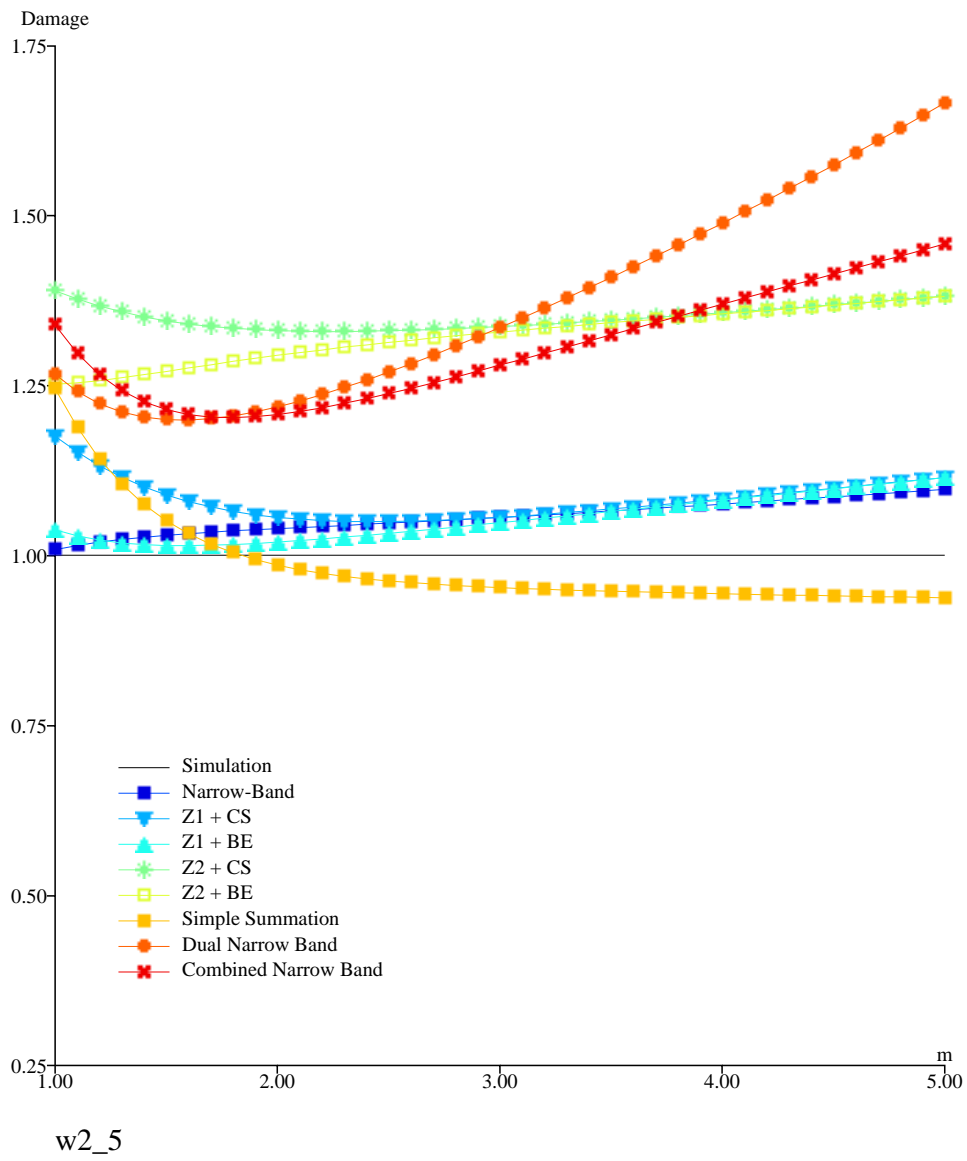


Figure 34: Comparison of the various methods for $\lambda = 1.25$ and $p = 5$

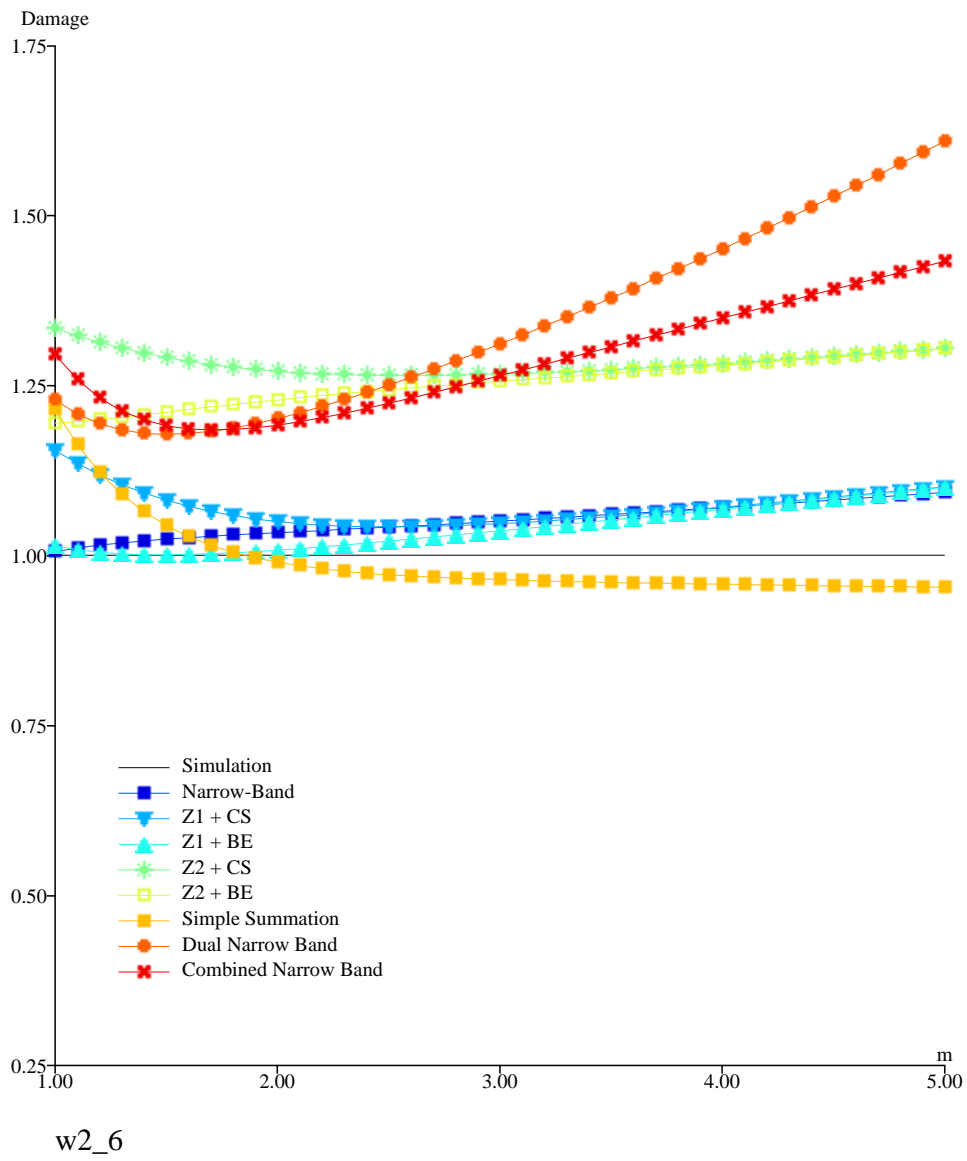


Figure 35: Comparison of the various methods for $\lambda = 1.25$ and $p = 6$

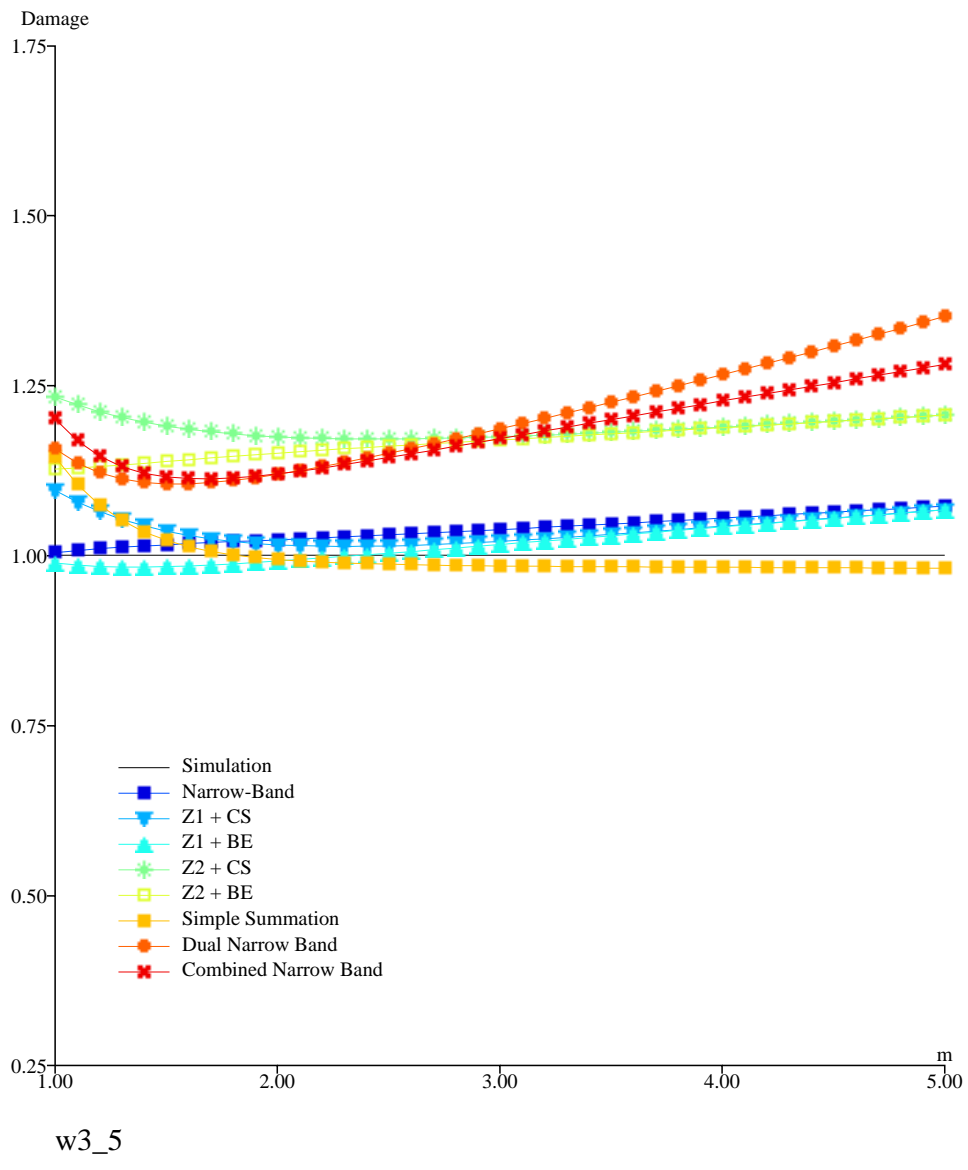


Figure 36: Comparison of the various methods for $\lambda = 1.75$ and $p = 5$

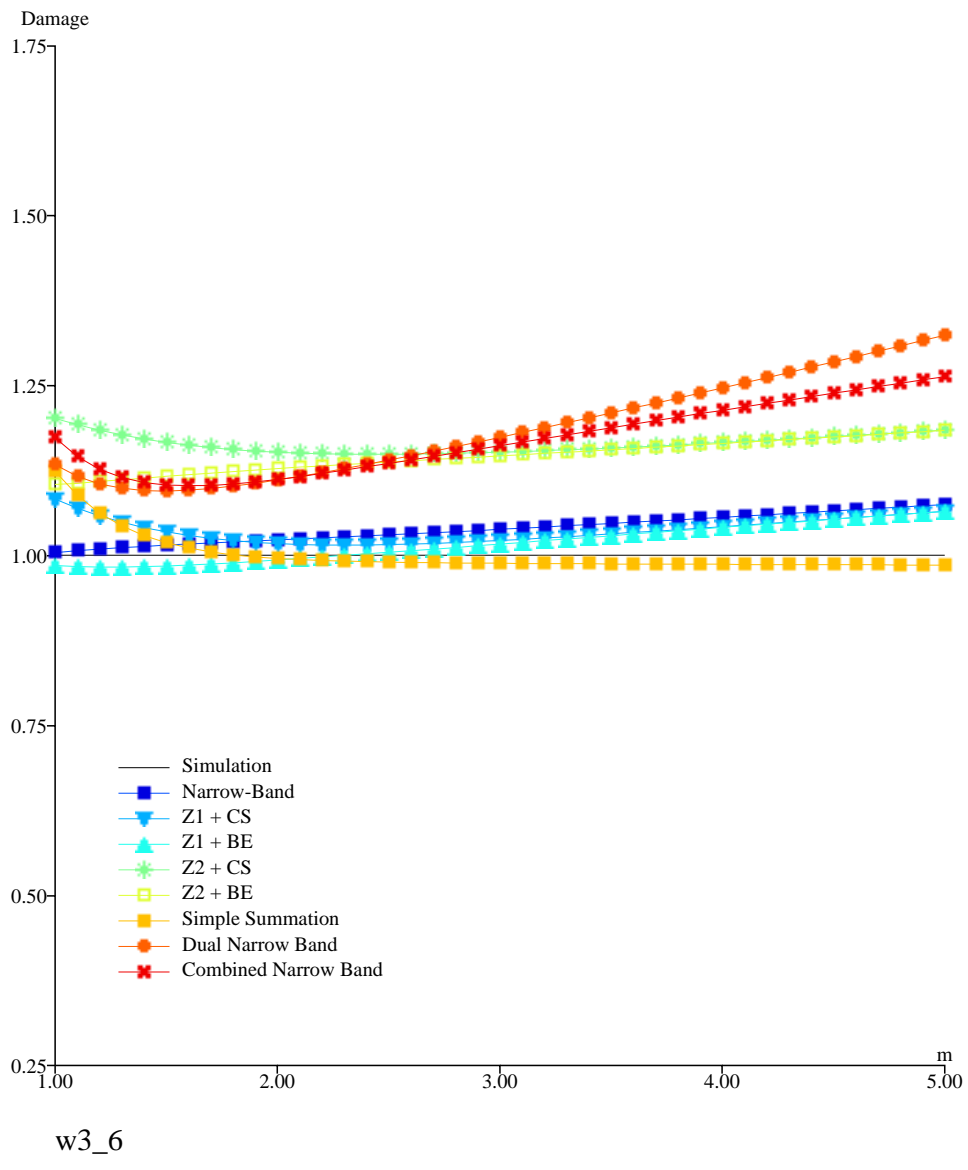


Figure 37: Comparison of the various methods for $\lambda = 1.75$ and $p = 6$

F.4 Conclusion

It can be seen that although the combined spectrum approximation provides in all cases very good results with little conservatism, the ICA method may also be applied with comparable levels of conservatism.